Changes in the Public IgM Repertoire and Its Idiotypic Connectivity in Alzheimer's Disease and Frontotemporal Dementia

Shina Pashova-Dimova[1], Peter Petrov[2], Sena Karachanak-Yankova[3], Diana Belezhanska[4], Yavor Zhelev[4], Shima Mehrabian[4], Draga Toncheva[3], Lachezar Traykov[4], Anastas Pashov[5]

[1] Institute of Biology and Immunology of Reproduction, Bulgarian Academy of Sciences, Sofia, Bulgaria,
[2] Institute of Mathematics and Informatics, Bulgarian Academy of Sciences, Sofia, Bulgaria,
[3] Department of Medical Genetics, Medical University, Sofia, Bulgaria,
[4] Clinic of Neurology, UH "Alexandrovska", Medical University, Sofia, Bulgaria,
[5] Department of Immunology, Institute of Microbiology, Bulgarian Academy of Sciences, Sofia, Bulgaria

Correspondence:
Anastas Pashov
a_pashov@microbio.bas.bg

Key words: antibody repertoire, public antibodies, Alzheimer's disease, frontotemporal dementia, IgOme, antibody reactivity graph, IgM

Abstract

Alzheimer's disease (AD) and frontotemporal dementia (FTD) are prevalent neurodegenerative disorders. Early diagnosis is challenging due to the lack of definitive biomarkers and reliance on invasive procedures. Immune biomarkers, particularly those reflecting the interaction between the central nervous system (CNS) and the peripheral immune system, have shown promise for non-invasive detection through blood samples. This study investigates the reactivity of serum IgM and IgG from AD and FTD patients against a library of mimotopes representing public IgM reactivities in healthy donors. Serum samples from AD, FTD, and other neurodegenerative dementias (ND) and controls were tested on peptide microarrays. The samples were pooled to mitigate individual variability. The reactivity data were analyzed using graphs to represent the cross-reactivity networks. The analysis revealed distinct reactivity patterns for the studied groups. Public IgM reactivities showed significant correlations with neurodegenerative conditions, with AD and FTD exhibiting loss or gain of specific IgM reactivities. Graph analysis highlighted significant differences between disease and control groups in graph density, clustering, and assortativity parameters. Mimotopes of IgM reactivities lost in dementia, particularly in AD, exhibited significant homology to HCDR3 sequences of human antibodies. Furthermore, clusters of reactivities showed significant distinctions between AD and FTD, with IgG reactivities providing additional differentiation. Several self-proteins related to neurodegeneration proved to have sequences homologous to disease-associated mimotopes. Interestingly, the beta-propeller signature sequence YWTD found in ApoE's receptor LRP1 proved a characteristic epitope for IgG in FTD but not AD. At the same time, the respective public |gM mimotope YWTDSSR coincides with a highly conserved sequence in many microorganisms and sequences found in human HCDR3. Thus, the public IgM repertoire, characterized by its broad reactivity and inherent autoreactivity, offers valuable insights into the immunological alterations in neurodegenerative diseases. The study supports the potential of IgM and IgG reactivity profiles as another compartment of non-invasive biomarkers for early diagnosis and differentiating AD and FTD.

1. Introduction

Alzheimer's disease (AD) and frontotemporal dementia (FTD) are among the most prevalent neurodegenerative disorders affecting the elderly population (Musa et al., 2020). Even the basic pathogenic mechanisms of these diseases are still debated (Castellani et al., 2022) But it is clear that they involve complex system-level interactions, including immunological mechanisms (Chen and Colonna, 2022). A better understanding of the pathogenesis of neurodegenerative disease serves the development of potential therapy approaches and better and earlier diagnosis. The diagnosis of AD and FTD remains a significant challenge due to the lack of definitive biomarkers and the need for invasive procedures like cerebrospinal fluid (CSF) analysis or positron emission tomography (PET) scans (Gifford et al., 2023; Shue et al., 2024). Recent advancements in plasma biomarkers and computational approaches have opened up new avenues for the early diagnosis of these neurodegenerative diseases. Immune biomarkers, particularly those related to the cross-talk between the central nervous system (CNS) and the immune system, have emerged as promising tools for the detection of AD and FTD (Krix et al., 2024). These serum biomarkers are more accessible and cost-effective than traditional methods, and their diversity justifies the use of machine learning approaches, combining them with further information (e.g., age, sex, APOE genotype) into predictive models supporting an earlier diagnosis.

Among the promising immunological biomarkers, antibodies have a unique role because of their highly diverse repertoire of specificities. Previous studies have demonstrated that patients with AD exhibit unique IgG antibody binding patterns compared to healthy controls and those with other types of dementia. For instance, Restrepo et al. (2011) explored the application of a peptide microarray containing 10,000 random sequence peptides to profile the antibody repertoire of AD patients and transgenic mouse models. The study found that AD patients and mice with cerebral amyloidosis displayed distinct immunoprofiles, suggesting the utility of the immunosignature technique in AD diagnosis (Restrepo et al., 2011). Some sets of IgG autoantibodies with better-defined autoantigen specificities have shown great promise for the development of multi-disease biomarkers, including for the early detection of AD (DeMarshall et al., 2017; DeMarshall et al., 2023; Nagele et al., 2011). Unlike the highly specific IgG, which is usually the product of an adaptive immune response, the IgM repertoire abounds in constitutively produced natural antibody, and at least 20% of them are physiologically autoreactive (Imkeller and Wardemann, 2018). Since it is also more diverse than its IgG counterpart and better overlapping with the public reactivities (Galson et al., 2015). Thus, the individual IgM repertoire is better poised as a sensor of the internal environment before the development of overt autoimmunity. With this working hypothesis, we started developing a diagnostic platform applicable to a very broad range of pathologies that is based on applying IgOme approaches (Ryvkin et al., 2012) for extracting patterns of diagnostic public IgM reactivities (Ferdinandov et al., 2023; Pashov et al., 2019; Pashova-Dimova et al., 2023; Pashova et al., 2022; Shivarov et al., 2020).

In this manuscript, we present our findings on the reactivity of serum IgM and IgG from AD and FTD patients to a large library of mimotopes of the public IgM reactivities found in healthy donors. In addition, the cross-reactivities to the same mimotopes in the IgG repertoire were tested, hoping to estimate the degree of the adaptive immune response contribution to the observed binding patterns. We focus on the differences in antibody reactivity graphs generated from the binding data as a formalism for cross-reactivity networks. Somewhat surprisingly, losing or gaining public IgM reactivities in AD and FTD

correlated with their cross-reactivity with human immunoglobulin HCDR3 sequences seen as potential idiotopes.

2. Materials and methods

2.1. Patients and sera

Patients were recruited at the Clinic of Neurology, Medical University - Sofia. The diagnosis of AD was made according to the NIA-AA criteria (McKhann et al., 2011). A diagnosis of behavioral variant of FTD and primary progressive aphasia (PPA) was considered based on the current revised diagnostic guidelines (Gorno-Tempini et al., 2011; Rascovsky et al., 2011). A group of patients with other neurodegenerative diseases (Lewy body disease, Parkinson's disease with dementia, and Huntington disease) was also included. A summary of the patients' clinical data is presented in Table 1. Sera were collected from three groups of 8 patients diagnosed with AD, FTD, or other neurodegenerative dementias and compared to sera from 6 sex and age-matched control group patients without dementia (C). All participants or their caregivers gave written informed consent to participation in the study. The informed consent forms and study protocols were approved by the local ethics committee, UH "Alexandrovska", and performed in harmony with the Helsinki Declaration.

2.2. IgM and IgG isolation

The serum samples were thawed and incubated at 37°C for 30 min to dissolve the IgM aggregates. After spinning for 10 min at 20,000 × g, the IgM concentration was determined by ELISA, and the sera were diluted to 10 µg/ml IgM. The samples used in the study were limited to 5 per diagnosis, so some of the samples had to be pooled. Pooling creates correlation between the samples, which makes cross-validation and machine learning impossible. Since this limitation was inevitable, it was decided that all samples would be pools of two patients' appropriately diluted sera as an intermediate averaging of reactivities in the groups and giving a slight advantage to public reactivities. The pooling schemes in terms of serum number were: AD – 1+6, 2+7, 3+8, 4+8, and 5+2, FTD - 1+6, 2+7, 3+8, 4+1, and 5+2, ND - 1+6, 2+7, 3+8, 4+1, and 5+2, and C – 1+3, 2+6, 3+4, 4+2, 5+1.

The patients' blood groups were detected by reverse blood group typing of the sera using the test erythrocytes kit Biotestcell (BioRad).

2.3. Peptide microarray binding assay

2.3.1. Sequence selection

Previously, we have studied a library of 2×10^5 peptide mimotopes of the public IgM of healthy donors (Pashov et al., 2019). The selection of public reactivities is assured by using IgM isolated from a blood plasma pool from 10 000 individuals, which substantially dilutes the private IgM specificities. Using a Gibbs sampling approach (Andreatta et al., 2013) (https://services.healthtech.dtu.dk/services/GibbsCluster-2.0/), the sequences were clustered optimally in 790 clusters (Pashov et al., 2019). Here, we further analyzed this grouping by constructing a graph of the clusters. For each primary cluster, the neighboring clusters were determined based on sequence proximity. The latter was based on the next best cluster information for each of the sequences of a given cluster as reported by the algorithm. If a cluster had more than n sequences close to the same alternative

cluster, the two clusters were connected by an edge. Most (675) of the clusters remained disconnected, but some formed the graph components connecting 2 to 10 clusters. The threshold n was adjusted to produce fewer than 730 components (a number defined by the peptide array format). These components were considered the secondary clusters (n=726). The singletons in this graph represent primary clusters, and the Gibbs Sampling algorithm provided the most relevant representative sequence from each cluster. Each of the secondary clusters was converted to an IgOme graph of sequences (Pashova et al., 2022), and the vertex with the highest eigencentrality was used to define the representative sequence. In this way, a set of 726 peptides that sampled symmetrically the space of the 7-mer mimotopes of the public IgM reactivities was selected and used to synthesize the peptide arrays.

2.3.2. Peptide microarrays design

PEPperPRINT™ (Heidelberg, Germany) produced custom peptide microarrays with 726 7 amino acid residues long linear peptides (see 2.3.1). The peptides were synthesized in situ and attached to the functionalized chip surface by their C-terminus and through a GSGSG spacer. The layout of the microarrays contained the respective peptide spots duplicated at random positions.

Supplementary Table 1 shows the sequences of the peptides used. The peptide arrays were blocked for 60 min using PBS, pH 7.4, and 0.05% Tween 20 with 1% BSA with constant shaking; washed 3 × 1 min with PBS, pH 7.4, and 0.05% Tween 20 followed by incubation with sera in dilutions equivalent to 0.01 mg/mL IgM (established by determining the immunoglobulin concentrations by ELISA) on an orbital shaker overnight at 4°C. After washing 3 × 1 min, the arrays were incubated with secondary antibodies at room temperature, washed, rinsed with distilled water, and dried by spinning vertically in empty 50 mL test tubes at 100×g for 2 min. Two different secondary antibodies were used to measure simultaneously the binding of IgG and IgM at wavelengths of detection, respectively, 544 nm and 647 nm.

2.4. Microarray data analysis

2.4.1. Acquisition, cleaning and normalization

The Innoscan 1100 (Innopsys, Carbonne, France) microarray scanner was used to acquire the stained microarray fluorescence images. MAPIX software was used for the subsequent densitometry. The analysis of the densitometry data was performed using publicly available packages from the R statistical environment (*Bioconductor, Biostrings, limma, pepStat, igraph, clvalid, gplots, future.apply, FactoMIneR, factoextra, stringi, stringdist, rBLAST, rgl,* etc.) as well as in-house developed R functions. The data and the scripts of the analysis are deposited at https://github.com/ansts/ADFTDIgOme. The cross-reactivity graph strategy was previously described (Ferdinandov et al., 2023). Here it is used with some modifications. Briefly, the raw data was cleaned based on the flags set during densitometry. The background was defined based on the gradients of staining between the randomly positioned duplicate peptide spots and subtracted (Pashov et al., 2019).

The logarithms of the data were normalized relative to the amino acid residue composition using the pepstat Bioconductor package as described previously (Pashov et al., 2019). This compensates for binding, which is dependent on the overall charge and hydrophobicity rather than on the sequence. Further, the data was normalized between arrays using the *limma*::normalizeCyclicLoess function with the “affy” method applied in 3 iterations separately for the IgM and IgG datasets. At the end of this stage, the datasets were based on 722 mimotopes.

2.4.2. Graph representation

Each of the isotype sets was used to generate a separate cross-reactivity graph. The criterion for cross-reactivity between two peptides used to define the edges of the graphs was a similarity measure. It was based on the reciprocal of the Manhattan distance between the respective profiles of reactivities with the 20 samples. Each pair of profiles was first scaled and centered using the median and the interquartile range. If M is the n×k matrix of the n reactivity values with k samples and $i1$ and $i2$ are two rows corresponding to two peptides (profiles), the quartiles of each row M_i being

$$Q^i_{0.25}, Q^i_{0.5}, Q^i_{0.75} = quantile(M_i, \{0.25, 0.5, 0.75\})$$

the similarity measure is calculated as:

$$s(M) = \frac{1}{\sum_{j:Q_{0.2}<D_j<Q_{0.8}} D_j}, D_j = \left| \frac{2\left(M_{i1,j} - Q^{(1)}_{0.5}\right)}{Q^{(1)}_{0.75} - Q^{(1)}_{0.25}} - \frac{2\left(M_{i2,j} - Q^{(2)}_{0.5}\right)}{Q^{(2)}_{0.75} - Q^{(2)}_{0.25}} \right| .$$

Only the D values between the quantiles 0.2 and 0.8 were used. The filtering out of the extreme values of D is done to prevent the decision about cross-reactivity from being taken on the basis of just a couple of similar values. The concept of defining cross-reactivity by testing multiple individual repertoires depends on the multiplicity of samples with correlated reactivities. The criterion was tested using the data form (Ferdinandov et al., 2023). The ROC curve and the selected threshold for connecting the vertices of the graphs were analyzed as previously described (Ferdinandov et al., 2023). The threshold selected ensured specificity of 0.9 and sensitivity of 0.6, thus emphasizing only the most probable cross-reactivities (Fig. 1).

An edge in a reactivity graph G can be interpreted as a cross-reactivity relation between two peptides. Since the cross-reactivity is inferred from similarity of the reactivity profiles across samples, the same peptide can be cross-reactive with other peptides based on different parts of the profile. The respective edges will represent potentially different antibody reactivities. Therefore, the topology of the reactivity graph does not represent the map of cross reactivities with the necessary detail unless the qualitative differences between the edges are figured in. To improve the clustering so that it can be used to formalize the concept of latent antibody reactivities, a second graph – GE, was constructed with vertices representing the edges in G. GE was not a line graph of G. The vertices in GE (originally edges in G) are connected not when they have a common incident vertex (like in a line graph) but when they stand for correlating profiles D_j. Given the reactivity graph G, and the raw data matrix M, from which G is constructed,

$$E_i = \{\, ends(G, e) \mid e \in E(G) \,\}$$

are the endpoints of each edge where $ends(G, e)$ represents the pair of vertices at the ends of the edge e in graph G. The distance matrix

$$A = \begin{pmatrix} d_{11} & \cdots & d_{1m} \\ \vdots & \ddots & \vdots \\ d_{m1} & \cdots & d_{mn} \end{pmatrix}$$

where the distances $d_{\{jk\}} = \left|\mu(M[l_j, :]) - \mu(M[l_k, :])\right|$ and μ is the vector of column-wise means of each row pair, l_j and l_k being the two pairs of indices of the respective pairs of profiles *j* and *k*. After setting

the diagonal of A to zero, this became effectively the adjacency matrix of the GE graph. The weights of the edges in this graph (as distances) are given by the elements of A. Next, a cluster size optimization was performed by varying the threshold w_i for edge deletion. The threshold c_t was determined by maximizing the product of the cluster sizes s_k of the clusters larger than 5 vertices:

$$c_t = arg \max_{w_i} \left(log_{10} \left(\prod_k t_k \mid t_k > 5 \right) \right)$$

The edges with distances greater than the optimal threshold c_t were deleted. The ultimate form of the graph GE, thus obtained, was clustered to obtain clusters of what are respectively edges in the context of the original graph G. They were labeled edge clusters. Every edge cluster was defined in terms of the vertices - its end points in the original graph G. The final grouping of reactivities was obtained as intersections of the G clusters with the vertex clustering derived from the GE edge clusters. The groups of reactivity obtained are not a partition (like the clusters) but a cover (they overlap) because different edges can have overlapping vertices as endpoints.

To test the significance of various graph parameters (like size of large component, number of clusters, assortativity of vertex parameters, degree and maximal clique distributions, etc.) the baseline values for these parameters were estimated using 2 sets of 100 random graphs generated using the same algorithm but starting with the scrambled raw data matrices for IgM and IgG reactivities respectively. All graph analysis was performed using the igraph package.

Let $\mathbf{1}_{dia_l}$ be the indicator function of the diagnosis group $\mathrm{dia}_l \in \{\text{"A"},\text{"C"},\text{"F"},\text{"ND"}\}$ and let $r_i = [r_{i1}, r_{i1}, \dots, r_{ik}]$ represent the *i-th* row (mimotope) of the reactivity data matrix M. The rows are ranked: $\mathbf{rank}(r_i) = \mathbf{r}_i^{\mathrm{rank}} = [r_{i1}^{\mathrm{rank}}, r_{i2}^{\mathrm{rank}}, \dots, r_{ik}^{\mathrm{rank}}]$, r_{ij}^{rank} denotes the *j-th* element of the *i-th* row. Then, the sum of ranks for the group dia_l for the *i-th* row is:

$$S_{i,dia_l} = \sum_{j=1}^{m} r_{ij}^{rank} \cdot \mathbf{1}_{dia_l}(l),$$

Where $\mathbf{1}_{dia_l}(l)$ is 1 if $dia_j = \mathbf{dia}_k$ and 0 otherwise. The S_{i,dia_l} was used to quantify the degree of association of each reactivity with each diagnosis.

For the visualization, the graphs were embedded using the eigenvectors of the graph Laplacian of each isotype graph (spectral embedding). The eigenvectors that corresponded to the k smallest eigenvalues were used. The cutoff to determine k was based on the irregular increase in the ordered eigenvalues (Suppl. Fig. 2). The exact position of the vertices in the two-dimensional projections is derived by UMAP embedding from k dimensions to two dimensions. UMAP was considered appropriate for the final 2D embedding because applying it to a relatively low-dimensional dataset reduces the distortion of distances. The 3D visualization was done with the help of the rgl package. The graph clustering was done using the Leiden algorithm with modularity optimization and resolution parameter 1.

2.5. Machine learning model

To mitigate the inter-sample correlation, a specific cross-validation scheme was applied to classify the three diagnoses using a support vector machine-based (SVM) model. The feature selection step included

a filtering step removing features with a Mahalanobis distance less than the 0.35 quantile of its distribution in the space of the samples. This was followed by a recursive feature elimination on the reduced feature set (typically about 400 features) using a compound clustering criterion based on Dunn's, the connectivity, and the Baker-Hubert Gamma criteria as previously described (Pashov et al., 2019). For the cross-validation, to disconnect the correlated pools, sets of samples were left out (1-3 per step), so that they contained no serum sample used in the rest of the pools. Because of the small number of samples, the labeling was only dichotomous and applied separately for AD/FTD vs C/ND, AD/C vs FTD/ND, and FTD/C vs AD/ND. The aim was to assess roughly the observed patterns' separability and generalizability. The optimized SVM parameters were: gamma = 0.001, and the constant was set at 35. Before training the model, the data was projected on the first six principal components following the n/3 rule for optimal dimensionality reductionrelative to size of the sample, prompted by the peaking phenomenon (Sima and Dougherty, 2008).

2.6. External data sources

The human immunoglobulin heavy chain junction regions found in the NCBI protein database (1 012 520 different entries) was used. The junction regions include the D gene product and correspond to the most diverse portion of the HCDR3 (heavy chain complementarity-determining region 3). From them, 4 433 252 unique overlapping 7-residues sequence frames were derived to compare the mimotopes and find potential linear idiotopes among the latter. The comparison to a given mimotope sequence was done by finding the number of HCDR3 region 7-mer sequences within a longest common subsequence (LCS) distance of 2, i.e. – with no more than 1 mismatch. A set of 217 442 7-mer sequences from a previously published analysis (Matochko et al., 2014; Matochko and Derda, 2013) amplified from the same PDL (Ph.D -7, New England Biolabs) without prior selection was used as a background non-selected library to bootstrap the frequency of idiotopes among mimotopes. To perform protein BLAST (using the rBLAST package), the human RefSeq protein database from NCBI was used (136 194 sequences). The filter was set to 1 mismatch. The criterion of editing distance of 2 (one deletion, one insertion) was previously established (Pashova et al., 2022) based on data from the Biopanning data bank (http://i.uestc.edu.cn/bdb/) (He et al., 2016), summarizing results from phage display screening with monoclonal antibodies.

2.7. Statistics

In this study, the groups were compared using non-parametric tests – the Wilcoxon rank sum test and Dunn's test for multiple comparisons with Benjamini-Hochberg (BH) adjustment of the p values where necessary. Principal component analysis (PCA) was used for data exploration and dimensionality reduction using the *FactoMineR* and *factoextra* packages. Each reactivity was compared to the blood group antigen score. The blood group antigen score equaled the number of pooled sera coming from patients expressing that antigen. Thus, it took only 3 values: 0, 1, and 2.

3. Results

An array of 722 representative mimotopes of public IgM reactivities in healthy donors (Pashov et al., 2019) were used to probe the repertoires of serum IgM and IgG from patients with neurodegenerative diseases. To this end, samples from AD (n=8), FTD (n=8), ND (n=8), and controls without clinical dementia (n=6) were pooled in pairs to yield four groups of five serum samples. These were tested on the IgM mimotopes in oriented planar peptide microarrays (Suppl. Table 1).

3.1. The reactivity data distinguishes diagnoses

After cleaning and normalization, the data from serum IgM and IgG binding to the array of public IgM mimotopes showed considerable correlation between all samples (Suppl. Fig. 1). Amino acid residue composition bias is most probably not the cause because the data was normalized with respect to that. Some part of this correlation may be due to testing public reactivities that reflect constant characteristics of the repertoire. Another contribution may be from the between-array normalization. In the overview of the data analyzed by PCA, the latent variable underlying this correlation was isolated in the first component. Excluding this factor, the other components separated the samples by diagnosis (Fig.2).

3.2. Graph representation of mimotope reactivities for a detailed analysis

The PCA, indicated that the public IgM reactivity repertoire contains information relevant to the neurodegenerative disease under study. To extract further detail, the cross-reactivity data for both isotypes were represented as graphs along the lines of the methodology published recently (Ferdinandov et al., 2023; Pashova-Dimova et al., 2023). The method for inferring cross-reactivities between peptides was improved by measuring the similarities between the profiles observed in the set of sera (see Materials and methods for a detailed description). The threshold of profile similarity for connecting two mimotope reactivities with an edge was adjusted to yield a large connected component of the graph with at least 700/722 reactivities. The connected components of the graphs were visualized in 2D using a two-step spectral embedding (Suppl. Fig. 2). A 3D final projection is also provided, which is of even higher fidelity to the four or 5D spectral embedding (Supplementary files IgM_AD_FTD_NDD_C.mp4 and IgG_AD_FTD_NDD_C.mp4). The visualizations illustrate a very clear distinction between the public reactivities lost (high in the controls) and those gained in the patients with dementia. Furthermore, there is also a clear distinction between the diagnoses, especially in the IgG graph.

3.3. Reactivity graph structure and parameters

To estimate the significance of some descriptive parameters of the graphs, the baseline values were simulated by using graphs generated by the same algorithm but based on the scrambled raw data matrices for each isotype. The graph density (the number of edges relative to the maximal number of possible edges) and the size of the large connected component were higher for both the IgM and the IgG graphs then for the random graphs (Fig. 3). Similarly, the degree distributions were shifted slightly to the right (Suppl. Fig. 3) and the maximal clique size distributions showed more cliques but with similar distribution as compared to the random graphs (Suppl. Fig. 3).

Next, the information about classes of public reactivities encoded in the topology of the graphs and their relation to neurodegenerative diseases was studied. Clusters of vertices were determined in the graphs

based on modularity (regions with denser edges within than to other parts of the graph) using the Leiden algorithm (https://github.com/TomKellyGenetics/leiden). The IgM graph had 47 clusters, with 13 consisting of single vertices and the largest containing 60 vertices. For the IgG graph, these values were 60, 22, and 33, respectively. The IgG graph clusters appeared more numerous and smaller in size, but these differences were not significant. Compared to the random graphs, both the IgM and the IgG graphs had a significantly lower number of clusters (Fig. 3), indicating that the repertoire of public reactivities at this coarse resolution exhibits large-scale modularity with relatively few clusters. Interestingly, compared to the random graphs, the modularity of the clustering was very different between IgM (high) and IgG (low), although the values for both graphs were rather similar. This can be interpreted as the public IgM repertoire clustering into a relatively small number of tight clusters, while the IgG reactivities to the IgM mimotopes form slightly more clusters that are significantly less well-defined.

The vertices of the graphs were assigned attributes corresponding to the rank sums of each mimotope's reactivities in different diagnoses. Thus, for instance, mimotopes with high reactivities in the control and low in the disease groups will have a high rank sum associated with the control group. The attributes also reflected blood group antigen cross-reactivity, as well as cross-labeling – assigning the IgM graph vertices the IgG attributes by diagnosis and vice versa. The latter approach was applied to check if the graph of each isotype reflects the diagnosis-associated relations of the other.

The degree of correlation of the graph structure with a quantitative attribute is measured by assortativity – the extent to which neighboring vertices have similar magnitudes of the attribute. Figure 4 compares the assortativities of several characteristics for both graphs compared to the respective sets of random graphs. Here, assortativity was intended to indicate the degree to which reactivities, correlating with the respective property, cluster. The highest assortativity was found for the control group-related reactivities (i.e., those lost in disease). The assortativity of the correlation with blood group antigens was comparable but somewhat lower, and the cross-labeling attribute assortativities were markedly lower, reaching insignificant levels in FTD (for IgM) and NDD (for IgG). The correlation between the reactivity profiles across isotypes (GMCR) did not show significant assortativity. Thus, the clusters of disease-specific cross-reactivities among these public IgM mimotopes did not match.

3.4. Idiotypy and neurodegenerative disease

In our previous studies, we stumbled upon a significantly high proportion of homologies to HCDR3 region sequences from human antibodies in the public IgM reactivity mimotopes (Pashov et al., 2019; Pashova et al., 2022). Such HCDR3 homologues of mimotopes could be considered, at least potentially, as idiotopes. Since the IgM mimotope array used in this study was shown previously to be significantly enriched in idiotipic mimotopes, we decided to check if this idiotope reactivity correlated with reactivity associated with neurodegenerative diseases. The nearest neighbors for each mimotope among a library of 4×10^6 7-residue frames from 10^6 human antibodies were determined using a criterion of at most one mismatch. Under this condition, 483/722 mimotopes had at least one nearest neighbor among the J region frames, and some had up to 187. Probably, the latter coincide with germline genes. Next, the number of nearest neighbors among idiotopes (NNNI) that best splits the data into groups correlated with diagnosis was determined. To that end, the mimotope set was repeatedly divided into two groups relative to each value of the sorted NNNI. The correlation between mean reactivity rank by disease and the grouping of NNNI low and high mimotopes was calculated using the Wilcoxon rank sum test at each step. Figure 5 shows that for IgM, the finding of 2 idiotopes among the nearest neighbors was the optimal criterion to detect

maximal correlation. The correlation was positive for the reactivities lost in the disease groups (high in the control group) and negative for the reactivities high in AD. The group of ND also had a positive correlation, although much lower than the group C, and the FTD group had a negative correlation similar to AD, but much lower. For IgG, these correlations were mainly insignificant. Unexpectedly and contrary to the IgM, the IgG reactivities lost in neurodegeneration (C) had a small but significant negative correlation. In contrast, the ND group had a slight positive correlation, like in AD. Thus, the public IgM reactivities lost in the neurodegenerative diseases tend to be more idiotypically connected, in contrast to, in particular, those gained in AD but also to some extent those found in FTD.

3.5. Public reactivity clusters associated with neurodegenerative diseases

The mean reactivities by diagnosis in each vertex cluster, defined in 3.3, were compared using the Dunn test (BH - Benjamini & Hochberg adjusted $p<0.01$). The clusters found to have significant differences between at least two diagnoses were 17/47 for the IgM graph and 17/60 for the IgG one. To summarize these results, each significant cluster was represented by the six differences between mean reactivities for the four diagnoses. The data was subjected to PCA and plotted as a biplot (Fig.6), which shows simultaneously the correlations between the axes as well as the mapping of the clusters onto the same space. The IgM graph clusters show differences mostly along the axis defined by differences between the controls vs AD and FTD, with a weak correlation between the control reactivities and the ND patients. The IgG clusters complemented these distinctions by differences between AD and FTD. The symmetric distribution of the clusters around the origin shows that there are approximately equal numbers of clusters representing positive or negative differences.

The repertoire probing with just 722 mimotopes provides too coarse a picture. The reactivity graphs clustering summarized the cross-reactivities based on profile similarities. The respective underlying reactivities are encoded in the pattern of similarities between the samples that generate an edge. So, although the reactivities in each cluster were generally related, augmenting the grouping by a further clustering of the edges would provide a higher resolution. Indeed, when each cluster was subdivided into (overlapping) subclusters connected by highly correlated edges, a new, more detailed clustering was obtained. It consisted of 211 clusters (sizes 3-47) for the IgM graph and 236 clusters (sizes 3-26) for the IgG graph. Applying similar strategy for statistical analysis as for the vertex clusters with a significance level of $p<1e-3$ after BH adjustment, 44 highly significant secondary clusters were found for the IgM graph and 21 – for IgG (Fig. 7). At an even higher level of significance ($p<1e-5$) 18 IgM clusters and 11 IgG clusters remained. Many of these clusters had the same type of difference between the diagnoses, so they could be grouped into seven groups for the IgM and four for the IgG (Suppl. Table 2). As concluded above, IgM reactivities did not differentiate between AD and FTD, but IgG clusters did. Since the final clusters of mimotopes were overlapping, their relations were examined using a Venn diagram (Suppl. Figure 5). The clusters with higher reactivity in the controls were only from the IgM set, while those with disease-associated reactivities tended to overlap between IgM and IgG. The IgG reactivities, which were high in disease, grouped in more diverse clusters. Interestingly, 2 clusters were high in the controls and low in FTD in IgG and vice versa for IgM.

3.6. Mapping the NNNI to clusters

Since the disease associated reactivities were clearly correlated to idiotypy, at least in the IgM data set, the mean NNNI of each of the final clusters were compared (Fig.8). As expected, for IgM the clusters of

reactivities higher in AD and FTD had lower NNNI then those lost in the dementia patients (C) or the overall mean for the remaining (not significant) clusters (labeled ALL). Among the reactivities lost in dementia as compared to the controls (high in C), only those higher in ND than in C had significantly more idiotope neighbors than the bulk (ALL). In IgG, surprisingly, only the clusters with reactivity higher in FTD than in the controls had significantly higher NNNI.

3.7. Mapping the altered reactivity mimotopes to potential self-antigen linear epitopes

The reactivity of public antibodies, especially IgM, could often be identified as directed to carbohydrate epitopes on bacteria. Still, many of these reactivities probably come from natural antibodies which have no nominal antigen in the sense of adaptively evolved specificity and are inherently poly/autospecific. Also, it is almost impossible to deconvolute conformational protein epitopes corresponding to mimotopes selected by a bulk repertoire. With these considerations, the only accessible specificity interpretation of the studied mimotopes was to check them against potential linear epitopes in the human proteome. BLAST search for sequences which had at most one mismatch with any of the studied mimotopes yielded 184/722 sequences with hits in 2182 proteins and 46/197 sequences with hits in 67 proteins for the mimotopes selected in the ultimate disease-associated clusters (Suppl. Table 3). Among the 67 putative targets, 31 were involved in brain metabolism and signaling. The proteins LRPs (LRP1B, LRP4, LRP6, and proLRP), sortilin, TIA-1, and BMAL1 are directly contributing to the pathogenesis of neurodegenerative disorders. The LRPs are endocytic receptors for the internalization of ApoE-containing lipoproteins, and sortilin is an endocytic receptor for the uptake of diverse proteins, including ApoE (Asaro et al., 2021; Carlo et al., 2013), amyloid beta (Saadipour et al., 2013), and α-synuclein (Ishiyama et al., 2023). These receptors had homologies with mimotopes that were part of a reactivity group overexpressed in IgG from FTD and ND patients. TIA-1 - a cytoplasmic scaffold protein of stress granules, was homologous to mimotopes of reactivities overexpressed in IgM from FTD and ND patients. BMAL1 – a transcription factor which is an important regulator of circadian rhythm, has a mimotope in a group of reactivities overexpressed in IgM from AD and FTD. Some other potentially targeted proteins with involvement in neurodegeneration are SMG7 (mRNA quality control), Tenascin C (neuroinflammation and association with core amyloid-beta plaques), FGF17 (cognitive processes), IRS2 (Insulin receptor signaling), Lon protease (protein quality control), UBXN1 (protein quality control), ZFYVE26 (autophagy), PlexinD1 (neuronal guidance) (Suppl. Table 4).

3.8. Generalizability

To assess the separability and generalizability of the observed patterns, a cross-validation scheme, leaving out sets of pools with no common serum with the rest of the samples, was applied to an SVM model. The Materials and Methods section gives details on the feature selection and cross-validation. The models were trained separately on the IgM and the IgG data and a joined data set of IgM and IgG reactivities. The only dichotomy that yielded significantly high accuracy (0.85) in the cross-validation scheme was AD/FTD vs C/ND in the IgM data set.

4. Discussion

The presented study aimed at exploring the capacity of the public IgM antibody repertoire to detect and react to different types of dementia. To this end, the public IgM repertoire and the IgG counterparts that are cross-reactive with it were analyzed using high-throughput binding assays and cross-reactivity graphs. The immune system's role in neurodegenerative diseases has been supported by extensive evidence, both in terms of cellular immunity (Chen et al., 2018; Reagin and Funk, 2023; Yang et al., 2022), inflammatory mechanisms (Baulch et al., 2020; Foley et al., 2024; Shue et al., 2024), and antibody-based biomarkers (DeMarshall et al., 2022; DeMarshall et al., 2023; Kheirkhah et al., 2020; Restrepo et al., 2013). Particularly, concerning the antibody repertoire, several groups have demonstrated the utility of IgG adaptive immunity responses as a source of biomarkers, including for early detection (DeMarshall et al., 2016; Reddy et al., 2011; Restrepo et al., 2013). The primary paradigm underlying these studies was basically autoimmunity, possibly a “protective” one (Yoles et al., 2001). At the same time, others considered the role of constitutively expressed natural antibodies (Rothstein, 2016), although in most cases, the term naturally occurring is used for antibodies elicited by self-antigens (Britschgi et al., 2009; Rosenmann et al., 2006; Szabo et al., 2008).

Enticed by the successful mining of the antibody repertoires for AD biomarkers (DeMarshall et al., 2015; DeMarshall et al., 2016; Restrepo et al., 2013), we looked for public IgM reactivities with the same properties. A recently developed approach was applied (Ferdinandov et al., 2023; Pashov et al., 2019; Pashova et al., 2022). It consists of combining IgOme repertoire analysis (Ryvkin et al., 2012) with the immunosignature concept (Restrepo et al., 2013). The sera were studied in pools of two to emphasize the public reactivities and reduce the cost of the microarrays. The small number of samples had already precluded the applicability of applicable machine learning models.

Compared to controls, we could demonstrate distinct patterns of public IgM and their cross-reactive IgG counterparts in AD, FTD, and ND patients. The loss or gain of specific IgM reactivities in AD and FTD indicates alterations in the natural and possibly the induced IgM repertoire. The loss of constitutive natural antibody reactivities has been observed before (Ferdinandov et al., 2023; Pashova et al., 2022). It probably represents a temporary exhaustion due to binding to some overexpressed self-antigens in terms of a scavenging function for cellular debris, as well as quantitative tolerance thresholds (Hennings et al., 2011). The opposite, reactivities increased in disease, is most easily explained as an adaptive immune response.

The concept of public clones has two aspects. Antibodies can be shared between individuals as clonotypes or just as a convergent specificity. In the latter, broader context, the IgM repertoire is not only more diverse but also organized in larger public specificity classes compared to IgG or IgA (Arora and Arnaout, 2022; Galson et al., 2015; Wu et al., 2022). It is also safe to assume that natural antibodies and public IgM overlap without being synonymous. Sometimes, the IgM compartment is considered to consist predominantly of ill-defined polyreactivities or even antibodies that are simply sticky (Ausserwöger et al., 2022; Cunningham et al., 2021). Previously, graphs were used to analyze the repertoire complexity (Miho et al., 2019) and antibody cross-reactivity patterns (Ferdinandov et al., 2023; Madi et al., 2011). The cross-reactivity graph provided a framework for visualizing and analyzing the IgM network of specificities inferred only from high-throughput binding assays. Spectral embedding ensured a well-defined visualization that can provide insight into the graph topology.

Our study found the cross-reactivity graphs to be dense and clustered in a relatively small number of clusters. It is possible that this is the image of the classes of overlapping reactivities discussed by Arora

and Arnout (Arora and Arnaout, 2022). It is seen at a relatively coarse resolution due to the low diversity of the mimotope library relative to the antibody diversity. The clusters had a higher modularity in IgM, indicating that their structure is less distinct in the IgG graph, probably due to addressing IgM mimotopes with IgG. Thus, the IgG reactivities were either randomly cross-reactive, IgG antibodies, or isotype-switched and probably mutated counterparts of the observed IgM. The characteristic large-scale cross-reactivity patterns of AD and FTD were manifested as high assortativity—neighboring mimotopes had similar levels of reactivity in a given diagnosis. The highest assortativity was observed for the control group, emphasizing the loss of IgM reactivities common to the different neurodegenerative diseases. Since the edges were defined as binding pattern correlations across samples, high assortativity indicates the prevalence of cross-reactivities between mimotopes for which the measured property is similar. Cross-reactivity groups can also be interpreted as footprints of major antibody reactivities with the respective properties. Like all other cross-reactivity graph observables, assortativity depends on the set of probes used. By sampling symmetrically the sequence space of a library of public IgM mimotopes, the probe set is optimized simultaneously for diversity and cross-reactivity (Pashov et al., 2019). Our results also show that it extracts information from the IgG repertoire with similar efficiency but different patterns, pointing to the relations between the public IgM repertoire and the induced IgG repertoire.

The observations from the assortativity analysis were studied in detail by the distribution pattern of these properties among the graphs' clusters. In the IgM network, the key distinction was between the controls (correlating with ND) vs AD and FTD. The latter were not well separated in the clusters. The good distinction between AD and FTD was apparent only in the IgG data set. Interestingly, FTD-associated IgG not only differed from those in AD but, unlike IgM, they were correlated with ND. Unlike AD, FTD IgG patterns appeared to have higher idiotypic connectivity. These facts point to the occurrence of new IgG reactivities in FTD, which are mostly unrelated to the public IgM repertoire. The distinction of ND from AD and FTD, and its similarity at times to the controls, could be characteristic of just some of the diagnoses in this heterogeneous group.

The BLAST search of the human proteome produced hits of proteins, potential targets of the reactivities found associated with dementia. Many of those putative autoantigens are implicated in neurodegeneration. This is especially true for the endocytic receptors LRPs and sortilin, which, although very different in structure, share ApoE and ApoE/amyloid beta complexes as ligands for internalization and subsequent endolysosomal degradation (Cam et al., 2004; Chow et al., 2021; Kanekiyo and Bu, 2014; Zhang et al., 2020) (Asaro et al., 2020). The clearance of amyloid beta from the brain was shown to depend on the level of expression of LRPs (Castellano et al., 2012), and sortilin-deficient mice present elevated levels of APOE and increased amyloid beta accumulation (Carlo et al., 2013). Additionally, LRP4 and LRP6 are engaged in Wnt/beta-catenin signaling, an important pathway promoting cell proliferation during early development, which is tightly controlled during aging and suppressed in neurodegeneration (Inestrosa and Toledo, 2008). Antibodies to these LRPs may contribute to the pathology of neurodegeneration by causing a loss of control over the Wnt/beta-catenin pathway. A tau-related neurodegenerative factor - TIA-1 was also identified as a target. It is an RNA-binding protein and a scaffold for the formation of stress granules (SG) in response to cellular stress. Downregulation of TIA-1 restrains the inclusion of tau in pathological and persistent stress granules, while overexpression of TIA1 stimulates tau-related degeneration (Apicco et al., 2018; Maziuk et al., 2018). Another target, a factor etiologically related to neurodegeneration and associated with sleep disturbances in AD, is the circadian transcription factor BMAL1. It is the main driver of circadian rhythm and is involved in the rhythmic transcription of about 5 to 10 % of expressed genes

(Hughes et al., 2009). BMAL1 has been shown to be aberrantly methylated and irregularly expressed in the brains of AD patients (Cronin et al., 2017; Hulme et al., 2020).

A number of previously discussed biomarkers for FTD and AD, like Nfl, progranulin, TDP-43, or GFA (Duran-Aniotz et al., 2021) were not among the potential targets of the antibody reactivities observed, most likely due to the coarse repertoire probing. Notably, a recent study found 7 specific serum autoantibodies to MAPT, DNAJC8, KDM4D, SERF1A, CDKN1A, AGER, and ASXL1 and proposed a classification model that differentiated AD from other neurodegenerative diseases with high accuracy (Fang et al., 2024). Furthermore, using proteome-wide autoantibody screening, Matsuda et al. identified 229 antibodies differentially elevated in AD or dementia with Lewy bodies (Matsuda et al., 2025). Autoantibodies targeting neuropeptide B and adhesion G protein-coupled receptor F5 showed significant correlations with clinical traits.

Previously, we found that the public IgM mimotope library is enriched in homologues to HCDR3 sequences of human immunoglobulins. Looking into this correlation, the public IgM reactivities lost in AD and FTD proved significantly cross-reactive with idiotopes. On the contrary, the IgM reactivities increased in AD (and partially those increased in FTD) were much less idiotypically connected. The correlation between idiotypic connectivity and disease-specific reactivities points to a potential mechanism of an AD-associated immune dysregulation, probably shaped by the induced autoimmunity. Interestingly, DeMarshall, et al. defined a diagnostic autoantibody reactivity panel for AD, including auto-light chain kappa antibodies (DeMarshall et al., 2023). Another interesting aspect is revealed concerning the recent finding on the pivotal role of the peripheral immune system in the brain-gut-periphery axis, potentially shaping the trajectory of AD (Han et al., 2018; Iban-Arias et al., 2024). The intriguing link necessitating further studies is through the role of the microbiome in shaping the IgM repertoire (Li et al., 2020) and the possibility that the idiotypic connectivity is at least partially, if not mainly, determined during repertoire selection (Detours et al., 1996; Kazatchkine et al., 1994).

Only 9/65 different proteins had putative linear epitopes differentially bound by IgM in the controls (reactivities disappearing in disease), in contrast to the prevalence of idiotypic connections in IgM compared to IgG. The mimotope sequence YWTDSSR has different one-residue-mismatched homologues in LRP1 B, LRP4, and LRP6 (see supplemental table 3). It represents the beta-propeller domain signature, found in most LRP, and is characterized by high polyspecificity to multiple ligands (Príncipe et al., 2021). A NCBI protein blast shows that the exact mimotope sequence is highly conserved across many species of bacteria and fungi. Furthermore, YWTDSSR proved to have seven idiotope neighbors in our analysis. Finally, it was found in the IgG cluster of reactivities increased in FTD and ND. Thus, at least some patients in the heterogeneous ND group showed similarity to FTD concerning this autoreactivity. So far, anti-LRP autoantibodies have been associated only with myasthenia gravis (Chuquisana et al., 2024). This interesting example highlights the connection between autoantibodies associated with neurodegeneration, antibody polyspecificity and other promiscuous protein binding patterns, public IgM, and HCDR3 idiotopes. Taken together, all these aspects of autoimmunity in neurodegenerative diseases are possibly related by processes involved in repertoire selection.

Thus, the differences in antibody public IgM reactivity profiles highlight another repertoire compartment with considerable potential as a source of non-invasive biomarkers for early disease diagnosis. Despite the promising findings, this study has several limitations. The experimental setting with small groups and overlapping serum pools precluded important model validation, so only a rudimentary classifier was trained to prove separability, at least of AD/FT vs C/ND. Furthermore, the overlapping pooling requires caution in interpreting correlations. Thus, the conclusions should be considered preliminary. Nevertheless,

our results also clearly indicate the utility of the reactivity graph approach and the significance of the association of idiotypically connected IgM reactivities with the immune pathogenesis of neurodegenerative diseases.

Additionally, the study primarily focused on linear mimotopes. Conformational epitope information is encoded in the clusters of linear mimotopes, but is hard to deconvolute without knowing in advance at least the target antigen, if not the exact epitope. This task remains to be addressed in future studies.

In conclusion, this study provides proof for the utility of public, idiotypically connected IgM reactivity profiles as biomarkers for AD and FTD. Applying cross-reactivity graphs to high-throughput antibody binding data offers a powerful tool for uncovering complex patterns and networks associated with disease states.

Declaration of generative AI and AI-assisted technologies in the writing process

During the preparation of this work, the author(s) used Grammarly to improve the style of the manuscript. After using this tool/service, the author(s) reviewed and edited the content as needed and took full responsibility for the content of the publication.

5. Acknowledgements

This work is supported by grants # KP 06 N 33/5/2019 and # KP 06 N 37/24/2019 from the Bulgarian National Science Fund. The Bulgarian cohort was supported by the European Union-NextGeneration EU (National Recovery and Resilience Plan of the Republic of Bulgaria, grant number BG-RRP-2.004-0004-C01).

6. References

Andreatta, M., Lund, O., Nielsen, M., 2013. Simultaneous alignment and clustering of peptide data using a Gibbs sampling approach. Bioinformatics 29, 8-14.

Apicco, D.J., Ash, P.E.A., Maziuk, B., LeBlang, C., Medalla, M., Al Abdullatif, A., Ferragud, A., Botelho, E., Ballance, H.I., Dhawan, U., Boudeau, S., Cruz, A.L., Kashy, D., Wong, A., Goldberg, L.R., Yazdani, N., Zhang, C., Ung, C.Y., Tripodis, Y., Kanaan, N.M., Ikezu, T., Cottone, P., Leszyk, J., Li, H., Luebke, J., Bryant, C.D., Wolozin, B., 2018. Reducing the RNA binding protein TIA1 protects against tau-mediated neurodegeneration in vivo. Nature Neuroscience 21, 72-80.

Arora, R., Arnaout, R., 2022. Repertoire-scale measures of antigen binding. Proceedings of the National Academy of Sciences 119, e2203505119.
Asaro, A., Carlo-Spiewok, A.S., Malik, A.R., Rothe, M., Schipke, C.G., Peters, O., Heeren, J., Willnow, T.E., 2020. Apolipoprotein E4 disrupts the neuroprotective action of sortilin in neuronal lipid metabolism and endocannabinoid signaling. Alzheimer's & dementia : the journal of the Alzheimer's Association 16, 1248-1258.
Asaro, A., Sinha, R., Bakun, M., Kalnytska, O., Carlo-Spiewok, A.S., Rubel, T., Rozeboom, A., Dadlez, M., Kaminska, B., Aronica, E., Malik, A.R., Willnow, T.E., 2021. ApoE4 disrupts interaction of sortilin with fatty acid-binding protein 7 essential to promote lipid signaling. J Cell Sci 134.
Baulch, J.E., Acharya, M.M., Agrawal, S., Apodaca, L.A., Monteiro, C., Agrawal, A., 2020. Immune and Inflammatory Determinants Underlying Alzheimer’s Disease Pathology. Journal of Neuroimmune Pharmacology.
Britschgi, M., Olin, C.E., Johns, H.T., Takeda-Uchimura, Y., LeMieux, M.C., Rufibach, K., Rajadas, J., Zhang, H., Tomooka, B., Robinson, W.H., Clark, C.M., Fagan, A.M., Galasko, D.R., Holtzman, D.M., Jutel, M., Kaye, J.A., Lemere, C.A., Leszek, J., Li, G., Peskind, E.R., Quinn, J.F., Yesavage, J.A., Ghiso, J.A., Wyss-Coray, T., 2009. Neuroprotective natural antibodies to assemblies of amyloidogenic peptides decrease with normal aging and advancing Alzheimer's disease. Proc Natl Acad Sci U S A 106, 12145-12150.
Cam, J.A., Zerbinatti, C.V., Knisely, J.M., Hecimovic, S., Li, Y., Bu, G., 2004. The low density lipoprotein receptor-related protein 1B retains beta-amyloid precursor protein at the cell surface and reduces amyloid-beta peptide production. J Biol Chem 279, 29639-29646.
Carlo, A.S., Gustafsen, C., Mastrobuoni, G., Nielsen, M.S., Burgert, T., Hartl, D., Rohe, M., Nykjaer, A., Herz, J., Heeren, J., Kempa, S., Petersen, C.M., Willnow, T.E., 2013. The pro-neurotrophin receptor sortilin is a major neuronal apolipoprotein E receptor for catabolism of amyloid-β peptide in the brain. J Neurosci 33, 358-370.

Castellani, R.J., Plascencia-Villa, G., Perry, G., 2022. Pathogenesis of Alzheimer’s Disease. In: Kostrzewa, R.M. (Ed.), Handbook of Neurotoxicity. Springer International Publishing, Cham, pp. 1709-1728.
Chen, H., Cho, K.-S., Vu, T.H.K., Shen, C.-H., Kaur, M., Chen, G., Mathew, R., McHam, M.L., Fazelat, A., Lashkari, K., Au, N.P.B., Tse, J.K.Y., Li, Y., Yu, H., Yang, L., Stein-Streilein, J., Ma, C.H.E., Woolf, C.J., Whary, M.T., Jager, M.J., Fox, J.G., Chen, J., Chen, D.F., 2018. Commensal microflora-induced T cell responses mediate progressive neurodegeneration in glaucoma. Nature communications 9, 3209.
Chen, Y., Colonna, M., 2022. Spontaneous and induced adaptive immune responses in Alzheimer’s disease: new insights into old observations. Current Opinion in Immunology 77, 102233.
Chow, H.M., Sun, J.K., Hart, R.P., Cheng, K.K., Hung, C.H.L., Lau, T.M., Kwan, K.M., 2021. Low-Density Lipoprotein Receptor-Related Protein 6 Cell Surface Availability Regulates Fuel Metabolism in Astrocytes. Advanced science (Weinheim, Baden-Wurttemberg, Germany) 8, e2004993.
Chuquisana, O., Stascheit, F., Keller, C.W., Pučić-Baković, M., Patenaude, A.M., Lauc, G., Tzartos, S., Wiendl, H., Willcox, N., Meisel, A., Lünemann, J.D., 2024. Functional Signature of LRP4 Antibodies in Myasthenia Gravis. Neurol Neuroimmunol Neuroinflamm 11, e200220.
Cronin, P., McCarthy, M.J., Lim, A.S.P., Salmon, D.P., Galasko, D., Masliah, E., De Jager, P.L., Bennett, D.A., Desplats, P., 2017. Circadian alterations during early stages of Alzheimer's disease are associated with aberrant cycles of DNA methylation in BMAL1. Alzheimer's & dementia : the journal of the Alzheimer's Association 13, 689-700.
DeMarshall, C., Goldwaser, E.L., Sarkar, A., Godsey, G.A., Acharya, N.K., Thayasivam, U., Belinka, B.A., Nagele, R.G., 2017. Autoantibodies as diagnostic biomarkers for the detection and subtyping of multiple sclerosis. J Neuroimmunol 309, 51-57.
DeMarshall, C., Viviano, J., Emrani, S., Godsey, G., Sarkar, A., Belinka, B., Libon, D., Nagele, R., Parkinson's Study Group, A.s.D.N.I., 2022. Preclinical Detection and Monitoring of Alzheimer’s Disease Using a

Multi-Disease Diagnostic Platform Employing Autoantibodies as Blood-based Biomarkers. Alzheimer's & Dementia 18, e066955.
DeMarshall, C.A., Han, M., Nagele, E.P., Sarkar, A., Acharya, N.K., Godsey, G., Goldwaser, E.L., Kosciuk, M., Thayasivam, U., Belinka, B., Nagele, R.G., 2015. Potential utility of autoantibodies as blood-based biomarkers for early detection and diagnosis of Parkinson's disease. Immunol Lett 168, 80-88.
DeMarshall, C.A., Nagele, E.P., Sarkar, A., Acharya, N.K., Godsey, G., Goldwaser, E.L., Kosciuk, M., Thayasivam, U., Han, M., Belinka, B., Nagele, R.G., 2016. Detection of Alzheimer's disease at mild cognitive impairment and disease progression using autoantibodies as blood-based biomarkers. Alzheimers Dement (Amst) 3, 51-62.
DeMarshall, C.A., Viviano, J., Emrani, S., Thayasivam, U., Godsey, G.A., Sarkar, A., Belinka, B., Libon, D.J., Nagele, R.G., 2023. Early Detection of Alzheimer's Disease-Related Pathology Using a Multi-Disease Diagnostic Platform Employing Autoantibodies as Blood-Based Biomarkers. Journal of Alzheimer's disease : JAD 92, 1077-1091.
Detours, V., Sulzer, B., Perelson, A.S., 1996. Size and connectivity of the idiotypic network are independent of the discreteness of the affinity distribution. J Theor Biol 183, 409-416.
Duran-Aniotz, C., Orellana, P., Leon Rodriguez, T., Henriquez, F., Cabello, V., Aguirre-Pinto, M.F., Escobedo, T., Takada, L.T., Pina-Escudero, S.D., Lopez, O., Yokoyama, J.S., Ibanez, A., Parra, M.A., Slachevsky, A., 2021. Systematic Review: Genetic, Neuroimaging, and Fluids Biomarkers for Frontotemporal Dementia Across Latin America Countries. Front Neurol 12, 663407.
Fang, L., Jiao, B., Liu, X., Wang, Z., Yuan, P., Zhou, H., Xiao, X., Cao, L., Guo, J., Tang, B., Shen, L., 2024. Specific serum autoantibodies predict the development and progression of Alzheimer's disease with high accuracy. Brain Behav Immun 115, 543-554.
Ferdinandov, D., Kostov, V., Hadzhieva, M., Shivarov, V., Petrov, P., Bussarsky, A., Pashov, A.D., 2023. Reactivity Graph Yields Interpretable

IgM Repertoire Signatures as Potential Tumor Biomarkers. International Journal of Molecular Sciences 24, 2597.
Foley, K.E., Winder, Z., Sudduth, T.L., Martin, B.J., Nelson, P.T., Jicha, G.A., Harp, J.P., Weekman, E.M., Wilcock, D.M., 2024. Alzheimer's disease and inflammatory biomarkers positively correlate in plasma in the UK-ADRC cohort. Alzheimer's & Dementia 20, 1374-1386.
Galson, J.D., Truck, J., Fowler, A., Munz, M., Cerundolo, V., Pollard, A.J., Lunter, G., Kelly, D.F., 2015. In-Depth Assessment of Within-Individual and Inter-Individual Variation in the B Cell Receptor Repertoire. Front Immunol 6, 531.
Gifford, A., Praschan, N., Newhouse, A., Chemali, Z., 2023. Biomarkers in frontotemporal dementia: Current landscape and future directions. Biomarkers in Neuropsychiatry 8, 100065.
Gorno-Tempini, M.L., Hillis, A.E., Weintraub, S., Kertesz, A., Mendez, M., Cappa, S.F., Ogar, J.M., Rohrer, J.D., Black, S., Boeve, B.F., Manes, F., Dronkers, N.F., Vandenberghe, R., Rascovsky, K., Patterson, K., Miller, B.L., Knopman, D.S., Hodges, J.R., Mesulam, M.M., Grossman, M., 2011. Classification of primary progressive aphasia and its variants. Neurology 76, 1006-1014.
Han, K.H., Arlian, B.M., Macauley, M.S., Paulson, J.C., Lerner, R.A., 2018. Migration-based selections of antibodies that convert bone marrow into trafficking microglia-like cells that reduce brain amyloid β. Proceedings of the National Academy of Sciences 115, E372-E381.
He, B., Chai, G., Duan, Y., Yan, Z., Qiu, L., Zhang, H., Liu, Z., He, Q., Han, K., Ru, B., Guo, F.B., Ding, H., Lin, H., Wang, X., Rao, N., Zhou, P., Huang, J., 2016. BDB: biopanning data bank. Nucleic Acids Res 44, D1127-1132.
Hennings, L., Artaud, C., Jousheghany, F., Monzavi-Karbassi, B., Pashov, A., Kieber-Emmons, T., 2011. Carbohydrate Mimetic Peptides Augment Carbohydrate-Reactive Immune Responses in the Absence of Immune Pathology. Cancers 3, 4151-4169.
Hughes, M.E., DiTacchio, L., Hayes, K.R., Vollmers, C., Pulivarthy, S., Baggs, J.E., Panda, S., Hogenesch, J.B., 2009. Harmonics of circadian gene transcription in mammals. PLoS genetics 5, e1000442.

Hulme, B., Didikoglu, A., Bradburn, S., Robinson, A., Canal, M., Payton, A., Pendleton, N., Murgatroyd, C., 2020. Epigenetic Regulation of BMAL1 with Sleep Disturbances and Alzheimer's Disease. Journal of Alzheimer's Disease 77, 1783-1792.
Iban-Arias, R., Yang, E.-J., Griggs, E., Soares Dias Portela, A., Osman, A., Trageser, K.J., Shahed, M., Maria Pasinetti, G., 2024. Ad-derived bone marrow transplant induces proinflammatory immune peripheral mechanisms accompanied by decreased neuroplasticity and reduced gut microbiome diversity affecting AD-like phenotype in the absence of Aβ neuropathology. Brain, Behavior, and Immunity 118, 252-272.
Imkeller, K., Wardemann, H., 2018. Assessing human B cell repertoire diversity and convergence. Immunol Rev 284, 51-66.
Inestrosa, N.C., Toledo, E.M., 2008. The role of Wnt signaling in neuronal dysfunction in Alzheimer's Disease. Mol Neurodegeneration 3, 9.
Ishiyama, S., Hasegawa, T., Sugeno, N., Kobayashi, J., Yoshida, S., Miki, Y., Wakabayashi, K., Fukuda, M., Kawata, Y., Nakamura, T., Sato, K., Ezura, M., Kikuchi, A., Takeda, A., Aoki, M., 2023. Sortilin acts as an endocytic receptor for α-synuclein fibril. Faseb j 37, e23017.
Kanekiyo, T., Bu, G., 2014. The low-density lipoprotein receptor-related protein 1 and amyloid-β clearance in Alzheimer's disease. Front Aging Neurosci 6, 93.
Kazatchkine, M.D., Dietrich, G., Hurez, V., Ronda, N., Bellon, B., Rossi, F., Kaveri, S.V., 1994. V region-mediated selection of autoreactive repertoires by intravenous immunoglobulin (i.v.Ig). Immunol Rev 139, 79-107.
Kheirkhah, R., DeMarshall, C., Sieber, F., Oh, E., Nagele, R.G., 2020. The origin and nature of the complex autoantibody profile in cerebrospinal fluid. Brain Behav Immun Health 2, 100032.
Krix, S., Wilczynski, E., Falgàs, N., Sánchez-Valle, R., Yoles, E., Nevo, U., Baruch, K., Fröhlich, H., 2024. Towards early diagnosis of Alzheimer's disease: advances in immune-related blood biomarkers and computational approaches. Frontiers in Immunology 15.

Li, H., Limenitakis, J.P., Greiff, V., Yilmaz, B., Schären, O., Urbaniak, C., Zünd, M., Lawson, M.A.E., Young, I.D., Rupp, S., Heikenwälder, M., McCoy, K.D., Hapfelmeier, S., Ganal-Vonarburg, S.C., Macpherson, A.J., 2020. Mucosal or systemic microbiota exposures shape the B cell repertoire. Nature.
Madi, A., Kenett, D.Y., Bransburg-Zabary, S., Merbl, Y., Quintana, F.J., Tauber, A.I., Cohen, I.R., Ben-Jacob, E., 2011. Network Theory Analysis of Antibody-Antigen Reactivity Data: The Immune Trees at Birth and Adulthood. PLoS ONE 6, e17445.
Matochko, W.L., Cory Li, S., Tang, S.K., Derda, R., 2014. Prospective identification of parasitic sequences in phage display screens. Nucleic Acids Res 42, 1784-1798.
Matochko, W.L., Derda, R., 2013. Error analysis of deep sequencing of phage libraries: peptides censored in sequencing. Comput Math Methods Med 2013, 491612.
Matsuda, K.M., Umeda-Kameyama, Y., Iwadoh, K., Miyawaki, M., Yakabe, M., Ishii, M., Ogawa, S., Akishita, M., Sato, S., Yoshizaki, A., 2025. Artificial intelligence and omics-based autoantibody profiling in dementia. Frontiers in Immunology Volume 16- 2025.
Maziuk, B.F., Apicco, D.J., Cruz, A.L., Jiang, L., Ash, P.E.A., da Rocha, E.L., Zhang, C., Yu, W.H., Leszyk, J., Abisambra, J.F., Li, H., Wolozin, B., 2018. RNA binding proteins co-localize with small tau inclusions in tauopathy. Acta Neuropathologica Communications 6, 71.
McKhann, G.M., Knopman, D.S., Chertkow, H., Hyman, B.T., Jack, C.R., Jr., Kawas, C.H., Klunk, W.E., Koroshetz, W.J., Manly, J.J., Mayeux, R., Mohs, R.C., Morris, J.C., Rossor, M.N., Scheltens, P., Carrillo, M.C., Thies, B., Weintraub, S., Phelps, C.H., 2011. The diagnosis of dementia due to Alzheimer's disease: recommendations from the National Institute on Aging-Alzheimer's Association workgroups on diagnostic guidelines for Alzheimer's disease. Alzheimer's & dementia : the journal of the Alzheimer's Association 7, 263-269.

Miho, E., Roškar, R., Greiff, V., Reddy, S.T., 2019. Large-scale network analysis reveals the sequence space architecture of antibody repertoires. Nature communications 10, 1321.
Musa, G., Slachevsky, A., Muñoz-Neira, C., Méndez-Orellana, C., Villagra, R., González-Billault, C., Ibáñez, A., Hornberger, M., Lillo, P., 2020. Alzheimer's Disease or Behavioral Variant Frontotemporal Dementia? Review of Key Points Toward an Accurate Clinical and Neuropsychological Diagnosis. Journal of Alzheimer's disease : JAD 73, 833-848.
Nagele, E., Han, M., Demarshall, C., Belinka, B., Nagele, R., 2011. Diagnosis of Alzheimer's disease based on disease-specific autoantibody profiles in human sera. PLoS ONE 6, e23112.
Pashov, A., Shivarov, V., Hadzhieva, M., Kostov, V., Ferdinandov, D., Heintz, K.-M., Pashova, S., Todorova, M., Vassilev, T., Kieber-Emmons, T., Meza-Zepeda, L.A., Hovig, E., 2019. Diagnostic Profiling of the Human Public IgM Repertoire With Scalable Mimotope Libraries. Frontiers in Immunology 10, 1-14.
Pashova-Dimova, S., Petrov, P., Karachanak-Yankova, S., Pashov, A., 2023. Neurodegenerative diseases associated antibody repertoire signatures in mimotope arrays based on cyclic versus linear peptides. Pharmacia 70, 1439-1447.
Pashova, S., Balabanski, L., Elmadjian, G., Savov, A., Stoyanova, E., Shivarov, V., Petrov, P., Pashov, A., 2022. Restriction of the Global IgM Repertoire in Antiphospholipid Syndrome. Frontiers in Immunology 13.
Príncipe, C., Dionísio de Sousa, I.J., Prazeres, H., Soares, P., Lima, R.T., 2021. LRP1B: A Giant Lost in Cancer Translation. Pharmaceuticals (Basel) 14.
Rascovsky, K., Hodges, J.R., Knopman, D., Mendez, M.F., Kramer, J.H., Neuhaus, J., van Swieten, J.C., Seelaar, H., Dopper, E.G., Onyike, C.U., Hillis, A.E., Josephs, K.A., Boeve, B.F., Kertesz, A., Seeley, W.W., Rankin, K.P., Johnson, J.K., Gorno-Tempini, M.L., Rosen, H., Prioleau-Latham, C.E., Lee, A., Kipps, C.M., Lillo, P., Piguet, O., Rohrer, J.D., Rossor, M.N., Warren, J.D., Fox, N.C., Galasko, D., Salmon, D.P., Black, S.E., Mesulam, M., Weintraub, S., Dickerson, B.C., Diehl-Schmid, J., Pasquier, F.,

Deramecourt, V., Lebert, F., Pijnenburg, Y., Chow, T.W., Manes, F., Grafman, J., Cappa, S.F., Freedman, M., Grossman, M., Miller, B.L., 2011. Sensitivity of revised diagnostic criteria for the behavioural variant of frontotemporal dementia. Brain 134, 2456-2477.
Reagin, K.L., Funk, K.E., 2023. CD8+ T cells pump the brakes on Alzheimer's disease. Nature immunology.
Reddy, M.M., Wilson, R., Wilson, J., Connell, S., Gocke, A., Hynan, L., German, D., Kodadek, T., 2011. Identification of Candidate IgG Biomarkers for Alzheimer's Disease via Combinatorial Library Screening. Cell 144, 132-142.
Restrepo, L., Stafford, P., Johnston, S.A., 2013. Feasibility of an early Alzheimer's disease immunosignature diagnostic test. J Neuroimmunol 254, 154-160.
Restrepo, L., Stafford, P., Magee, D.M., Johnston, S.A., 2011. Application of immunosignatures to the assessment of Alzheimer's disease. Ann Neurol 70, 286-295.
Rosenmann, H., Meiner, Z., Geylis, V., Abramsky, O., Steinitz, M., 2006. Detection of circulating antibodies against tau protein in its unphosphorylated and in its neurofibrillary tangles-related phosphorylated state in Alzheimer's disease and healthy subjects. Neurosci Lett 410, 90-93.
Rothstein, T.L., 2016. Natural Antibodies as Rheostats for Susceptibility to Chronic Diseases in the Aged. Front Immunol 7, 127.
Ryvkin, A., Ashkenazy, H., Smelyanski, L., Kaplan, G., Penn, O., Weiss-Ottolenghi, Y., Privman, E., Ngam, P.B., Woodward, J.E., May, G.D., Bell, C., Pupko, T., Gershoni, J.M., 2012. Deep Panning: steps towards probing the IgOme. PLoS ONE 7, e41469.
Saadipour, K., Yang, M., Lim, Y., Georgiou, K., Sun, Y., Keating, D., Liu, J., Wang, Y.R., Gai, W.P., Zhong, J.H., Wang, Y.J., Zhou, X.F., 2013. Amyloid beta$_{1-42}$ (Aβ_{42}) up-regulates the expression of sortilin via the p75(NTR)/RhoA signaling pathway. J Neurochem 127, 152-162.
Shivarov, V., Petrov, P.K., Pashov, A.D., 2020. Potential SARS-CoV-2 Preimmune IgM Epitopes. Frontiers in Immunology 11.

Shue, F., White, L.J., Hendrix, R., Ulrich, J., Henson, R.L., Knight, W., Martens, Y.A., Wang, N., Roy, B., Starling, S.C., Ren, Y., Xiong, C., Asmann, Y.W., Syrjanen, J.A., Vassilaki, M., Mielke, M.M., Timsina, J., Sung, Y.J., Cruchaga, C., Holtzman, D.M., Bu, G., Petersen, R.C., Heckman, M.G., Kanekiyo, T., 2024. CSF biomarkers of immune activation and Alzheimer's disease for predicting cognitive impairment risk in the elderly. Science advances 10, eadk3674.
Sima, C., Dougherty, E.R., 2008. The peaking phenomenon in the presence of feature-selection. Pattern Recognition Letters 29, 1667-1674.
Szabo, P., Relkin, N., Weksler, M.E., 2008. Natural human antibodies to amyloid beta peptide. Autoimmunity Reviews 7, 415-420.
Wu, H., Zhou, Z., Xie, S., Yan, R., Gong, M., Tian, X., Wang, Z., 2022. Similarity measurements of B cell receptor repertoire in baseline mice showed spectrum convergence of IgM. BMC Immunology 23, 11.
Yang, H.S., Zhang, C., Carlyle, B.C., Zhen, S.Y., Trombetta, B.A., Schultz, A.P., Pruzin, J.J., Fitzpatrick, C.D., Yau, W.W., Kirn, D.R., Rentz, D.M., Arnold, S.E., Johnson, K.A., Sperling, R.A., Chhatwal, J.P., Tanzi, R.E., 2022. Plasma IL-12/IFN-gamma axis predicts cognitive trajectories in cognitively unimpaired older adults. Alzheimer's & dementia : the journal of the Alzheimer's Association 18, 645-653.
Yoles, E., Hauben, E., Palgi, O., Agranov, E., Gothilf, A., Cohen, A., Kuchroo, V., Cohen, I.R., Weiner, H., Schwartz, M., 2001. Protective autoimmunity is a physiological response to CNS trauma. J Neurosci 21, 3740-3748.
Zhang, H., Chen, W., Tan, Z., Zhang, L., Dong, Z., Cui, W., Zhao, K., Wang, H., Jing, H., Cao, R., Kim, C., Safar, J.G., Xiong, W.C., Mei, L., 2020. A Role of Low-Density Lipoprotein Receptor-Related Protein 4 (LRP4) in Astrocytic Aβ Clearance. J Neurosci 40, 5347-5361.

7. Table

Table 1. Summary of the clinical data of the patients included.

Characteristics	AD (n=8)	FTD (n=8)	Other dementias (ND) (n=8)
Age at diagnosis (±SD)	60,33,2±5,98	59,14±6,08	61,14±7,54
Debut age (±SD)	58,77 6,65	55,28 6,72	58,14 8,59
Education (±SD)	13,66±2,03	11,42 ± 2,00	14,62 ±2,27
Gender (F/M)	(4/4)	(2/6)	(5/3)
MMSE(±SD)	20,22±3,19	22,85±4,29	23,71± 4,66
CSF β-amyloid	409,22±195,16	685±126,87	668,42± 170,76
CSF T-tau	686,33±309,89	245,83± 28,99	383,28 ±259,96
CSF P-tau	79,42±16,26	39±41,01	56±25,35

AD-Alzheimer's disease, FTD-frontotemporal dementia, CSF-cerebrospinal fluid;

Mean age of the control group 70.5 ± 3.73.

Other dementias include diagnosis of Lewy body disease, Parkinson's disease with dementia, and Huntington disease.

8. Figure Legends

Figure 1. Tuning the similarity measure used to construct the graph. A and B - Examples of profile pairs of cross-reactive (A) and not cross-reactive peptides (B), C - ROC curve illustrating the capacity of the similarity criterion to classify 4150 pairs of peptides overlapping in 11/15 positions as a model of cross-reactive peptide pairs compared to a set of 10,000 pairs of dissimilar peptides sharing a longest common subsequence of fewer than 3/15 position (data from (Ferdinandov et al., 2023)). The tradeoff between sensitivity and specificity chosen log10(s)=-1.1 (specificity = 0.905, sensitivity = 0.604, AUC=0.848)**.**

Figure 2. Principal component analysis (PCA) of the binding data of IgM (top) and IgG (bottom) from patients with AD (red), FTD (green), NDD (blue), and healthy controls (black) to an array of 722 7-mer mimotopes of human public IgM reactivities. The PCA analysis was used to characterize the reactivities by their patterns across patients, so the layout is transposed, and "individuals" refers to individual reactivities. The variables are the respective serum samples. Left – correlation of serum reactivities mapped to the first two components – the first component correlates highly with all sera and accounts for 60% of the

variation. The raw data have been normalized for the physicochemical properties of the amino acid residues in the peptides. Right – individual mimotope reactivities color coded for the four diagnostic groups studied, mapped to factors 2 and 4 (IgM) and 2 and 3 (IgG) .

Figure 3. Some parameters of the IgM and IgG reactivity graphs. Each parameter has been bootstrapped by generating 100 graphs constructed using the same algorithm but using scrambled matrices of the raw data. The antibody reactivity graphs are dense and clustered into fewer clusters than the random graphs. Still, the modularity of the clustering is very different for IgM (higher) and IgG (lower) than that of the random graphs. **Figure 4.** Assortativity of the properties associated with the vertices (mimotopes) for the IgM (left) and the IgG (right) reactivity graphs. The assortativity measures the degree to which vertices with similar values are connected; respectively, a highly assortative property segregates the mimotopes in the space of their reactivities. The values for the studied sera are compared to the values obtained for random graphs (100 graphs constructed using the same algorithm but using scrambled matrices of the raw data) and using the same labeling of the vertices. The highest assortativity is observed for the control samples (C), as well as for the AD (A) and FTD (F). Cross-labeling the vertices using the reactivity magnitude seen in IgM for the IgG graph and vice versa gives much lower assortativity.

Figure 5. Correlations between IgM and IgG reactivity averaged by diagnosis and number of nearest neighbors among idiotopes. Red – AD (A), green – FTD (F), blue – NDD (ND), and black – controls (C). Wilcoxon rank sum test was used to compare the reactivities in the peptides dichotomously grouped by splitting the mimotope set relative to the number of neighboring idiotopes of each peptide. The test was performed at each split point indicated on the abscissa. The resulting z-score is on the ordinate. The shaded area indicates a significance level $p \geq 0.05$, so the portions of the curves outside of the shaded area correspond to a significant difference. The insets show Spearman's correlation coefficient for the reactivity vs the number of idiotope neighbors. The IgM reactivities, higher in the controls (i.e., lost in the other patients), show the highest positive correlation with idiotypy, while those increased in AD show the highest negative correlation.

Figure 6. Biplot from the PCA results on the differences between the mean reactivities by diagnosis in the established clusters in the IgM and the IgG graphs. Only the clusters for which the differences are significant at the level $p<0.05$ after adjusting for false discovery rate using the Benjamini-Hochberg correction are used. IgM shows a simpler separation of the clusters, mainly between those with high reactivity in AD and FTD and those with low reactivity in the patients (high in the controls). The IgG clusters show higher diversity, some differentiating AD and FTD or NDD, but their differences were generally smaller than those in the IgM clusters.

Figure 7. Biplot from the PCA results on the differences between the mean reactivities by diagnosis in the established combined (vertex and edge) clusters in the IgM and the IgG graphs. The statistical parameters are the same as for Fig.7. Again, no IgM cluster differentiates AD and FTD, while IgG clusters do. The cluster numbers comprise the vertex cluster separated from the subdividing edge cluster by a point.

Figure 8. Distribution of the decimal logarithms of the number of idiotope neighbors by cluster groups. Since many significant clusters had the same reactivity pattern across diagnoses, they were reunited to form cluster groups with the same difference in reactivity between diagnoses. These cluster groups are analyzed to determine the distribution of the number of idiotope neighbors per peptide. For comparison, the set of tested mimotopes not included in the selected clusters was added as a separate group (All). The groups are sorted by the increasing mean number of idiotope neighbors. Dunn's test showed that, for the

IgM graph, the clusters to the left of the red asterisk have fewer idiotope neighbors than the rest. Also, the groups with higher expression in the controls as compared to AD and FTD (C>F.A) had more idiotope neighbors than the mean for those not included in the significant clusters (black asterisk). For IgG, only the reactivities in FTD had more idiotope neighbors than those not included in the significant clusters.

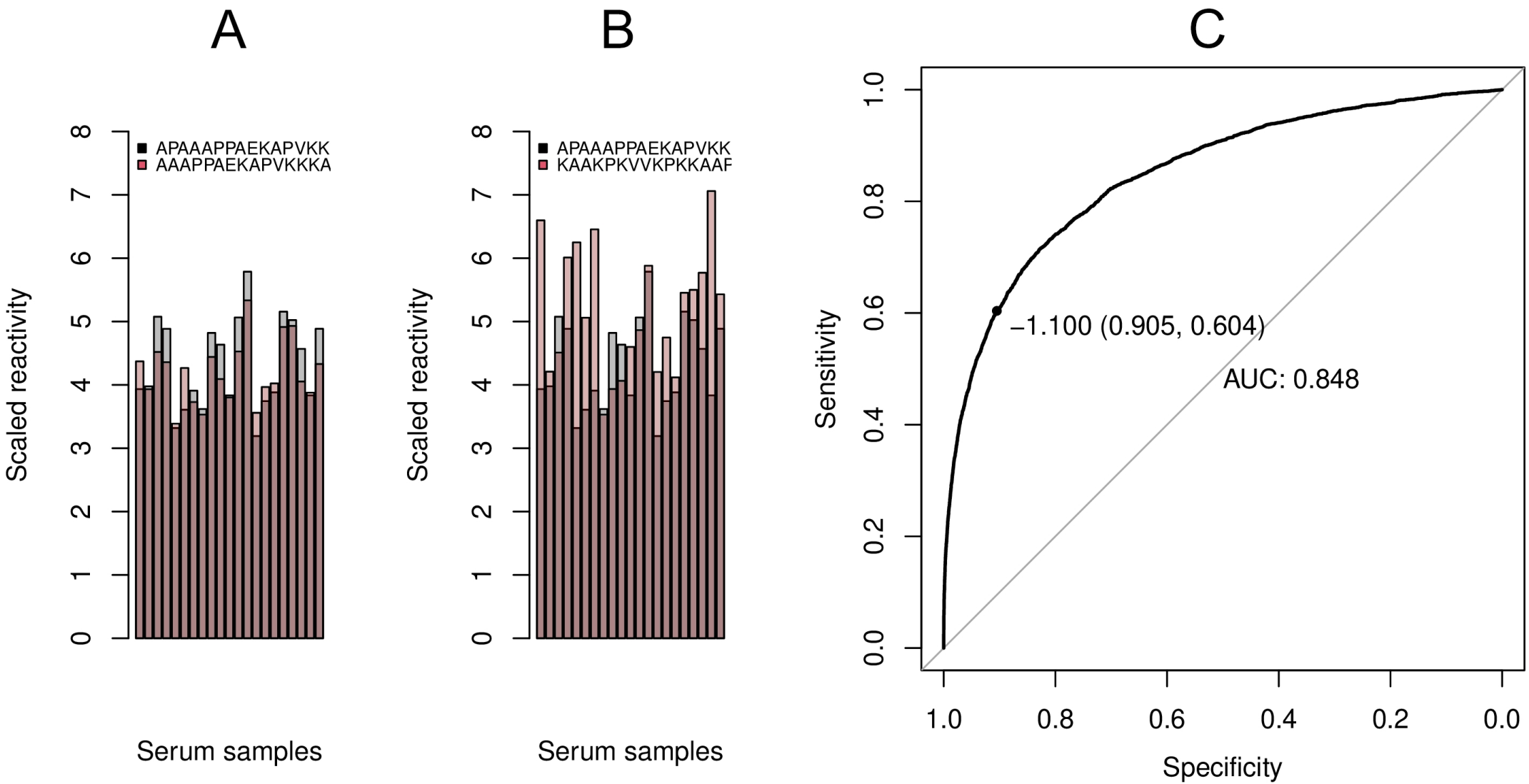
A
APAAAPPAEKAPVKK
AAAPPAEKAPVKKKA
Scaled reactivity
Serum samples
B
APAAAPPAEKAPVKK
KAAKPKVVKPKKAAF
Scaled reactivity
Serum samples
C
−1.100 (0.905, 0.604)
AUC: 0.848
Sensitivity
Specificity

IgM

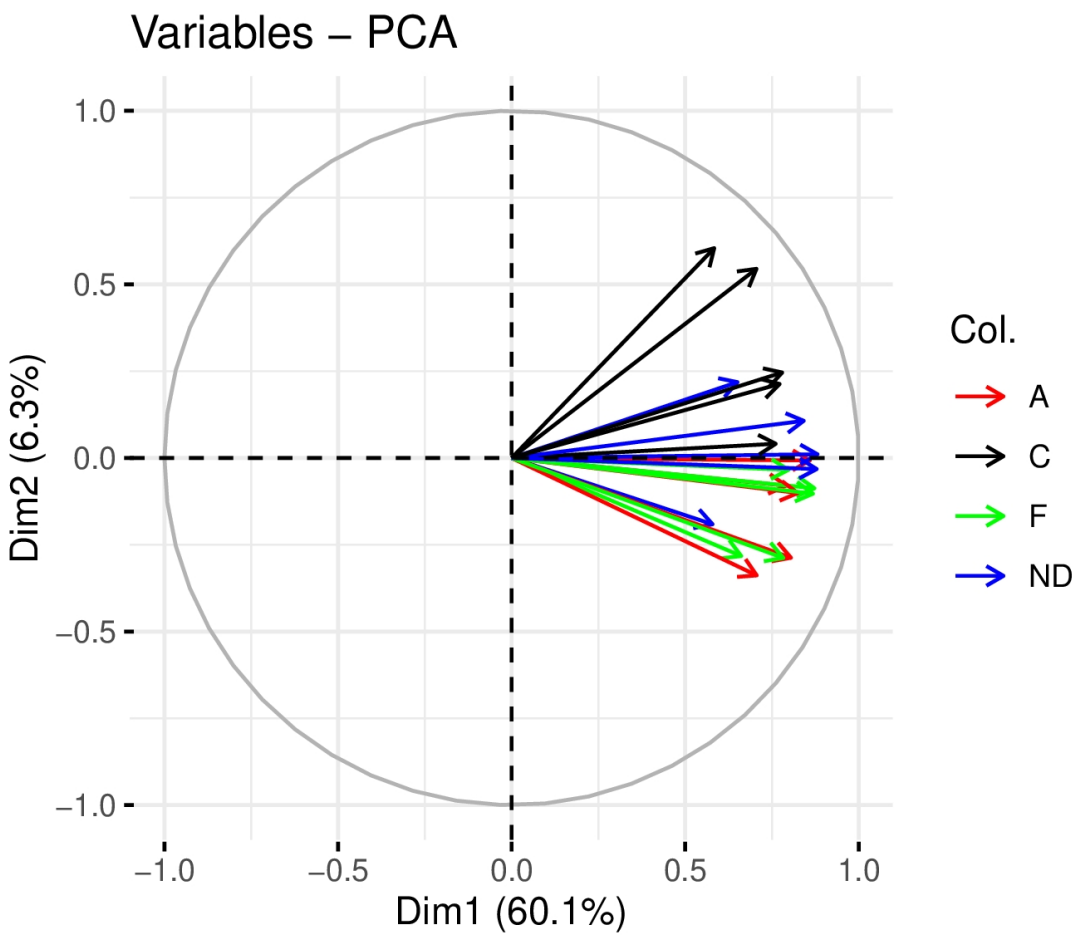
Variables – PCA
Dim1 (60.1%)
Dim2 (6.3%)
1.0
0.5
0.0
−0.5
−1.0
Col.
A
C
F
ND

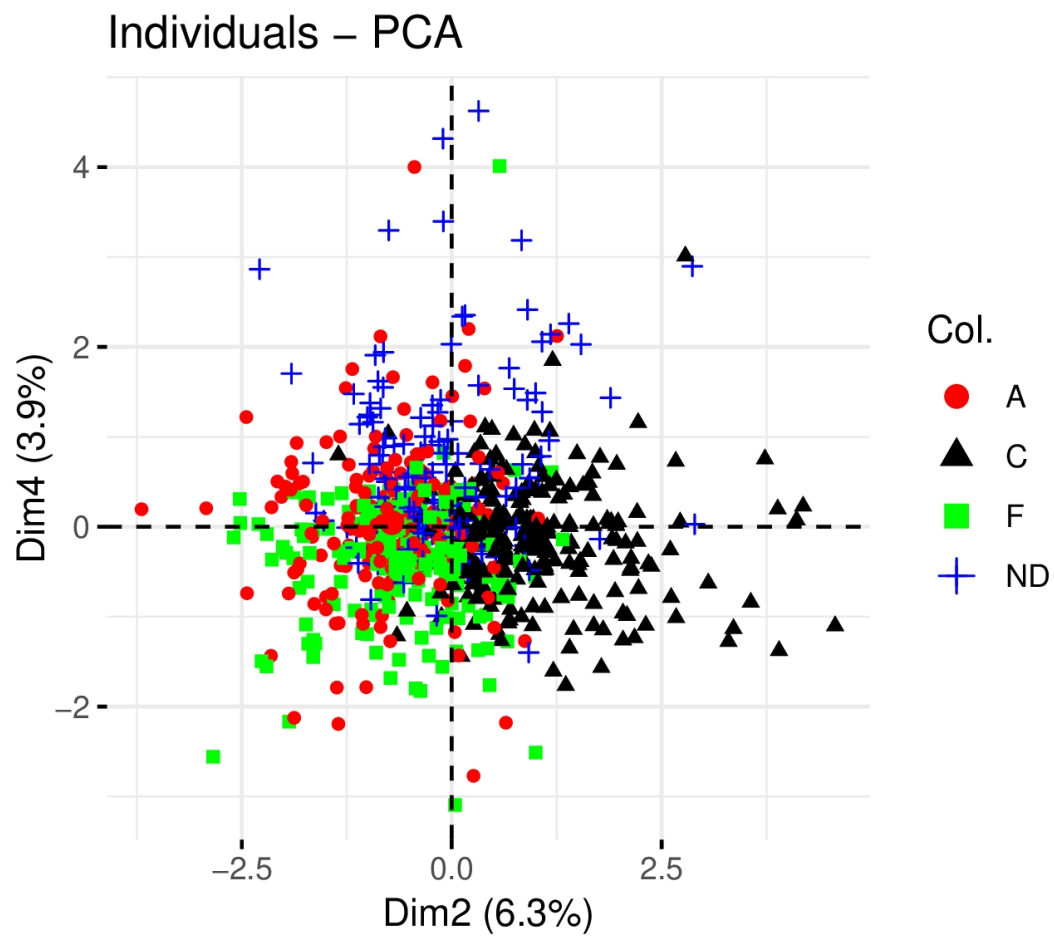
Individuals – PCA
Dim2 (6.3%)
Dim4 (3.9%)
4
2
0
−2
−2.5
0.0
2.5
Col.
A
C
F
ND

IgG

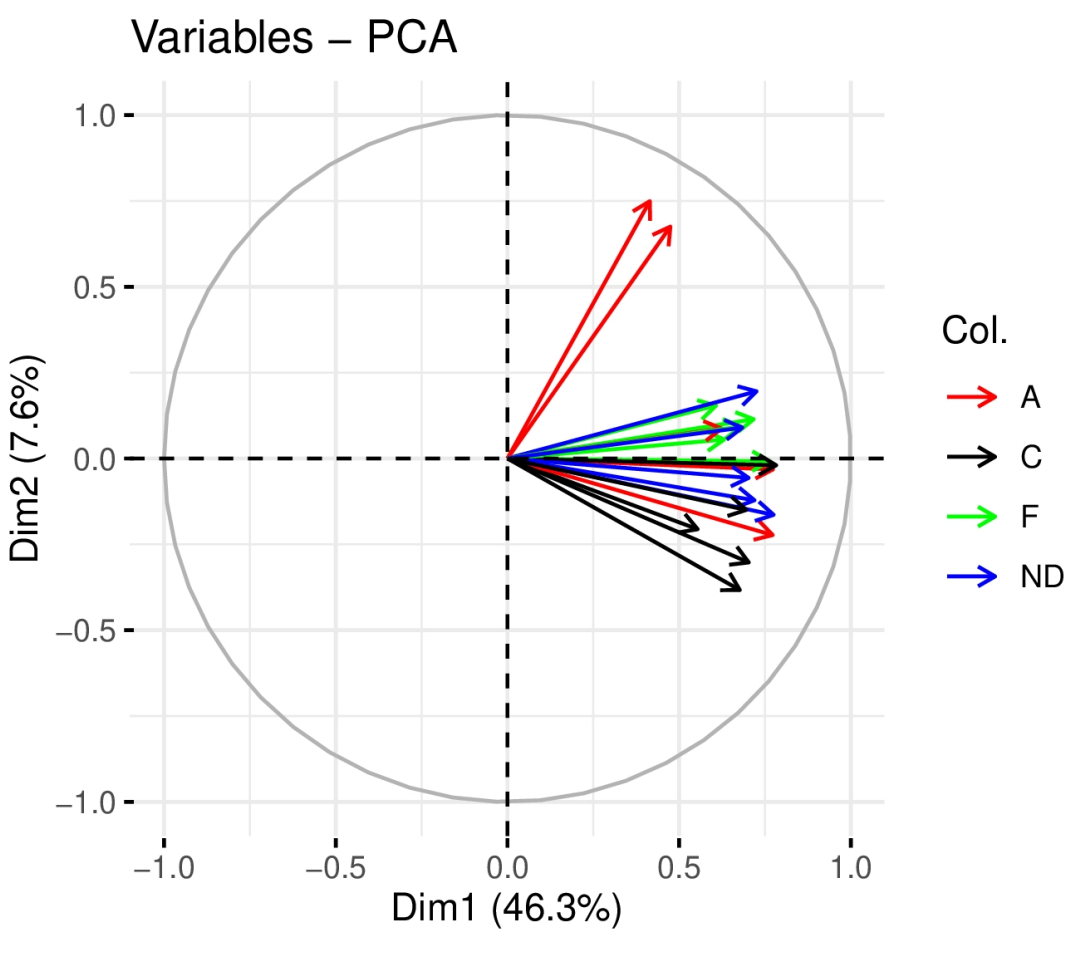
Variables – PCA
Dim1 (46.3%)
Dim2 (7.6%)
1.0
0.5
0.0
−0.5
−1.0
Col.
A
C
F
ND

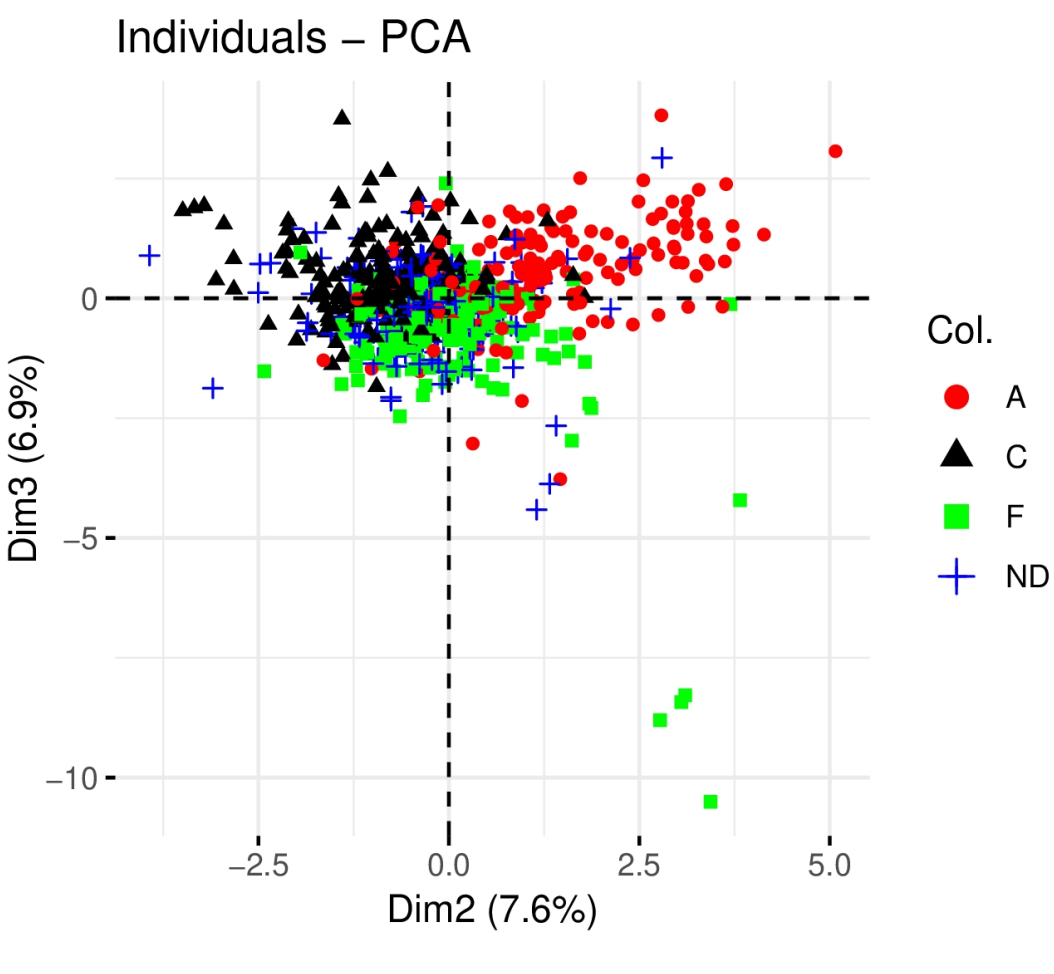
Individuals – PCA
Dim2 (7.6%)
Dim3 (6.9%)
0
−5
−10
−2.5
0.0
2.5
5.0
Col.
A
C
F
ND

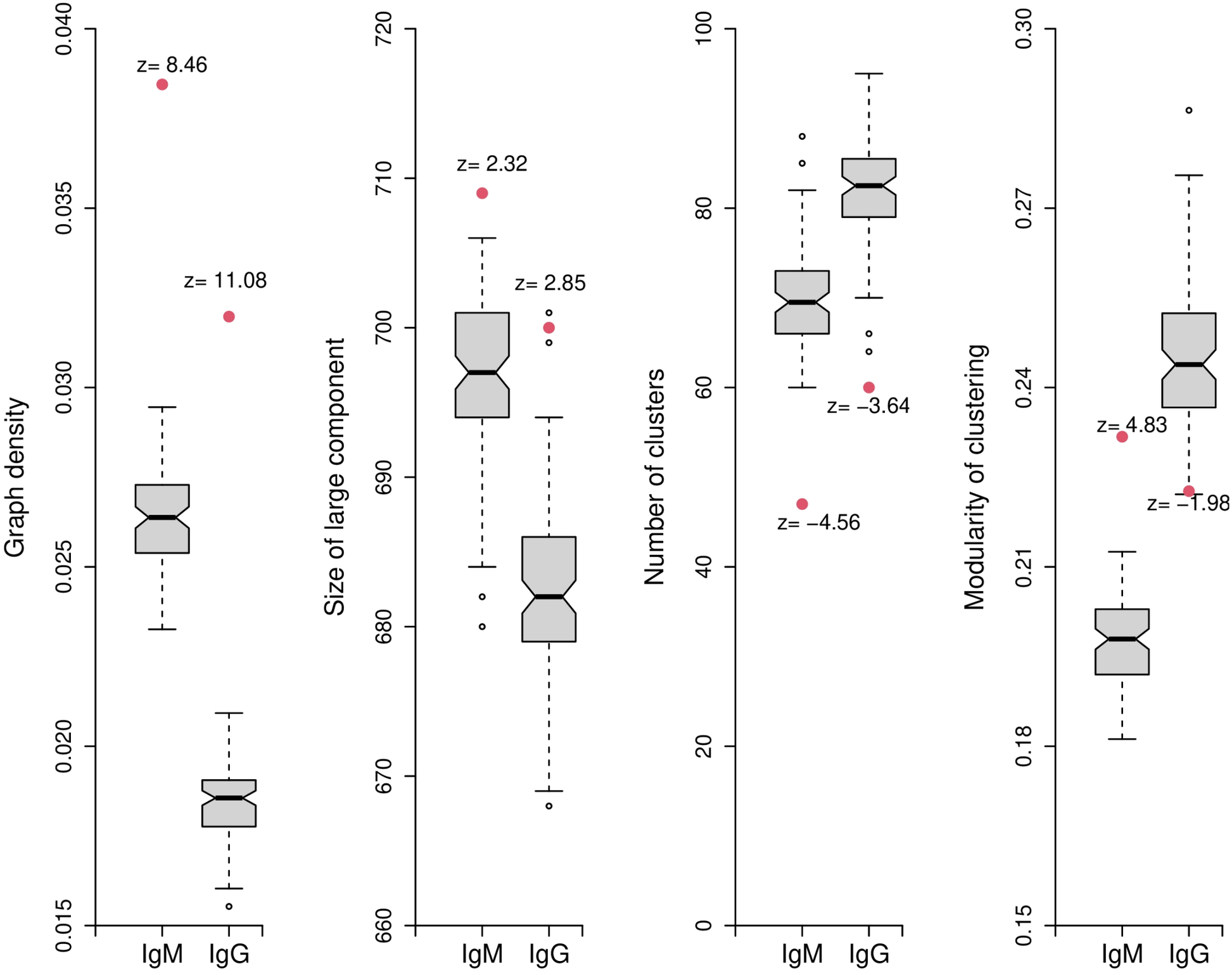
Graph density
0.015
0.020
0.025
0.030
0.035
0.040
z= 8.46
z= 11.08
IgM
IgG
Size of large component
660
670
680
690
700
710
720
z= 2.32
z= 2.85
IgM
IgG
Number of clusters
0
20
40
60
80
100
z= −3.64
z= −4.56
IgM
IgG
Modularity of clustering
0.15
0.18
0.21
0.24
0.27
0.30
z= 4.83
z= −1.98
IgM
IgG

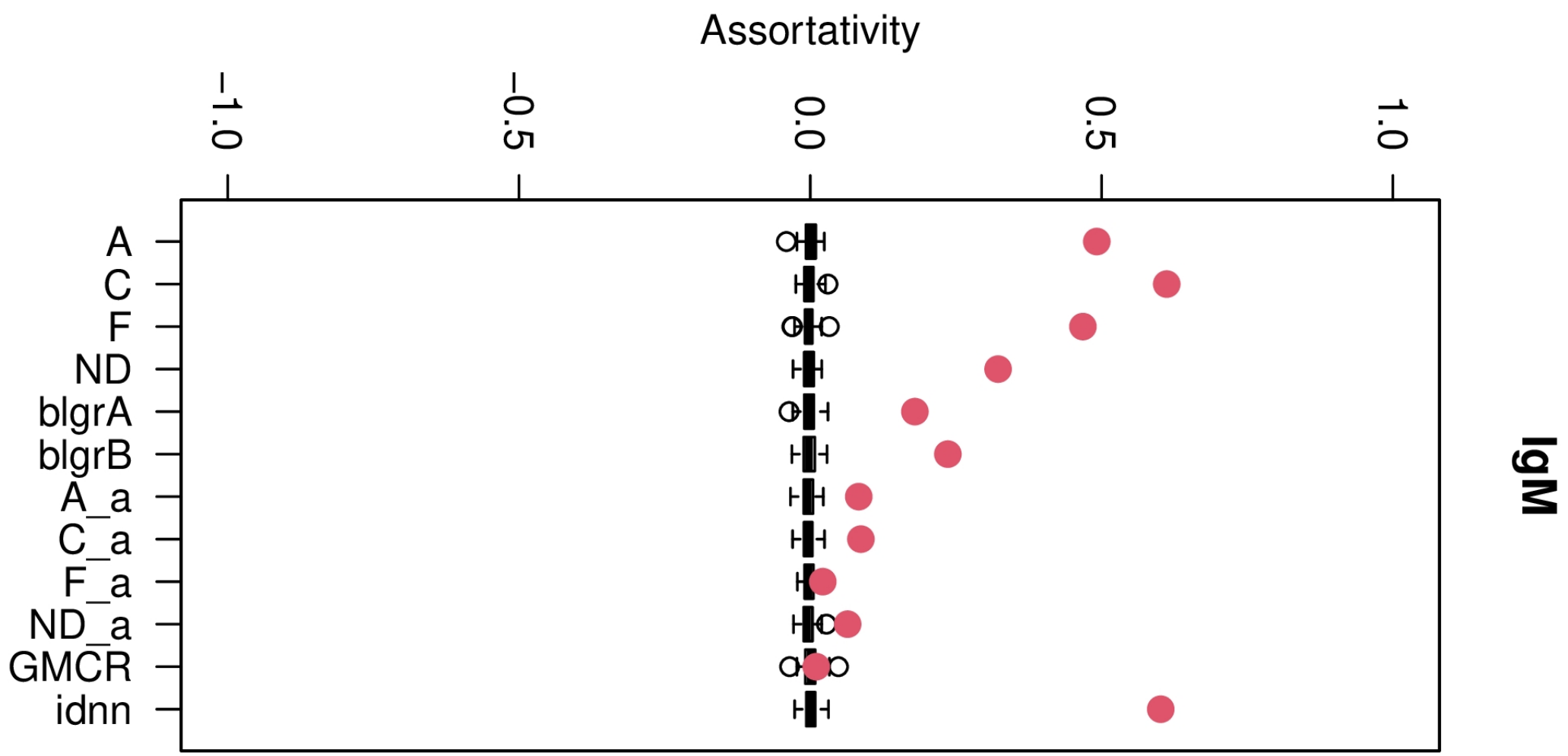
IgM
Assortativity
−1.0
−0.5
0.0
0.5
1.0
A
C
F
ND
blgrA
blgrB
A_a
C_a
F_a
ND_a
GMCR
idnn

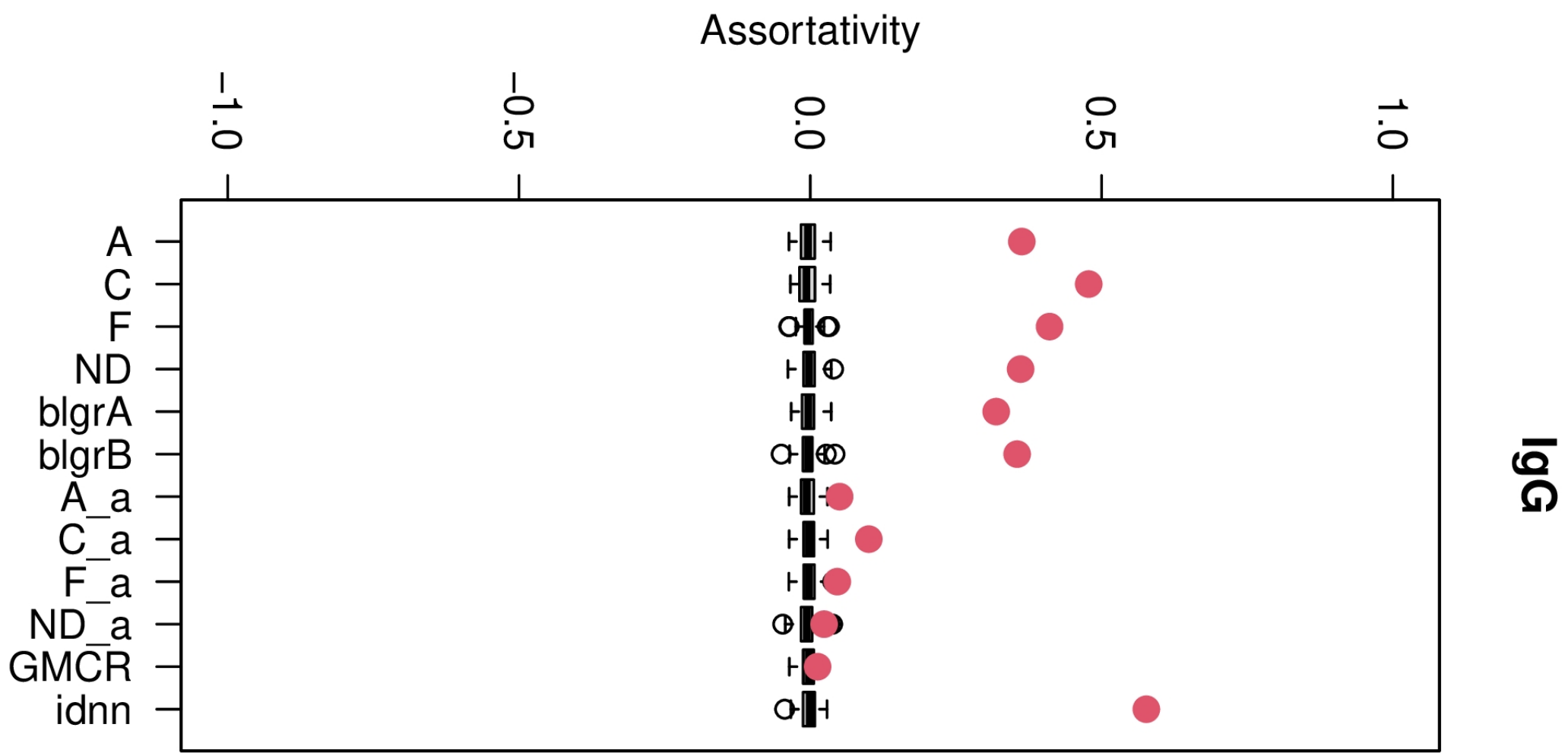
IgG
Assortativity
−1.0
−0.5
0.0
0.5
1.0
A
C
F
ND
blgrA
blgrB
A_a
C_a
F_a
ND_a
GMCR
idnn

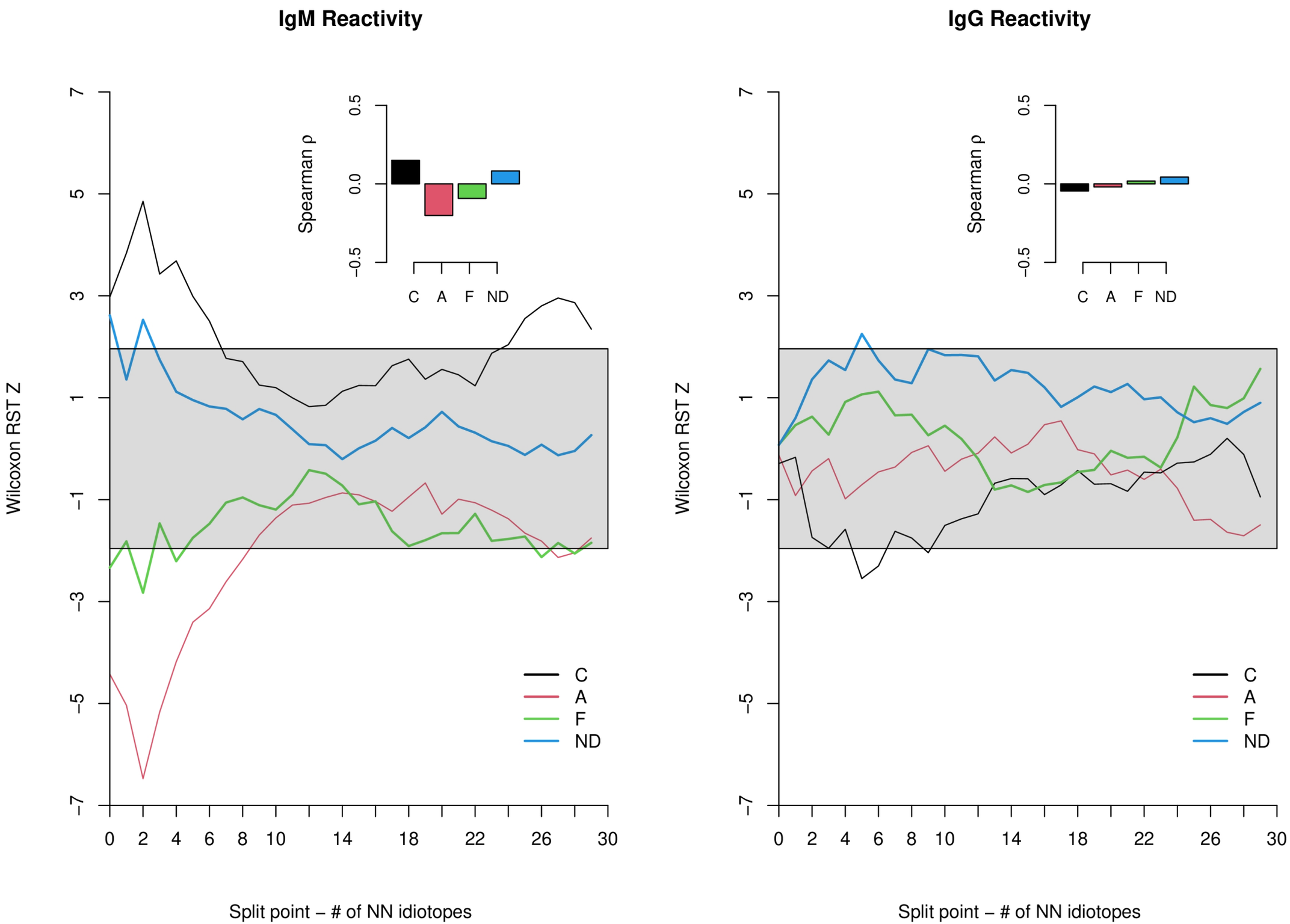
IgM Reactivity
IgG Reactivity
Wilcoxon RST Z
Split point – # of NN idiotopes
Spearman ρ
C
A
F
ND
7
5
3
1
−1
−3
−5
−7
0
2
4
6
8
10
14
18
22
26
30
0.5
0.0
−0.5

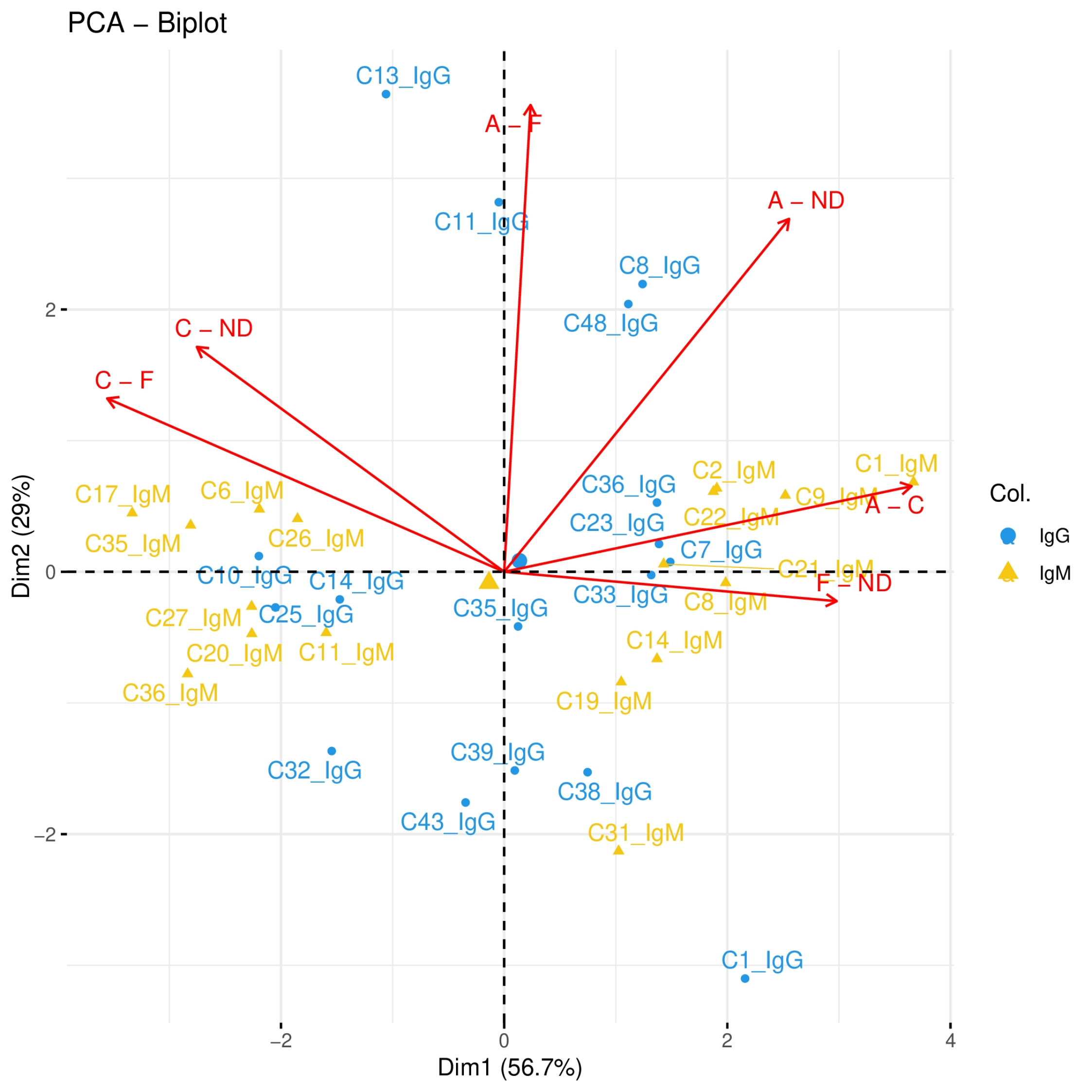
PCA – Biplot
C13_IgG
A – F
A – ND
C11_IgG
C8_IgG
C48_IgG
C – ND
C – F
C1_IgM
C2_IgM
C36_IgG
C9_IgM
A – C
C17_IgM
C6_IgM
C23_IgG
C22_IgM
C35_IgM
C26_IgM
C7_IgG
C21_IgM
C10_IgG
C14_IgG
F – ND
C33_IgG
C8_IgM
C35_IgG
C27_IgM
C25_IgG
C14_IgM
C20_IgM
C11_IgM
C36_IgM
C19_IgM
C39_IgG
C32_IgG
C38_IgG
C43_IgG
C31_IgM
C1_IgG
Dim2 (29%)
Dim1 (56.7%)
2
0
–2
–2
0
2
4
Col.
IgG
IgM

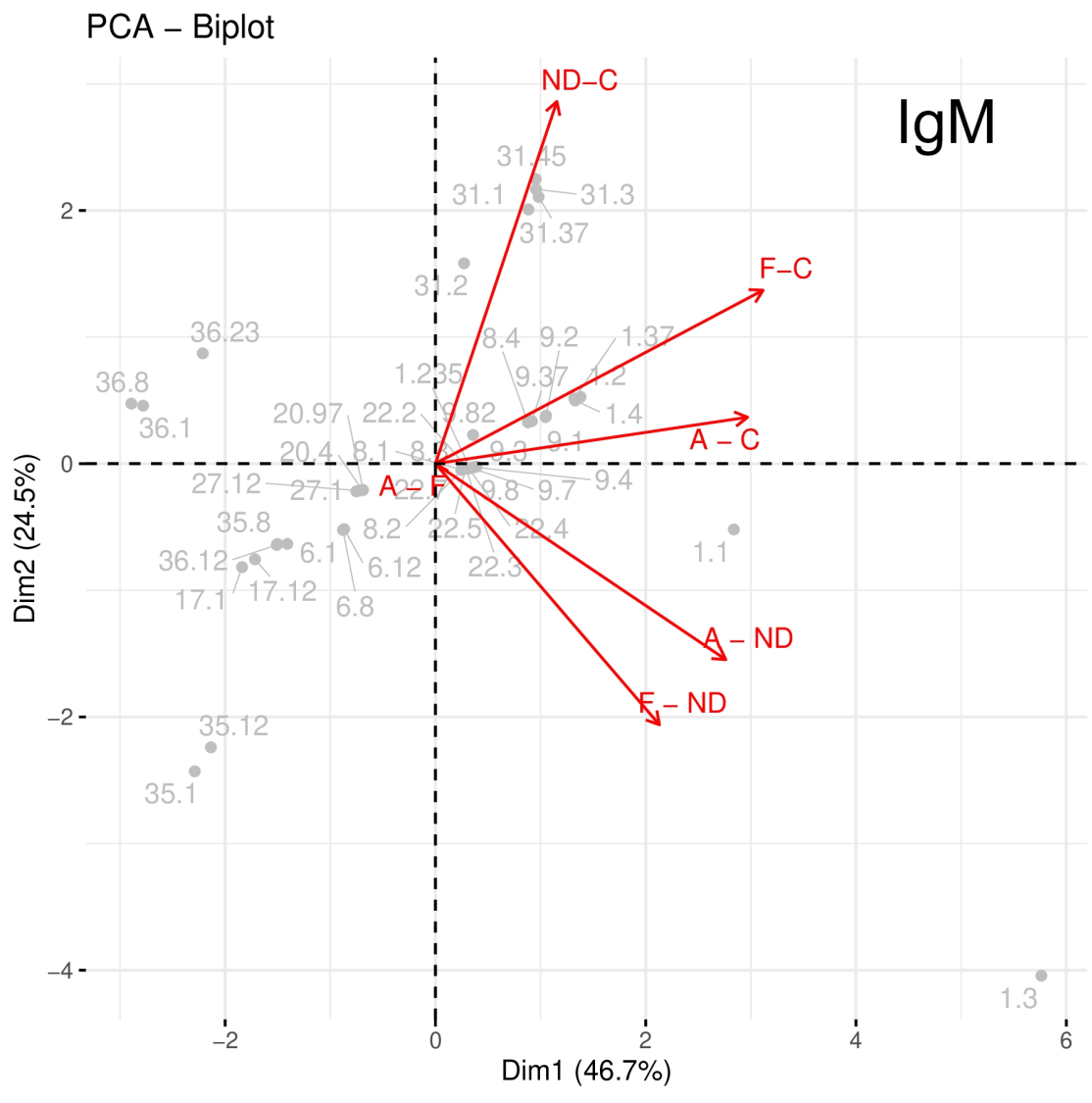
PCA – Biplot
IgM
ND–C
F–C
A – C
A – ND
F – ND
A
F
Dim1 (46.7%)
Dim2 (24.5%)

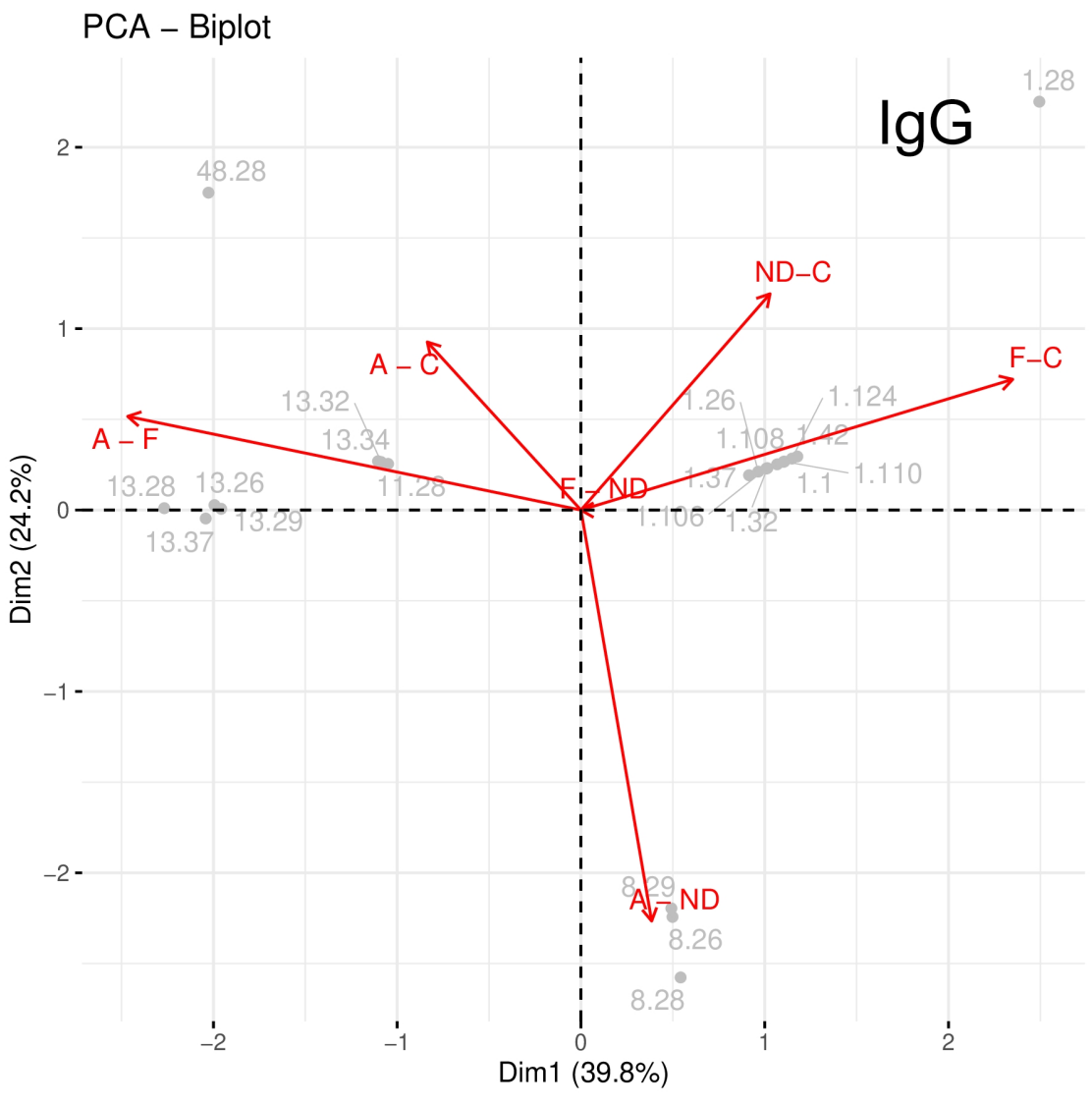
PCA – Biplot
IgG
ND–C
F–C
A – C
A – F
F – ND
A – ND
Dim1 (39.8%)
Dim2 (24.2%)

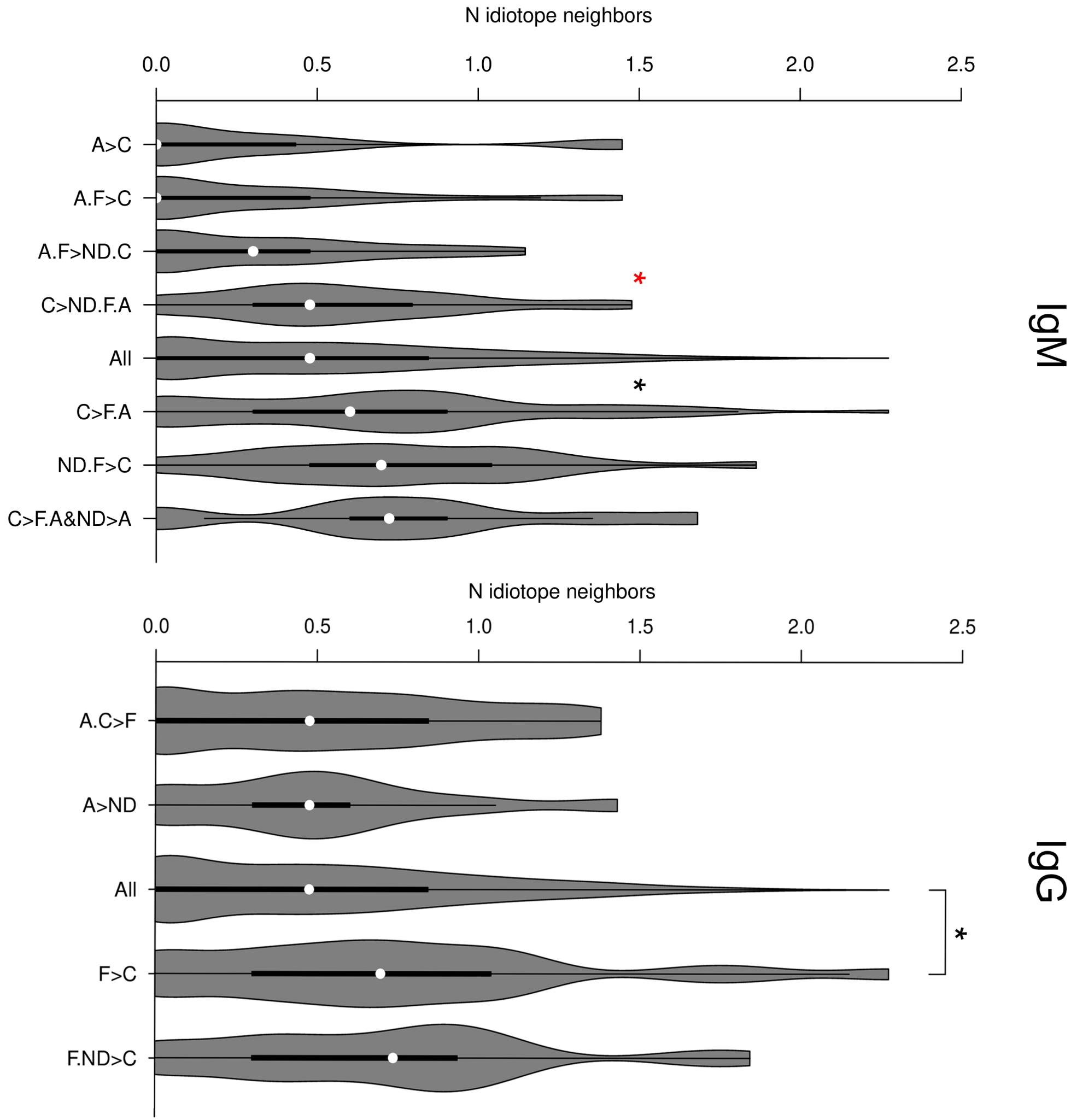
N idiotope neighbors
0.0
0.5
1.0
1.5
2.0
2.5
A>C
A.F>C
A.F>ND.C
C>ND.F.A
All
C>F.A
ND.F>C
C>F.A&ND>A
*
*
IgM
N idiotope neighbors
0.0
0.5
1.0
1.5
2.0
2.5
A.C>F
A>ND
All
F>C
F.ND>C
*
IgG

Supplementary Materials

Supplementary Table 1. Sequences of the peptide mimotopes used in the study.

AAANSRM	ARDLGNV	EEPERWV	GKTLSDV	GYPGLWS	KPSNPEW	NGEPLIP	RTTCDHC	TGSPHTA	TTMSLVT
AAGNASL	ARPAEMS	EERHYPE	GKYFIRN	HAKSIGQ	KPTTGLY	NHWQLRW	RTTPPHY	TGSSWLV	TTPIRWP
AAGSYLP	ARSVHPI	EEVQIPV	GLCLDCR	HAMWPSR	KPVEWRV	NKQHEVP	RWDPFPA	TGTPWSP	TTPMVPW
AAIHQIR	ASVYCGR	EGLLDRN	GLCSSRL	HAQMQFV	KPYFLPH	NLAPRPH	RWIDKVP	TGVTRDS	TTPNFIL
AAISQRY	ATAFKIG	EGNKPMN	GLDIKLH	HDESFFR	KQMLPFR	NPALWCC	SAITHAL	THLAQDV	TTSSTLR
AAMDRLM	ATRADYF	EGWAREP	GLENLSH	HDGLIPS	KQPCILK	NPHHVTR	SAYWNAF	THPELAL	TTTVHLT
AANINLR	ATRGQLH	EHFRHWF	GLKSWPP	HDIQSWH	KWADLAR	NPVQAHY	SCWWCPE	THPTSSF	TTYDQSP
AASHVVT	AVAIDPR	EHIAKVF	GLLRPSP	HDLMWHR	KWPEYKY	NRYPTQI	SDAPWYN	THRWSLS	TVAHGKQ
AATQLWW	AVDGTDR	EHLDRRS	GLPITQT	HDYENRG	LDGPRPH	NTCDICW	SGALITG	THSNREV	TVCGWAC
AAYKGEE	AVGSPRS	EHSLETE	GMHLSNW	HEEQVMM	MDARPAT	NVAGLLS	SGTATLR	THVWFPS	TVLLPRD
ACCQDRM	AVGYPVR	EHVPRIL	GMPHYRE	HEIGSQL	MDCCAGG	QAFPFHP	SGWNEMV	THWENSG	TVPYRFF
ACRLQCN	AVPDLRW	EHWEAPY	GMPTRTF	HGLLERD	MDTDALT	QAMMKLR	SHELFVS	TIPRSLV	TVTRFPL
ADDACPR	AVRFSPY	ELRLIVV	GMSHLNN	HGPRCCW	MDTFTML	QANTSVR	SHQRYLS	TITSSWS	TVVAPVP
ADDRSSW	AVTDRWI	ELVRTND	GNCGQPF	HGSSAFR	MDWKVTP	QDGRDPL	SHTQKLL	TIWGADF	TVVPNGF
ADGPGMI	AVTQNYH	ELWEKTN	GNDFPPV	HGTMYPD	MEGEYWH	QDMPRLP	SITKPGN	TIWHPGL	TWPGGMR
ADMDTQA	AVVNKLI	EPLHRFI	GNRVAYV	HGTQRSH	MEMRDPY	QDQICHC	SMHLGFI	TKHIGSG	TYAEPVR
ADPGYHS	AWARHES	EPVIPRS	GPAVTTS	HGYFRFS	MEPQVII	QETPFFA	SMSFASP	TKIPLWS	TYNPRDS
ADPRNKI	AWKWDFI	EPVTSYL	GPCCRSV	HKDLWPG	MEREIPH	QEVQTVI	SPDDLRV	TKIYPQH	TYPSRPI
ADRLSFS	AWRVIPI	EQSAWRE	GPGFNKT	HKVTDVF	METFTAG	QEWHWKV	SPIDTWS	TKNSMPW	VASGTAG
ADSNLSR	AWSTGRT	ERLTCEF	GPGSQAT	HLGPYLR	MGASSFL	QFTMATF	SPIGSPR	TKTVTER	VASTSTP
ADTCWAC	AWTESLP	ETVFWRM	GPKTMLN	HLTCPKC	MGIRQND	QHDTQIM	SPNWLRL	TLARTAP	VATNPAL
ADVARTH	AWVNDLQ	ETWIGPI	GPLNLQM	HMATHPW	MGQIRYN	QIAWIRQ	SPVQSHC	TLEEFPF	VERMYTP
ADYQPPR	AYEPSLI	EVERPQI	GPLPNMD	HMKAFAR	MGTPKED	QIYAPFI	SPWSLIN	TLHMTQT	VERSRYL
AEECNIC	AYVDPRY	EVGKPHI	GPNTCHC	HMKQNSP	MGTQQDP	QLPGGSA	SQGHLKT	TLHNPRW	VERTLSY
AEHIRAF	CCLAWDP	EVPYDRR	GPPGVSR	HNAFRYD	MGVQTEV	QLWASYP	SQGYSMH	TLIPPRA	VGLTFTQ
AEKSARL	CLRYTNC	GAEWRNG	GPPLTWK	HNAIVFG	MHKNYGQ	QMQINLD	SQTHKVV	TLITSFW	VPRPMSD
AENNGSL	CNMPSRC	GAHMRWQ	GPRIPPL	HPDFWPI	MHKQINP	QPNKHFD	SRFVEPP	TLPMHHQ	VQGLTPG
AESKLAY	CPASKCW	GALQSAT	GPTNTAR	HPGCSAR	MHQEQCR	QPRVVIF	STFWKFP	TLRPWEP	VQNMWPV
AFPPWRV	CPFGCKN	GAPKHWL	GPWRSVH	HPGWAWQ	MIHDKRY	QPSPMFL	STLERLS	TMDNYFV	VWPQIIG
AGGFEWR	CPSHGCT	GARMISD	GPYTLSL	HPLLSNS	MLCSKCQ	QQLPFIW	STMQVFR	TMHEILP	VYKPKNP
AGGTPRD	CPWWCEE	GASLRPG	GQAGGLI	HPLRHSG	MLKPQVK	QSDWSSF	STYMTNF	TMMGVPR	WAERASL
AGTSRCN	CWARSVG	GATGAYN	GQHQGRI	HPNYYGL	MLRTADT	QSGHNQR	SWAMRGN	TMPDPWT	WAKGMCC
AGVAPRL	CWRSPQS	GATGSLP	GQIALSS	HPPAGIL	MMGTQRN	QSGRAPQ	SWHFQKN	TMRYPDP	WAPRIIA
AGWSPVN	CWYPSCM	GATGSYP	GQIDKIP	HPSGSSL	MMQRMSP	QSRHPEP	SWQAPFY	TNGPLSV	WCTRCFQ
AHNRTLS	DAEGFTK	GCASFAR	GQNVTAP	HQCHNCW	MMSEWQA	QSSMLER	SYPRYAW	TNGQTQS	WCVHCVQ
AHNTLRD	DAFIHTR	GCCAMHW	GQTCPCT	HQKQDLL	MPAEFLR	QTFQVLS	SYQCCAW	TNNWPFL	WDKCRDA
AHNWWFD	DAGPCRP	GCCGADP	GQVFTYP	HRLNAEW	MPCQGCS	QTGKSLH	TAAFAFT	TNPHGDT	WDMRSSF
AHPRNYS	DAHVRLA	GCSNCLY	GRWSDSY	HRWPDVM	MPDGRVY	QTGSSFP	TADGLNI	TNVHLQS	WDRNIHL
AHSIPFR	DALNAFR	GDEARDG	GSDSSDY	HTMSNPS	MPDMRVP	QTHLFSS	TAFAIKL	TNWDTTV	WERDCCT
AKGWHYP	DAPLSIK	GDLKHGN	GSGPCCS	HTQPCVD	MPFKTGH	QTMRTWN	TAGRVDS	TPGKYPA	WGGLDVT
AKVFHGR	DARADLL	GEHLLLR	GSIIFHR	HTQSHKF	MPFTDFR	QTSNRSY	TALGSRG	TPLPRAV	WGIKLRH
AKVPYTE	DARSGKW	GEHRWPW	GSYEAIG	HTRADVV	MPHKNDF	QTSSVFR	TALMILP	TPQNSLP	WGKPTLR
ALERTSK	DAVSCAR	GEPVYNP	GTATTLP	HTRTTLS	MPHLDPF	QTVEWYR	TALPVTS	TPRLVTT	WGNQYRI
ALNVATL	DCSRHPC	GEPWRYE	GTGHHVY	HTTLVYP	MPHTPRD	QTVIMRD	TANHQHL	TPSPDLW	WGPWIIP
ALTKNHT	DEGWCNC	GGAHLVT	GTGLLPT	HVNGFSK	MPIRGPM	QTYLLTP	TANNHKF	TPSRYVV	WGTTRVA
ALYALPR	DGASNLP	GGAWRES	GTHLLTR	HVNGTVQ	MPMSPPS	QTYVSRY	TANTFTI	TPTLFPQ	WHERPWY
AMFPRND	DGGLIRI	GGCQTGL	GTIPGQP	HVPLNNP	MPTYVNR	QVATYSY	TAPRDPV	TPTSSRL	WHGVQNI
AMFTPIK	DGWEAAS	GGIPCCT	GTPVLSH	HVRLPWT	MQCPNDC	QVHMHLK	TARDSAH	TPVFHGC	WHQTSRM
AMMSGFI	DHCFARR	GGKHASW	GTQNKTL	HWEPMRN	MQQTSST	QVIPFNH	TARFYGT	TPYPPFP	WMPQVSF
AMPDKLT	DHCGAPC	GGKPYLV	GTSKFDL	HWRYSPY	MQSTGHQ	QVKIPLS	TCAASLL	TQADPYR	WNGPWRI
AMPIIYG	DHQVRFT	GGRLDST	GTSMIVP	HYTCPQC	MQVSMIP	QVNPPLS	TDCTDGW	TQEYWRG	WPLMLMP
AMWDKPR	DHRMLSK	GGTLVPP	GTTAGTM	IAEMWTA	MRDPIYF	QVPSFWY	TDEIHQM	TQGFQTM	WPSQIGH
ANAPLLM	DHRNSIR	GHANPPD	GTTQVLG	IAGCHHC	MRGDLVP	QVTYMIV	TDERNFL	TQIWNSQ	WPYFSLG
ANFPSPW	DIRYHGY	GHARLSP	GTTSLAG	IANRAEQ	MRLDPDE	QYMSIPQ	TDRANWW	TQLSGVP	WQFKGLA
ANLYLPW	DKAEIWH	GHCISRP	GTTSLLS	IGLPSYS	MRPFVPC	RAADEYS	TDRVRAQ	TQMYITS	WQGRPPQ
ANQIHND	DPAGHLN	GHCRMNM	GVDRSRF	IPRIPYT	MRTDGVL	RADIYAP	TEAKLYR	TQNYAAI	WRDASMP
ANYTQRL	DPGLRYS	GHGKLSR	GVDSNWR	IPRLSPL	MSGTHQT	RAWPEAY	TEKPKNW	TQQAYLH	WRSHPQM
APGNCCR	DQPHVWN	GHLPVWS	GVLPMRF	IPTLHRP	MTDMSLL	RCCHNVF	TELKEMI	TQQTLNP	WSLAKYT
APNPYIG	DRALPSR	GHQDKSG	GVLQAAG	IRVVESG	MTPFFPV	RDMEFSN	TENWVHQ	TRCLTSC	WSPNHTS
APSNKFT	DRCCVLD	GHQSWLG	GVPQNSN	KAELIKP	MTPHNLP	RDVLDVY	TEPDYRE	TRMPATI	WTGFPLR
APTKFSL	DRHASYH	GHQVPDL	GVQMRML	KANCCRV	MTPYTQK	RFPVDQH	TEQLMRT	TSAPSYS	WTKGEHF
APWFPIG	DRLELGQ	GHSLKPR	GVRCPPQ	KENAWWR	MTVGNRL	RIAQNHP	TFATAGP	TSGLEKL	WTKVPSP
APWVTGQ	DSGCGHQ	GHWWKEG	GWCRTPM	KEVPPFR	MVKNYAD	RLDDTSY	TFQARSM	TTDARIH	WTNPFPQ
APYKSYR	DTSKAGR	GIDPGVP	GWHAIVH	KHDSISF	MVNAPWY	RLPHPLP	TGADNYR	TTDIPAR	WTPPQLR
AQALNMR	DTTLQNS	GIHTMPH	GWQHPNL	KHLLLWP	MVVDSRS	RLPMPDS	TGCFGPC	TTDRTMM	WVGQLLR

AQDCCLN	EAFQMIA	GILTPNQ	GWSYPWV	KLPARIP	MYGVDQN	RMEITNL	TGDVVLP	TTELLVA	WVKPWWP
AQGDINR	EAHYRGP	GIQGHPL	GWTESFL	KLVDLYA	MYTDPGW	RPDMLRY	TGFHGHK	TTFRLPD	WYPKHVF
AQIKHVL	EAIDPIY	GIVSYPG	GYALDPD	KMAPGPS	NALLDCT	RPFVYEY	TGHFSLR	TTHVSTG	YAGQRSW
AQLKVST	EALHWAK	GIWRDPW	GYASPPQ	KPCDCPP	NAQCCGT	RPMLQIV	TGINKTY	TTIMLPR	YPRWITE
AQMKREP	EANSIAF	GKHCWSC	GYAWITD	KPCTPCH	NAQTTVS	RPSTFHL	TGMKSPG	TTLPLPT	YQNMPWI
AQPSILR	EDCKWCR	GKHITMW	GYCQLCR	KPGSGWP	NAVPLRY	RSTDLYT	TGNWLLR	TTLSPKN	YTQCPKC
AQSMEFV	EEGLIRG	GKPPLHA	GYCRESC	KPLYVHL	NEPRDTK	RTNHMTP	TGPIAPT	TTMCCSL	YTSTLNP
ARDFTMS									YWTDSSR

Supplemental Table 2. Mimotope clusters with significantly different expression in the different diagnoses after the final clustering.

IgM							IgG			
C>ND.F.A	**C>F.A&ND>A**	**C>F.A**	**ND.F>C**	**A.F>ND.C**	**A>C**	**A.F>C**	**A.C>F**	**A>ND**	**F.ND>C**	**F>C**
DQPHVWN	GAPKHWL	AENNGSL	AWSTGRT	AAANSRM	ACRLQCN	ARDFTMS	AFPPWRV	KHLLLWP	ARDFTMS	ARDFTMS
GEHLLLR	GILTPNQ	DIRYHGY	DGASNLP	ARDFTMS	CNMPSRC	GSGPCCS	AMMSGFI	MGVQTEV	DRHASYH	DRHASYH
GHQVPDL	GIVSYPG	DPAGHLN	DPGLRYS	DTTLQNS	HAMWPSR	MDTDALT	ANFPSPW	RPSTFHL	MGASSFL	GSDSSDY
GHSLKPR	GPGFNKT	GAEWRNG	MEPQVII	GKHITMW	MPMSPPS	MDTFTML	AVGSPRS	RTNHMTP	MRDPIYF	MGASSFL
GIQGHPL	GPGSQAT	GATGAYN	MRPFVPC	GSGPCCS	MYTDPGW	MDWKVTP	CNMPSRC	SPWSLIN	MRPFVPC	MRDPIYF
GNCGQPF	GPPLTWK	GCCAMHW	RTTCDHC	HEEQVMM	NHWQLRW	MEMRDPY	EPVIPRS	TFATAGP	MTPFFPV	MRPFVPC
GTSKFDL	HPNYYGL	GCSNCLY	TGSPHTA	HMATHPW	QDMPRLP	MIHDKRY	ETVFWRM	THVWFPS	QLWASYP	MTPFFPV
GWTESFL	TSGLEKL	GEPVYNP	TGTPWSP	HTMSNPS	QTGSSFP	RDMEFSN	GMPTRTF	TTMSLVT	QSDWSSF	QLWASYP
GYAWITD	WGKPTLR	GGCQTGL	TLRPWEP	MDARPAT	SMSFASP	SRFVEPP	GPWRSVH	TVTRFPL	QTSSVFR	QSDWSSF
HDYENRG	WGIKLRH	GHLPVWS	TNWDTTV	MDTFTML	TTPIRWP	TDEIHQM	GVLPMRF	VERMYTP	QYMSIPQ	QYMSIPQ
HGPRCCW		GHQDKSG	TKIPLWS	MDWKVTP	MHKQINP	TTMCCSL	HWEPMRN	WGNQYRI	SMSFASP	SMSFASP
HQKQDLL		GLDIKLH	TGADNYR	MHQEQCR	WTNPFPQ	WDKCRDA	KQMLPFR	WRSHPQM	TALGSRG	TALGSRG
KPTTGLY		GLENLSH	TLHMTQT	MIHDKRY	RWIDKVP	MQCPNDC	NHWQLRW	WSLAKYT	TGSSWLV	TFQARSM
MRTDGVL		GMHLSNW	WRDASMP	MQCPNDC	VERMYTP	MTDMSLL	SPNWLRL		THRWSLS	THRWSLS
TQLSGVP		GQTCPCT	TEQLMRT	QVTYMIV	HYTCPQC	MVNAPWY	SQGYSMH		TQIWNSQ	TQIWNSQ
WDRNIHL		GRWSDSY	TYNPRDS	RDMEFSN	CPSHGCT	AAANSRM	TARFYGT		TFQARSM	KHDSISF
WPSQIGH		GSDSSDY	GTGLLPT	SGWNEMV	DHQVRFT	AAMDRLM	THLAQDV		YWTDSSR	GVPQNSN
WSPNHTS		GVDRSRF	QTYLLTP	SRFVEPP	GTTSLLS	ADMDTQA	YAGQRSW		TARDSAH	YQNMPWI
TGHFSLR		GVDSNWR	RSTDLYT	TDEIHQM	IANRAEQ	DTTLQNS	TPSPDLW		QTYLLTP	AAANSRM
WQFKGLA		GWSYPWV	TARFYGT	TTMCCSL	MQQTSST	GKHITMW	GWCRTPM		YQNMPWI	AWSTGRT
		HDGLIPS	TGVTRDS	ADMDTQA	SGALITG	HMATHPW	TTPIRWP			TGSSWLV
		MRGDLVP		MVNAPWY	MPCQGCS	HTMSNPS	ADDRSSW			QTSSVFR
		TNPHGDT		QEWHWKV		HWEPMRN	TEPDYRE			TPQNSLP
		GWQHPNL		VQNMWPV		QEWHWKV	QVNPPLS			
		DQPHVWN		WDKCRDA		QVTYMIV	GWSYPWV			
		GHSLKPR		WDMRSSF		QEVQTVI	TPLPRAV			
		GTSKFDL		AAMDRLM		MHQEQCR	DTSKAGR			
		GWTESFL		HRWPDVM		WDMRSSF	TGTPWSP			
		GYAWITD		MDTDALT		MDARPAT	GPRIPPL			
		HDYENRG		MTDMSLL		VQNMWPV				
		HQKQDLL		QEVQTVI		ACRLQCN				
		KPTTGLY				CNMPSRC				
		MRTDGVL				CPSHGCT				
		TQLSGVP				CWYPSCM				
		WSPNHTS				DHQVRFT				
		SHELFVS				GHCISRP				
		WQFKGLA				GTSMIVP				
		EAHYRGP				HAMWPSR				
		GAPKHWL				HYTCPQC				
		GDLKHGN				MMSEWQA				
		GILTPNQ				MPCQGCS				
		GIVSYPG				MPMSPPS				
		GMPTRTF				MQQTSST				
		GPGSQAT				MYTDPGW				
		GPNTCHC				NHWQLRW				
		GPPLTWK				QDMPRLP				
		GYPGLWS				RWIDKVP				
		HPNYYGL				VERMYTP				
		TIWHPGL				SGALITG				
		TSGLEKL				TTLPLPT				
		WGIKLRH				TTMSLVT				
		WGKPTLR				QTGSSFP				
		GPGFNKT				WTNPFPQ				
						SMSFASP				
						TTPIRWP				
						EGNKPMN				
						GLKSWPP				
						IANRAEQ				
						MHKQINP				
						HWRYSPY				

Supplementary Table 3. Proteins containing potential linear epitopes homologous to the mimotopes with differentially expressed antibody reactivities in AD and FTD.

Cluster type	Mimotope Sequence	Protein name/ protein sequence	Localization	Associated process	Function and relation to neurodegeneration	Reference
F.ND>C:IgG	YWTDSSR	Low-density lipoprotein, receptor-related protein 1B (LRP1B), YWIDSSR, YWTDHSR	Membrane	Endocytosis	Receptor for ApoE-carrying lipoproteins. LRP1B interacts with APP, leading to a decrease in APP processing to Aβ.	(Real et al., 2022), (Haas et al., 2011),(Cam et al., 2004)
F.ND>C:IgG	YWTDSSR	Low-density lipoprotein, receptor-related protein 4 (LRP4), YWTDSGTSR	Membrane	Endocytosis	Promotes Aβ uptake by interacting with ApoE. Involved in the maintenance of the synapse between motor neuron and skeletal muscle, as well as the synapse function in the CNS.	(Pohlkamp et al., 2015; Zhang et al., 2020), (Gomez et al., 2014), (Aoki et al., 2020), (Kim et al., 2008)
F.ND>C:IgG	YWTDSSR	Low-density lipoprotein receptor-related protein 6 (LRP6), YWTDWSR	Membrane	Endocytosis, Wnt signaling	Co-receptor of synaptic Wnt signaling. Maintain the functional integrity of the synaptic connections in the adult brain.	(Chow et al., 2021; Wood, 2023), (Buechler and Salinas, 2018)
F>C:IgG, F.ND>C:IgG	MRDPIYF	Sortilin, SORT1 RDPIYF	Membrane	Endocytosis	ApoE receptor	(Saadipour et al., 2013), (Asaro et al., 2020), (Ruan et al., 2018) (Hu et al., 2017a)
ND.F>C:IgM	TEQLMRT	Cytotoxic granule associated RNA binding protein TIA-1 TEQLMR	Intracellular	Post-transcriptional regulation of Gene expression	Interaction between TIA1 and tau lead to insoluble tau aggregates in stress granules. Reduced levels of TIA1 restrain the inclusion of tau in pathological and persistent stress granules while overexpression of TIA1 stimulates tau-related degeneration. High expression in GS where binds to and controls multitude of specific transcripts during B-cell positive selection.	(Vanderweyde et al., 2016), (Osma-Garcia et al., 2023), (Maziuk et al., 2018)
A.F>C:IgM	GLKSWPP	Basic helix-loop-helix ARNT-like protein 1 BMAL1 LKSWPP	Intracellular	Regulation of transcription	Circadian transcription factor which is important regulator of circadian rhythm. DNA methylation and rhythmic expression of Bmal1 is aberrant in brains of AD.	(Cronin et al., 2017; Hulme et al., 2020)
A.C>F:IgG ND.F>C:IgM	TGTPWSP	Nonsense-mediated mRNA decay factor SMG7	Intracellular	Nonsense-mediated	SMG7 is part of the mRNA decay complex. It directs aberrant mRNA for degradation by SMG6	(Boehm et al., 2021),

		GTPWSP		mRNA decay; RNA quality control	endonuclease, also part of the complex. Inhibition of the mRNA decay complex results in massive transcriptomic alterations.	(Unterholzner and Izaurralde, 2004), (Weskamp and Barmada, 2018)
A.C>F:IgG	GPRIPPL	Fibroblast growth factor 17, FGF 17, GPRIPPL	Secreted	Signalling	Enriched in the brain; Required for normal brain development; FGF17 improves memory in aging brains; blocking of FGF17 impairs cognitive processes.	(Iram et al., 2022)
A.F>C:IgM A.F>ND.C:IgM	MDTDALT	Plexin-D1 MDTDTLT	Membrane	Cell signaling, Neuronal guidance	Glycoprotein receptor for semaphorin 3E. Plexin-D1 signaling positively mediates synapse formation and has a role in ensuring the specificity of synapse formation. A missense mutation variant in PLXND1 gene is enriched among AD patients.	(Wang et al., 2015), (Balabanski et al., 2021), (Burk et al., 2017),(Pecho-Vrieseling et al., 2009),(Ding et al., 2011)
A.F>C:IgM A.F>ND.C:IgM	MQCPNDC	Tenascin X QCPNDC	Extracellular	Cell adhesion	Regulate tissue structures through anti-adhesive interaction with collagen.	(Aktar et al., 2018), (Okuda-Ashitaka and Matsumoto, 2023)
A.F>C:IgM A.F>ND.C:IgM	MQCPNDC	Tenascin C MSCPNDC	Extracellular	Cell adhesion	Anti-adhesive effects. Blood level of Tenascin C may increase in AD patients. Tenascin C can be deposited together with amyloid beta plaques in AD patients.	(Soares et al., 2012) ,(Mi et al., 2016)
A.F>C:IgM A>C:IgM	MPMSPPS	Insulin receptor substrate 2 IRS2 MPMSPAS	Intracellular	Insulin/IGF-1 signaling pathway	Signaling through the Insulin receptor/IRS2 is associated with the amount of amyloid beta accumulation in the brain.	(Schubert et al., 2003), (Sano et al., 2023), (Ochiai et al., 2021)
A.F>C:IgM A>C:IgM	MPMSPPS	Zinc finger and BTB domain-containing protein 5, ZBTB5 LPMSPPS	Intracellular	Transcription factor	Participates in cell fate decision as a repressor of the cell cycle arrest gene p21. Proto-oncogene that stimulates cell proliferation in the presence of p53 and apoptosis in the absence of p53.	(Choi et al., 2020; Koh et al., 2009)
A.F>C:IgM	GLKSWPP	Catenin alpha-1 GLKGWPP	Intracellular	Cell adhesion; Wnt signaling suppression	Beyond its involvement in adherent junctions, alpha-catenin is reported to repress Wnt/beta-catenin target genes.	(Choi et al., 2013)
A.C>F:IgG	SPNWLRL	Brain mitochondrial carrier protein 1, UCP5 PNWLRL	Intracellular	Mitochondrial energy metabolism	Passes protons through the inner mitochondrial membrane, thus controlling ATP synthesis from ADP. Improper functioning leads to elevated reactive oxygen species and mitochondrial dysfunction.	(Ramsden et al., 2012; Tracy et al., 2022; Wang et al., 2020)
C>F.A:IgM	GRWSDSY	Actin-binding protein IPP, Profilin I GRWSDS	Intracellular	Regulation of the actin cytosceleton	Localized at synaptic sites in the brain and is involved in activity-dependent mechanisms at dendritic spine synapses.	(Neuhoff et al., 2005)
C>F.A:IgM	GCCAMHW	Adhesion G protein-coupled receptor E1, ADGRE1, GCCVMHSW	Membrane	Adhesion	Plays a regulatory role in creating contact sites between the endoplasmic reticulum and mitochondria.	(Rasul et al., 2021)

A.C>F:IgG A.F>C:IgM	HWEPMRN	E3 ubiquitin-protein ligase TRIM4, HWEPLR	Intracellular	Innate immune signaling	The activator of innate immune response triggered by RIG-I	(Yan et al., 2014),(Fernández-de Frutos et al., 2019)
A.F>C:IgM A>C:IgM	HAMWPSR	Proteasome adapter and scaffold protein ECM29 HAMWNSR	Intracellular	Protein degradation	Involved in the regulation of the proteasomal distribution during neuronal maturation. Oxidative stress promotes proteasome disassembly.	(Wang et al., 2017), (Lee et al., 2020),
A.F>C:IgM A.F>ND.C:IgM	MTDMSLL	Intermembrane lipid transfer protein VPS13C MTDMSIL	Intracellular	Transfer of lipids; vesicle trafficking	Mediates the transfer of lipids between membranes at organelle contact sites. Mutations in VPS13C might relate to impaired lysosomal degradation.	(Kumar et al., 2018), (Hancock-Cerutti et al., 2022)
A.F>C:IgM A>C:IgM A>ND:IgG	VERMYTP	lon protease homolog, mitochondrial VERMYDVTP	Intracellular	Hydrolysis of mitochondrial proteins	Degradation of oxidatively damaged proteins.	(Bezawork-Geleta et al., 2015)
A.F>ND.C:IgM	SGWNEMV	TBC1 domain family TBC1D SGAWNEMV	Intracellular	Various	Some family members may be indirectly related to ND. For example, TBC1D24 regulates autophagy, and TBC1D1 regulates GLUT4 trafficking and glucose uptake via VPS13C.	(Finelli and Oliver, 2017), (Hook et al., 2020)
C>ND.F.A:IgM	GHQVPDL	RNA/RNP complex-1-interacting phosphatase, DUSP11, GHQVPD	Intracellular	RNA metabolism	Reduce the exposure of intracellular RNA to RIG-1, thus preventing activation of the innate immune response.	(Choi and Sullivan, 2021)
A.F>C:IgM A.F>ND.C:IgM	AAMDRLM	UBX domain-containing protein 1 UBXN1 AAMDWLM	Intracellular	Protein degradation	Inhibit NFκB signaling. Regulatory adaptor for proteasome degradation of ubiquitylated proteins	(Hu et al., 2017b), (Ganji et al., 2018)
A.F>C:IgM	TTLPLPT	Zinc finger FYVE domain-containing protein 26, ZFYVE26, TTLPLPT	Intracellular	Autophagy	ZFYVE26 mutations lead to defects in the fusion between autophagosomes and endosomes.	(Vantaggiato et al., 2019), (Khundadze et al., 2013)
A.F>C:IgM A.F>ND.C:IgM	QVTYMIV	Dynein axonemal intermediate chain 3 QITYMI	Intracellular	Cellular transport	Transports intracellular cargos towards the minus end of microtubules.	(Chen et al., 2014)
A.F>C:IgM	HWRYSPY	Rho GTPase- activating protein 32, ARHGAP32, HYRYSPY	Intracellular	Signaling, energy metabolism	Dysregulation of Rho GTPases, regulated by ARHGAP32, has been implicated in conditions like Alzheimer's disease.	(Aguilar et al., 2017)
F.ND>C:IgG F>C:IgG	TALGSRG	Sigma non-opioid intracellular receptor 1 TALGSRG	Intracellular	Calcium signaling	During healthy aging, the density of σ1R increases, but in diseases like Alzheimer's, there appears to be a reduction in σ1R expression.	(Prasanth et al., 2021)

A.F>C:IgM A.F>ND.C:IgM	GSGPCCS	Tumor necrosis factor receptor superfamily SGPCCS	Membrane	TNF signaling	For example, Death receptor 6 (DR6, TNFRSF21) has been implicated in Alzheimer's disease pathogenesis. It interacts with the amyloid precursor protein APP.	(Ren et al., 2022)
A.F>C:IgM A>C:IgM	HYTCPQC	Zinc finger protein 214 ZNF231 YTCPEC	Intracellular	Regulation of transcription	Brain-specific gene that is implicated in the neurodegenerative disease MSA.	(Hashida et al., 1998)
A.F>C:IgM A.F>ND.C:IgM	RDMEFSN	Leucine-rich repeat-containing protein 66 RDLEFSN	Membrane	Cell adhesion	-	-
F>C:IgG ND.F>C:IgM	AWSTGRT	S arrestin WSTGRT	intracellular	Signaling	Rho signal termination; S-arrestin is immunogenic	(Baldin et al., 2019), (Velez et al., 2016)
C>F.A&ND>A:IgM C>F.A:IgM	GAPKHWL	Signal peptide, CUB and EGF-like domain-containing protein 2, GAPKHWM	Secreted	Signaling	Enhancer of proteolytic truncation for soluble Shh	(Jakobs et al., 2014)
A.F>C:IgM A>C:IgM	MPMSPPS	Transmembrane serine protease 9, LPMSPPS	Membrane	-	TMPRSS9 may induce changes in cell adhesion and contribute to cancer cell invasion	(Fontanil et al., 2014)
A.F>C:IgM A.F>ND.C:IgM	HMATHPW	Trinucleotide repeat-containing gene 18 protein TNRC18, HLATHPW	Intracellular	Chromatin regulation	mediate the silencing of ERV class I (ERV1)	(Zhao et al., 2023)
A.F>C:IgM A>C:IgM	HYTCPQC	Zinc finger protein 311, ZNF311, HYGCPQC	Intracellular	-	-	-
A.F>C:IgM A.F>C:IgM A.F>ND.C:IgM A>C:IgM	WDMRSSF HYTCPQC WDMRSSF HYTCPQC	Zinc finger protein 532 DMRSSF, YTCPEC	Intracellular	DNA-binding	Transcriptional activation of the expression ZNF532 is poor biomarker for laryngeal carcinoma progression.	(Fan et al., 2022)
F.ND>C:IgG F>C:IgG	QSDWSSF SDWSSF	zinc finger protein-like 1, ZFPL1	Membrane, Intracellular (different isoforms)	-	structural component of the Golgi apparatus; Identified as a significantly different and down regulated in FTD as compared to controls	(Bronner et al., 2009)
ND.F>C:IgM	DPGLRYS	Sorting nexin-29, SNX29 DPGLRYS	Intracellular	Cell trafficking	Involved in intracellular trafficking of proteins; regulator of myocyte differentiation	(Vieira et al., 2021)
ND.F>C:IgM	GTGLLPT	Protein PRRC1 GTGLLPT	Membrane, Intracellular	Cell trafficking	The cellular function of PRRC1 is unknown; it facilitates ER-to-Golgi trafficking of proteins.	(Huang et al., 2021)
A>ND:IgG	WRSHPQM	Nuclear cap-binding protein subunit 1, WRNHPQM	Intracellular	Nuclear export	Component of the cap-binding complex (CBC)	(Kim and Taylor, 2017)

A.C>F:IgG	GWCRTPM	Mismatch repair endonuclease PMS2 GWCRTP	Intracellular	Mismatch repair	Part of the mismatch repair complex. PMS2 deficiency leads to increased genomic mutation rates.	(van Oers et al., 2010)
A.C>F:IgG	GPRIPPL	Ly6/PLAUR domain-containing protein 3, LYPD3 PRIPPL	Membrane, No brain expression	Focal adhesion	Supports cell migration, associated with metastasis	(Ngora et al., 2012)
A.C>F:IgG	EPVIPRS	general transcription factor 3C, polypeptide 2, TFIIIC110 EPVVPRS	Intracellular	Transcription	Subunit of human TFIIIC complex which is specific for RNA pol III and essential for transcription of tRNA and other type 2 genes.	(Schaffer et al., 2019), (Crepaldi et al., 2013)
A>ND:IgG	SPWSLIN	Acid sphingomyelinase-like phosphodiesterase 3b/ SPWALIN	Membrane	Lipid metabolism	GPI-anchored glycoprotein, negative regulator of TLR and insulin receptor signaling.	(Heinz et al., 2015; Mitrofanova et al., 2019)
A.F>ND.C:IgM	HEEQVMM	Spliceosome RNA helicase DDX39B, HEKQVMM	Intracellular	Nuclear mRNA export	Controls the splicing of FOXP3	(Nagasawa et al., 2024)
A.F>C:IgM	CWYPSCM	Outer dense fiber protein 2, ODF2, CWFPSC	Intracellular	Structural protein	The cytoskeletal structure protein of the sperm tail attaches to the microtubules.	(Donkor et al., 2004)
A.F>C:IgM A.F>ND.C:IgM	SRFVEPP	Dynein axonemal heavy chain 2, SRFIEPP	Intracellular	Cellular movement	Generate force for the movement of microtubules in beating cilia, cell division, and intracellular transport.	(Schmidt and Carter, 2016)
A.C>F:IgG	SPNWLRL	Kidney mitochondrial carrier protein 1 UCP6/PNWLRL	Intracellular	Mitochondrial energy metabolism	Highly homologous to UCP5 (Brain mitochondrial carrier protein 1). Passes protons through the inner mitochondrial membrane, thus controlling ATP synthesis from ADP	(Gorgoglione et al., 2019)
A.C>F:IgG C>F.A:IgM	GWSYPWV	Proline-rich protein 23E WAYPWV	-	-	-	-
C>F.A:IgM	GRWSDSY	Olfactomedin-like protein 2B, GRWSNSY	Intracellular	-	-	-
A.F>C:IgM	GHCISRP	Maestro heat-like repeat-containing protein family GHCISRP	Intracellular	-	-	-
A.F>C:IgM	GHCISRP	Chymotrypsin-like elastase family preproprotein GHCISR	Secreted	Hydrolysis of proteins,	Expression restricted to the pancreas; digestive function protease.	
F.ND>C:IgG F>C:IgG ND.F>C:IgM	MRPFVPC	Cerebral cavernous malformations 2 protein-like, MRPFIP	Intracellular	Signaling	Part of CCM signaling complex	(Whitehead et al., 2009)
A.F>C:IgM A.F>ND.C:IgM	GSGPCCS	Disintegrin and metalloproteinase domain-containing protein 18 GSGPCC	Membrane	Cell-matrix interaction	Possibly involved in spermatogenesis	-

A.F>C:IgM A.F>ND.C:IgM	GSGPCCS	Disintegrin and metalloproteinase domain-containing protein 18, GSGPCC	Membrane	Cell-matrix interaction	-	-
C>ND.F.A:IgM	GEHLLLR	Helicase with zinc finger domain 2, HELZ2, GDHLLLR	Intracellular	Regulation of transcription	Interferon-stimulated gene, transcriptional coactivator, degrades mRNA of L1 retrotransposons.	(Luqman-Fatah et al., 2023)
C>F.A:IgM	GLDIKLH	Keratin, type I cytoskeletal 25, LDIKLH	-	-	-	
C>F.A:IgM	GPNTCHC	Multiple epidermal growth factor-like domains protein 11, MEGF11/PDTCHC	Membrane		Involved in neuronal mosaic arrangements. Upregulated in triple-negative breast cancer.	(Chiu et al., 2020; Kay et al., 2012)
A.F>ND.C:IgM	HEEQVMM	Plakophilin-1 QEQVMM	Intracellular	Cytoskeleton/ cell membrane interactions	Linker molecule at the adherens junctions.	(McGrath et al., 1997)
A.F>C:IgM A>C:IgM	HYTCPQC	Zinc finger protein 497 YTCPEC	-	-	Predicted to be involved in the regulation of transcription by RNA polymerase II.	-
A.F>C:IgM A>C:IgM	HYTCPQC	zinc finger protein 500 YTCPEC	Intracellular	-	Elevated in breast cancer cells. Binds and activates p53, thus suppressing the proliferation of breast cancer cells.	(Ma et al., 2023)
A.F>C:IgM A>C:IgM	HYTCPQC	Zinc finger protein 668 YTCPEC	Intracellular	-	Tumor suppressor involved in the regulation and stabilization of p53.	(Hu et al., 2011)
A.F>C:IgM A>C:IgM	HYTCPQC	Zinc finger protein 777 YTCPEC	Intracellular	Transcription	Overexpression inhibits cell proliferation	(Yuki et al., 2015)
A.F>C:IgM A>C:IgM	HYTCPQC	Zinc finger protein 835 YTCPEC	Intracellular	Transcription	Differentially expressed in colorectal cancer.	(Jovov et al., 2012)

References to Suppl. Table 4.

- Aguilar, B.J., Zhu, Y., Lu, Q., 2017. Rho GTPases as therapeutic targets in Alzheimer's disease. Alzheimer's Research & Therapy 9, 97.
- Aktar, R., Peiris, M., Fikree, A., Cibert-Goton, V., Walmsley, M., Tough, I.R., Watanabe, P., Araujo, E.J.A., Mohammed, S.D., Delalande, J.M., Bulmer, D.C., Scott, S.M., Cox, H.M., Voermans, N.C., Aziz, Q., Blackshaw, L.A., 2018. The extracellular matrix glycoprotein tenascin-X regulates peripheral sensory and motor neurones. J Physiol 596, 4237-4251.
- Aoki, S., Nagashima, K., Furuta, M., Makioka, K., Fujita, Y., Saito, K., Kashima, T., Nakajima, N., Ikota, H., Higuchi, O., Ikeda, Y., 2020. Anti-LRP4 Antibody-associated Myasthenia Gravis with a Rare Complication of Thymoma Successfully Treated by Thymectomy. Internal medicine (Tokyo, Japan) 59, 1219-1222.
- Asaro, A., Carlo-Spiewok, A.S., Malik, A.R., Rothe, M., Schipke, C.G., Peters, O., Heeren, J., Willnow, T.E., 2020. Apolipoprotein E4 disrupts the neuroprotective action of sortilin in neuronal lipid metabolism and endocannabinoid signaling. Alzheimer's & dementia : the journal of the Alzheimer's Association 16, 1248-1258.
- Balabanski, L., Serbezov, D., Atanasoska, M., Karachanak-Yankova, S., Hadjidekova, S., Nikolova, D., Boyanova, O., Staneva, R., Vazharova, R., Mihailova, M., Damyanova, V., Nesheva, D., Belejanska, D., Mehrabian, S., Traykov, L., Toncheva, D., 2021. Rare genetic variants prioritize molecular pathways for semaphorin interactions in Alzheimer's disease patients. Biotechnology & Biotechnological Equipment 35, 1256-1262.
- Baldin, A.V., Grishina, A.N., Korolev, D.O., Kuznetsova, E.B., Golovastova, M.O., Kalpinskiy, A.S., Alekseev, B.Y., Kaprin, A.D., Zinchenko, D.V., Savvateeva, L.V., Varshavsky, V.A., Zernii, E.Y., Vinarov, A.Z., Bazhin, A.V., Philippov, P.P., Zamyatnin, A.A., Jr., 2019. Autoantibody against arrestin-1 as a potential biomarker of renal cell carcinoma. Biochimie 157, 26-37.
- Bezawork-Geleta, A., Brodie, E.J., Dougan, D.A., Truscott, K.N., 2015. LON is the master protease that protects against protein aggregation in human mitochondria through direct degradation of misfolded proteins. Scientific reports 5, 17397.
- Boehm, V., Kueckelmann, S., Gerbracht, J.V., Kallabis, S., Britto-Borges, T., Altmüller, J., Krüger, M., Dieterich, C., Gehring, N.H., 2021. SMG5-SMG7 authorize nonsense-mediated mRNA decay by enabling SMG6 endonucleolytic activity. Nature communications 12, 3965.
- Bronner, I.F., Bochdanovits, Z., Rizzu, P., Kamphorst, W., Ravid, R., van Swieten, J.C., Heutink, P., 2009. Comprehensive mRNA expression profiling distinguishes tauopathies and identifies shared molecular pathways. PLoS ONE 4, e6826.
- Buechler, J., Salinas, P.C., 2018. Deficient Wnt Signaling and Synaptic Vulnerability in Alzheimer's Disease: Emerging Roles for the LRP6 Receptor. Frontiers in synaptic neuroscience 10, 38.
- Burk, K., Mire, E., Bellon, A., Hocine, M., Guillot, J., Moraes, F., Yoshida, Y., Simons, M., Chauvet, S., Mann, F., 2017. Post-endocytic sorting of Plexin-D1 controls signal transduction and development of axonal and vascular circuits. Nature communications 8, 14508.
- Cam, J.A., Zerbinatti, C.V., Knisely, J.M., Hecimovic, S., Li, Y., Bu, G., 2004. The low density lipoprotein receptor-related protein 1B retains beta-amyloid precursor protein at the cell surface and reduces amyloid-beta peptide production. J Biol Chem 279, 29639-29646.
- Chen, X.J., Xu, H., Cooper, H.M., Liu, Y., 2014. Cytoplasmic dynein: a key player in neurodegenerative and neurodevelopmental diseases. Science China. Life sciences 57, 372-377.
- Chiu, J.H., Tseng, L.M., Huang, T.T., Liu, C.Y., Wang, J.Y., Huang, C.P., Tsai, Y.F., Hsu, C.Y., 2020. MEGF11 is related to tumour recurrence in triple negative breast cancer via chemokine upregulation. Scientific reports 10, 8060.
- Choi, J.H., Sullivan, C.S., 2021. DUSP11 and triphosphate RNA balance during virus infection. PLoS Pathog 17, e1009145.
- Choi, S.-H., Koh, D.-I., Ahn, H., Kim, J.Y., Kim, Y., Hur, M.-W., 2020. Cell fate decisions by c-Myc depend on ZBTB5 and p53. Biochemical and Biophysical Research Communications 533, 1247-1254.
- Choi, S.H., Estarás, C., Moresco, J.J., Yates, J.R., 3rd, Jones, K.A., 2013. α-Catenin interacts with APC to regulate β-catenin proteolysis and transcriptional repression of Wnt target genes. Genes Dev 27, 2473-2488.
- Chow, H.M., Sun, J.K., Hart, R.P., Cheng, K.K., Hung, C.H.L., Lau, T.M., Kwan, K.M., 2021. Low-Density Lipoprotein Receptor-Related Protein 6 Cell Surface Availability Regulates Fuel Metabolism in Astrocytes. Advanced science (Weinheim, Baden-Wurttemberg, Germany) 8, e2004993.
- Crepaldi, L., Policarpi, C., Coatti, A., Sherlock, W.T., Jongbloets, B.C., Down, T.A., Riccio, A., 2013. Binding of TFIIIC to sine elements controls the relocation of activity-dependent neuronal genes to transcription factories. PLoS genetics 9, e1003699.
- Cronin, P., McCarthy, M.J., Lim, A.S.P., Salmon, D.P., Galasko, D., Masliah, E., De Jager, P.L., Bennett, D.A., Desplats, P., 2017. Circadian alterations during early stages of Alzheimer's disease are associated with aberrant cycles of DNA methylation in BMAL1. Alzheimer's & dementia : the journal of the Alzheimer's Association 13, 689-700.
- Ding, J.B., Oh, W.J., Sabatini, B.L., Gu, C., 2011. Semaphorin 3E-Plexin-D1 signaling controls pathway-specific synapse formation in the striatum. Nat Neurosci 15, 215-223.

- Donkor, F.F., Mönnich, M., Czirr, E., Hollemann, T., Hoyer-Fender, S., 2004. Outer dense fibre protein 2 (ODF2) is a self-interacting centrosomal protein with affinity for microtubules. J Cell Sci 117, 4643-4651.
- Fan, L., Wang, J., Deng, P., Wang, Y., Zhang, A., Yang, M., Zeng, G., 2022. Foxhead box D1 promotes the partial epithelial-to-mesenchymal transition of laryngeal squamous cell carcinoma cells via transcriptionally activating the expression of zinc finger protein 532. Bioengineered 13, 3057-3069.
- Fernández-de Frutos, M., Galán-Chilet, I., Goedeke, L., Kim, B., Pardo-Marqués, V., Pérez-García, A., Herrero, J.I., Fernández-Hernando, C., Kim, J., Ramírez, C.M., 2019. MicroRNA 7 Impairs Insulin Signaling and Regulates Aβ Levels through Posttranscriptional Regulation of the Insulin Receptor Substrate 2, Insulin Receptor, Insulin-Degrading Enzyme, and Liver X Receptor Pathway. Mol Cell Biol 39.
- Finelli, M.J., Oliver, P.L., 2017. TLDc proteins: new players in the oxidative stress response and neurological disease. Mamm Genome 28, 395-406.
- Fontanil, T., Mohamedi, Y., Esteban, M.M., Obaya, A.J., Cal, S., 2014. Polyserase-1/TMPRSS9 induces pro-tumor effects in pancreatic cancer cells by activation of pro-uPA. Oncol Rep 31, 2792-2796.
- Ganji, R., Mukkavalli, S., Somanji, F., Raman, M., 2018. The VCP-UBXN1 Complex Mediates Triage of Ubiquitylated Cytosolic Proteins Bound to the BAG6 Complex. Mol Cell Biol 38.
- Gomez, A.M., Froemke, R.C., Burden, S.J., 2014. Synaptic plasticity and cognitive function are disrupted in the absence of Lrp4. eLife 3, e04287.
- Gorgoglione, R., Porcelli, V., Santoro, A., Daddabbo, L., Vozza, A., Monné, M., Di Noia, M.A., Palmieri, L., Fiermonte, G., Palmieri, F., 2019. The human uncoupling proteins 5 and 6 (UCP5/SLC25A14 and UCP6/SLC25A30) transport sulfur oxyanions, phosphate and dicarboxylates. Biochimica et Biophysica Acta (BBA) - Bioenergetics 1860, 724-733.
- Haas, J., Beer, A.G., Widschwendter, P., Oberdanner, J., Salzmann, K., Sarg, B., Lindner, H., Herz, J., Patsch, J.R., Marschang, P., 2011. LRP1b shows restricted expression in human tissues and binds to several extracellular ligands, including fibrinogen and apoE-carrying lipoproteins. Atherosclerosis 216, 342-347.
- Hancock-Cerutti, W., Wu, Z., Xu, P., Yadavalli, N., Leonzino, M., Tharkeshwar, A.K., Ferguson, S.M., Shadel, G.S., De Camilli, P., 2022. ER-lysosome lipid transfer protein VPS13C/PARK23 prevents aberrant mtDNA-dependent STING signaling. J Cell Biol 221.
- Hashida, H., Goto, J., Zhao, N., Takahashi, N., Hirai, M., Kanazawa, I., Sakaki, Y., 1998. Cloning and mapping of ZNF231, a novel brain-specific gene encoding neuronal double zinc finger protein whose expression is enhanced in a neurodegenerative disorder, multiple system atrophy (MSA). Genomics 54, 50-58.
- Heinz, L.X., Baumann, C.L., Köberlin, M.S., Snijder, B., Gawish, R., Shui, G., Sharif, O., Aspalter, I.M., Müller, A.C., Kandasamy, R.K., Breitwieser, F.P., Pichlmair, A., Bruckner, M., Rebsamen, M., Blüml, S., Karonitsch, T., Fauster, A., Colinge, J., Bennett, K.L., Knapp, S., Wenk, M.R., Superti-Furga, G., 2015. The Lipid-Modifying Enzyme SMPDL3B Negatively Regulates Innate Immunity. Cell reports 11, 1919-1928.
- Hook, S.C., Chadt, A., Heesom, K.J., Kishida, S., Al-Hasani, H., Tavaré, J.M., Thomas, E.C., 2020. TBC1D1 interacting proteins, VPS13A and VPS13C, regulate GLUT4 homeostasis in C2C12 myotubes. Scientific reports 10, 17953.
- Hu, R., Peng, G., Dai, H., Breuer, E.K., Stemke-Hale, K., Li, K., Gonzalez-Angulo, A.M., Mills, G.B., Lin, S.Y., 2011. ZNF668 functions as a tumor suppressor by regulating p53 stability and function in breast cancer. Cancer Res 71, 6524-6534.
- Hu, X., Hu, Z.L., Li, Z., Ruan, C.S., Qiu, W.Y., Pan, A., Li, C.Q., Cai, Y., Shen, L., Chu, Y., Tang, B.S., Cai, H., Zhou, X.F., Ma, C., Yan, X.X., 2017a. Sortilin Fragments Deposit at Senile Plaques in Human Cerebrum. Frontiers in neuroanatomy 11, 45.
- Hu, Y., O'Boyle, K., Auer, J., Raju, S., You, F., Wang, P., Fikrig, E., Sutton, R.E., 2017b. Multiple UBXN family members inhibit retrovirus and lentivirus production and canonical NFκB signaling by stabilizing IκBα. PLoS Pathog 13, e1006187.
- Huang, Y., Yin, H., Li, B., Wu, Q., Liu, Y., Poljak, K., Maldutyte, J., Tang, X., Wang, M., Wu, Z., Miller, E.A., Jiang, L., Yao, Z.P., Guo, Y., 2021. An in vitro vesicle formation assay reveals cargo clients and factors that mediate vesicular trafficking. Proc Natl Acad Sci U S A 118.
- Hulme, B., Didikoglu, A., Bradburn, S., Robinson, A., Canal, M., Payton, A., Pendleton, N., Murgatroyd, C., 2020. Epigenetic Regulation of BMAL1 with Sleep Disturbances and Alzheimer's Disease. Journal of Alzheimer's Disease 77, 1783-1792.
- Iram, T., Kern, F., Kaur, A., Myneni, S., Morningstar, A.R., Shin, H., Garcia, M.A., Yerra, L., Palovics, R., Yang, A.C., Hahn, O., Lu, N., Shuken, S.R., Haney, M.S., Lehallier, B., Iyer, M., Luo, J., Zetterberg, H., Keller, A., Zuchero, J.B., Wyss-Coray, T., 2022. Young CSF restores oligodendrogenesis and memory in aged mice via Fgf17. Nature 605, 509-515.
- Jakobs, P., Exner, S., Schürmann, S., Pickhinke, U., Bandari, S., Ortmann, C., Kupich, S., Schulz, P., Hansen, U., Seidler, D.G., Grobe, K., 2014. Scube2 enhances proteolytic Shh processing from the surface of Shh-producing cells. J Cell Sci 127, 1726-1737.
- Jovov, B., Araujo-Perez, F., Sigel, C.S., Stratford, J.K., McCoy, A.N., Yeh, J.J., Keku, T., 2012. Differential gene expression between African American and European American colorectal cancer patients. PLoS ONE 7, e30168.
- Kay, J.N., Chu, M.W., Sanes, J.R., 2012. MEGF10 and MEGF11 mediate homotypic interactions required for mosaic spacing of retinal neurons. Nature 483, 465-469.

- Khundadze, M., Kollmann, K., Koch, N., Biskup, C., Nietzsche, S., Zimmer, G., Hennings, J.C., Huebner, A.K., Symmank, J., Jahic, A., Ilina, E.I., Karle, K., Schöls, L., Kessels, M., Braulke, T., Qualmann, B., Kurth, I., Beetz, C., Hübner, C.A., 2013. A hereditary spastic paraplegia mouse model supports a role of ZFYVE26/SPASTIZIN for the endolysosomal system. PLoS genetics 9, e1003988.
- Kim, H.J., Taylor, J.P., 2017. Lost in Transportation: Nucleocytoplasmic Transport Defects in ALS and Other Neurodegenerative Diseases. Neuron 96, 285-297.
- Kim, N., Stiegler, A.L., Cameron, T.O., Hallock, P.T., Gomez, A.M., Huang, J.H., Hubbard, S.R., Dustin, M.L., Burden, S.J., 2008. Lrp4 is a receptor for Agrin and forms a complex with MuSK. Cell 135, 334-342.
- Koh, D.I., Choi, W.I., Jeon, B.N., Lee, C.E., Yun, C.O., Hur, M.W., 2009. A novel POK family transcription factor, ZBTB5, represses transcription of p21CIP1 gene. J Biol Chem 284, 19856-19866.
- Kumar, N., Leonzino, M., Hancock-Cerutti, W., Horenkamp, F.A., Li, P., Lees, J.A., Wheeler, H., Reinisch, K.M., De Camilli, P., 2018. VPS13A and VPS13C are lipid transport proteins differentially localized at ER contact sites. J Cell Biol 217, 3625-3639.
- Lee, M., Liu, Y.C., Chen, C., Lu, C.H., Lu, S.T., Huang, T.N., Hsu, M.T., Hsueh, Y.P., Cheng, P.L., 2020. Ecm29-mediated proteasomal distribution modulates excitatory GABA responses in the developing brain. J Cell Biol 219.
- Luqman-Fatah, A., Watanabe, Y., Uno, K., Ishikawa, F., Moran, J.V., Miyoshi, T., 2023. The interferon stimulated gene-encoded protein HELZ2 inhibits human LINE-1 retrotransposition and LINE-1 RNA-mediated type I interferon induction. Nature communications 14, 203.
- Ma, X., Fan, M., Yang, K., Wang, Y., Hu, R., Guan, M., Hou, Y., Ying, J., Deng, N., Li, Q., Jiang, G., Zhang, Y., Zhang, X., 2023. ZNF500 abolishes breast cancer proliferation and sensitizes chemotherapy by stabilizing P53 via competing with MDM2. Cancer Sci 114, 4237-4251.
- Maziuk, B.F., Apicco, D.J., Cruz, A.L., Jiang, L., Ash, P.E.A., da Rocha, E.L., Zhang, C., Yu, W.H., Leszyk, J., Abisambra, J.F., Li, H., Wolozin, B., 2018. RNA binding proteins co-localize with small tau inclusions in tauopathy. Acta Neuropathologica Communications 6, 71.
- McGrath, J.A., McMillan, J.R., Shemanko, C.S., Runswick, S.K., Leigh, I.M., Lane, E.B., Garrod, D.R., Eady, R.A., 1997. Mutations in the plakophilin 1 gene result in ectodermal dysplasia/skin fragility syndrome. Nat Genet 17, 240-244.
- Mi, Z., Halfter, W., Abrahamson, E.E., Klunk, W.E., Mathis, C.A., Mufson, E.J., Ikonomovic, M.D., 2016. Tenascin-C Is Associated with Cored Amyloid-β Plaques in Alzheimer Disease and Pathology Burdened Cognitively Normal Elderly. J Neuropathol Exp Neurol 75, 868-876.
- Mitrofanova, A., Mallela, S.K., Ducasa, G.M., Yoo, T.H., Rosenfeld-Gur, E., Zelnik, I.D., Molina, J., Varona Santos, J., Ge, M., Sloan, A., Kim, J.J., Pedigo, C., Bryn, J., Volosenco, I., Faul, C., Zeidan, Y.H., Garcia Hernandez, C., Mendez, A.J., Leibiger, I., Burke, G.W., Futerman, A.H., Barisoni, L., Ishimoto, Y., Inagi, R., Merscher, S., Fornoni, A., 2019. SMPDL3b modulates insulin receptor signaling in diabetic kidney disease. Nature communications 10, 2692.
- Nagasawa, C.K., Bailey, A.O., Russell, W., Garcia-Blanco, M.A., 2024. Inefficient recruitment of DDX39B impedes pre-spliceosome assembly on FOXP3 introns. RNA (New York, N.Y.).
- Neuhoff, H., Sassoè-Pognetto, M., Panzanelli, P., Maas, C., Witke, W., Kneussel, M., 2005. The actin-binding protein profilin I is localized at synaptic sites in an activity-regulated manner. The European journal of neuroscience 21, 15-25.
- Ngora, H., Galli, U.M., Miyazaki, K., Zöller, M., 2012. Membrane-bound and exosomal metastasis-associated C4.4A promotes migration by associating with the α(6)β(4) integrin and MT1-MMP. Neoplasia 14, 95-107.
- Ochiai, T., Sano, T., Nagayama, T., Kubota, N., Kadowaki, T., Wakabayashi, T., Iwatsubo, T., 2021. Differential involvement of insulin receptor substrate (IRS)-1 and IRS-2 in brain insulin signaling is associated with the effects on amyloid pathology in a mouse model of Alzheimer's disease. Neurobiology of Disease 159, 105510.
- Okuda-Ashitaka, E., Matsumoto, K.I., 2023. Tenascin-X as a causal gene for classical-like Ehlers-Danlos syndrome. Front Genet 14, 1107787.
- Osma-Garcia, I.C., Mouysset, M., Capitan-Sobrino, D., Aubert, Y., Turner, M., Diaz-Muñoz, M.D., 2023. The RNA binding proteins TIA1 and TIAL1 promote Mcl1 mRNA translation to protect germinal center responses from apoptosis. Cellular & molecular immunology 20, 1063-1076.
- Pecho-Vrieseling, E., Sigrist, M., Yoshida, Y., Jessell, T.M., Arber, S., 2009. Specificity of sensory-motor connections encoded by Sema3e-Plxnd1 recognition. Nature 459, 842-846.
- Pohlkamp, T., Durakoglugil, M., Lane-Donovan, C., Xian, X., Johnson, E.B., Hammer, R.E., Herz, J., 2015. Lrp4 domains differentially regulate limb/brain development and synaptic plasticity. PLoS ONE 10, e0116701.
- Prasanth, M.I., Malar, D.S., Tencomnao, T., Brimson, J.M., 2021. The emerging role of the sigma-1 receptor in autophagy: hand-in-hand targets for the treatment of Alzheimer's. Expert Opin Ther Targets 25, 401-414.
- Ramsden, D.B., Ho, P.W., Ho, J.W., Liu, H.F., So, D.H., Tse, H.M., Chan, K.H., Ho, S.L., 2012. Human neuronal uncoupling proteins 4 and 5 (UCP4 and UCP5): structural properties, regulation, and physiological role in protection against oxidative stress and mitochondrial dysfunction. Brain and behavior 2, 468-478.

- Rasul, F., Zheng, F., Dong, F., He, J., Liu, L., Liu, W., Cheema, J.Y., Wei, W., Fu, C., 2021. Emr1 regulates the number of foci of the endoplasmic reticulum-mitochondria encounter structure complex. Nature communications 12, 521.
- Real, R., Martinez-Carrasco, A., Reynolds, R.H., Lawton, M.A., Tan, M.M.X., Shoai, M., Corvol, J.-C., Ryten, M., Bresner, C., Hubbard, L., Brice, A., Lesage, S., Faouzi, J., Elbaz, A., Artaud, F., Williams, N., Hu, M.T.M., Ben-Shlomo, Y., Grosset, D.G., Hardy, J., Morris, H.R., 2022. Association between the LRP1B and APOE loci and the development of Parkinson's disease dementia. Brain 146, 1873-1887.
- Ren, X., Lin, Z., Yuan, W., 2022. A Structural and Functional Perspective of Death Receptor 6. Frontiers in pharmacology 13, 836614.
- Ruan, C.S., Liu, J., Yang, M., Saadipour, K., Zeng, Y.Q., Liao, H., Wang, Y.J., Bobrovskaya, L., Zhou, X.F., 2018. Sortilin inhibits amyloid pathology by regulating non-specific degradation of APP. Exp Neurol 299, 75-85.
- Saadipour, K., Yang, M., Lim, Y., Georgiou, K., Sun, Y., Keating, D., Liu, J., Wang, Y.R., Gai, W.P., Zhong, J.H., Wang, Y.J., Zhou, X.F., 2013. Amyloid beta$_{1-42}$ (Aβ_{42}) up-regulates the expression of sortilin via the p75(NTR)/RhoA signaling pathway. J Neurochem 127, 152-162.
- Sano, T., Ochiai, T., Nagayama, T., Nakamura, A., Kubota, N., Kadowaki, T., Wakabayashi, T., Iwatsubo, T., 2023. Genetic Reduction of Insulin Signaling Mitigates Amyloid-β Deposition by Promoting Expression of Extracellular Matrix Proteins in the Brain. J Neurosci 43, 7226-7241.
- Schaffer, A.E., Pinkard, O., Coller, J.M., 2019. tRNA Metabolism and Neurodevelopmental Disorders. Annual review of genomics and human genetics 20, 359-387.
- Schmidt, H., Carter, A.P., 2016. Review: Structure and mechanism of the dynein motor ATPase. Biopolymers 105, 557-567.
- Schubert, M., Brazil, D.P., Burks, D.J., Kushner, J.A., Ye, J., Flint, C.L., Farhang-Fallah, J., Dikkes, P., Warot, X.M., Rio, C., Corfas, G., White, M.F., 2003. Insulin receptor substrate-2 deficiency impairs brain growth and promotes tau phosphorylation. J Neurosci 23, 7084-7092.
- Soares, H.D., Potter, W.Z., Pickering, E., Kuhn, M., Immermann, F.W., Shera, D.M., Ferm, M., Dean, R.A., Simon, A.J., Swenson, F., Siuciak, J.A., Kaplow, J., Thambisetty, M., Zagouras, P., Koroshetz, W.J., Wan, H.I., Trojanowski, J.Q., Shaw, L.M., 2012. Plasma biomarkers associated with the apolipoprotein E genotype and Alzheimer disease. Archives of neurology 69, 1310-1317.
- Tracy, T.E., Madero-Pérez, J., Swaney, D.L., Chang, T.S., Moritz, M., Konrad, C., Ward, M.E., Stevenson, E., Hüttenhain, R., Kauwe, G., Mercedes, M., Sweetland-Martin, L., Chen, X., Mok, S.A., Wong, M.Y., Telpoukhovskaia, M., Min, S.W., Wang, C., Sohn, P.D., Martin, J., Zhou, Y., Luo, W., Trojanowski, J.Q., Lee, V.M.Y., Gong, S., Manfredi, G., Coppola, G., Krogan, N.J., Geschwind, D.H., Gan, L., 2022. Tau interactome maps synaptic and mitochondrial processes associated with neurodegeneration. Cell 185, 712-728.e714.
- Unterholzner, L., Izaurralde, E., 2004. SMG7 acts as a molecular link between mRNA surveillance and mRNA decay. Mol Cell 16, 587-596.
- van Oers, J.M., Roa, S., Werling, U., Liu, Y., Genschel, J., Hou, H., Jr., Sellers, R.S., Modrich, P., Scharff, M.D., Edelmann, W., 2010. PMS2 endonuclease activity has distinct biological functions and is essential for genome maintenance. Proc Natl Acad Sci U S A 107, 13384-13389.
- Vanderweyde, T., Apicco, D.J., Youmans-Kidder, K., Ash, P.E.A., Cook, C., Lummertz da Rocha, E., Jansen-West, K., Frame, A.A., Citro, A., Leszyk, J.D., Ivanov, P., Abisambra, J.F., Steffen, M., Li, H., Petrucelli, L., Wolozin, B., 2016. Interaction of tau with the RNA-Binding Protein TIA1 Regulates tau Pathophysiology and Toxicity. Cell reports 15, 1455-1466.
- Vantaggiato, C., Panzeri, E., Castelli, M., Citterio, A., Arnoldi, A., Santorelli, F.M., Liguori, R., Scarlato, M., Musumeci, O., Toscano, A., Clementi, E., Bassi, M.T., 2019. ZFYVE26/SPASTIZIN and SPG11/SPATACSIN mutations in hereditary spastic paraplegia types AR-SPG15 and AR-SPG11 have different effects on autophagy and endocytosis. Autophagy 15, 34-57.
- Velez, G., Roybal, C.N., Colgan, D., Tsang, S.H., Bassuk, A.G., Mahajan, V.B., 2016. Precision Medicine: Personalized Proteomics for the Diagnosis and Treatment of Idiopathic Inflammatory Disease. JAMA ophthalmology 134, 444-448.
- Vieira, N., Rito, T., Correia-Neves, M., Sousa, N., 2021. Sorting Out Sorting Nexins Functions in the Nervous System in Health and Disease. Molecular Neurobiology 58, 4070-4106.
- Wang, F., Eagleson, K.L., Levitt, P., 2015. Positive regulation of neocortical synapse formation by the Plexin-D1 receptor. Brain Research 1616, 157-165.
- Wang, H., Dey, K.K., Chen, P.C., Li, Y., Niu, M., Cho, J.H., Wang, X., Bai, B., Jiao, Y., Chepyala, S.R., Haroutunian, V., Zhang, B., Beach, T.G., Peng, J., 2020. Integrated analysis of ultra-deep proteomes in cortex, cerebrospinal fluid and serum reveals a mitochondrial signature in Alzheimer's disease. Mol Neurodegener 15, 43.
- Wang, X., Chemmama, I.E., Yu, C., Huszagh, A., Xu, Y., Viner, R., Block, S.A., Cimermancic, P., Rychnovsky, S.D., Ye, Y., Sali, A., Huang, L., 2017. The proteasome-interacting Ecm29 protein disassembles the 26S proteasome in response to oxidative stress. J Biol Chem 292, 16310-16320.
- Weskamp, K., Barmada, S.J., 2018. RNA Degradation in Neurodegenerative Disease. Advances in neurobiology 20, 103-142.
- Whitehead, K.J., Chan, A.C., Navankasattusas, S., Koh, W., London, N.R., Ling, J., Mayo, A.H., Drakos, S.G., Jones, C.A., Zhu, W., Marchuk, D.A., Davis, G.E., Li, D.Y., 2009. The cerebral cavernous malformation signaling pathway promotes vascular integrity via Rho GTPases. Nature medicine 15, 177-184.
- Wood, H., 2023. WNT receptor variant linked to synaptic degeneration. Nature Reviews Neurology 19, 129-129.

- Yan, J., Li, Q., Mao, A.P., Hu, M.M., Shu, H.B., 2014. TRIM4 modulates type I interferon induction and cellular antiviral response by targeting RIG-I for K63-linked ubiquitination. J Mol Cell Biol 6, 154-163.
- Yuki, R., Aoyama, K., Kubota, S., Yamaguchi, N., Kubota, S., Hasegawa, H., Morii, M., Huang, X., Liu, K., Williams, R., Fukuda, M.N., Yamaguchi, N., 2015. Overexpression of zinc-finger protein 777 (ZNF777) inhibits proliferation at low cell density through down-regulation of FAM129A. J Cell Biochem 116, 954-968.
- Zhang, H., Chen, W., Tan, Z., Zhang, L., Dong, Z., Cui, W., Zhao, K., Wang, H., Jing, H., Cao, R., Kim, C., Safar, J.G., Xiong, W.C., Mei, L., 2020. A Role of Low-Density Lipoprotein Receptor-Related Protein 4 (LRP4) in Astrocytic Aβ Clearance. J Neurosci 40, 5347-5361.
- Zhao, S., Lu, J., Pan, B., Fan, H., Byrum, S.D., Xu, C., Kim, A., Guo, Y., Kanchi, K.L., Gong, W., Sun, T., Storey, A.J., Burkholder, N.T., Mackintosh, S.G., Kuhlers, P.C., Edmondson, R.D., Strahl, B.D., Diao, Y., Tackett, A.J., Raab, J.R., Cai, L., Song, J., Wang, G.G., 2023. TNRC18 engages H3K9me3 to mediate silencing of endogenous retrotransposons. Nature 623, 633-642.

Supplementary Figure 1. Pairwise scatter plots of the raw data after between array and compositional bias (dependence on charge, hydrophobicity, etc. general physicochemical properties of the residues) normalization.

Supplementary Figure 2. Cross-reactivity graph spectral embeddings for the IgM (left) and the IgG (center) graphs. The embedding uses the eigenvectors of the graph Laplacian that correspond to the smallest eigenvalues with a cut off based on irregular increase in the ordered eigenvalues (right) – 4 dimensions for IgM and five dimensions for IgG. The exact position of the vertices in the two-dimensional projections is derived by UMAP transformation from 4 (5) dimensions to two dimensions. The vertices are color-coded with high values corresponding to the high expression in the respective diagnosis. The values mapped to them in this way correspond to the levels of reactivity as sums of the ranks of the indicated samples by group (AD, FTD, ND, and control - C), or to the number of nearest neighbors among the idiotopes. The edges inherit their color from their incident vertices by averaging. A clear separation is observed between the reactivities higher in the C vs those higher in AD or FTD. ND related reactivities differ from all.

Supplementary Figure 3. Degree distribution for the IgM/IgG graphs compared to the distributions of 100 graphs generated after scrambling the respective raw data matrices. The graphs have degree distribution drawn to the right, which corresponds to their higher the density as compared to randomly generated graphs.

Supplementary Figure 4. Maximal clique size distribution for the IgM and IgG graphs compared to the distributions of 100 graphs generated after scrambling the respective raw data matrices. The graphs have the same size but more cliques as compared to randomly generated graphs.

Supplementary Figure 5. Venn diagram of the overlap between the ultimate cluster groups defined by the type of significant changes in the different diagnoses (annotation example: C>F.A ND>A:IgM – the reactivity in the controls is higher than that in FTD and AD plus NDD is only higher than AD, an IgM set clusters). The numbers indicate the number of mimotopes in this section. Some overlaps are between opposing characteristics, respectively from the IgM and the IgG sets (e.g. – some reactivities higher in FTD and NDD relative to the controls in IgG are found also in the group with the opposite ratios in IgM).

The supplementary files IgM_AD_FTD_NDD_C.mp4 and IgG_AD_FTD_NDD_C.mp4 visualize 3D embedding of the files in motion. The color code is mapping the rank sums by diagnosis AD, FTD and NDD scaled respectively as the red, green and blue components of the color while the luminosity codes for the reciprocal of the rank sum of the controls. Thus, the darker or black vertices correspond to reactivities found high in the controls but lost in the neurodegenerative diseases. In the IgM graph a considerable portion of the vertices with very light colors (reactivities not found in the controls) are colored red and green yielding a spectrum of predominantly yellow hues – the overlap of AD and FTD associated reactivities. In the IgG graph AD and FTD reactivities are separated in bright red and green clusters.

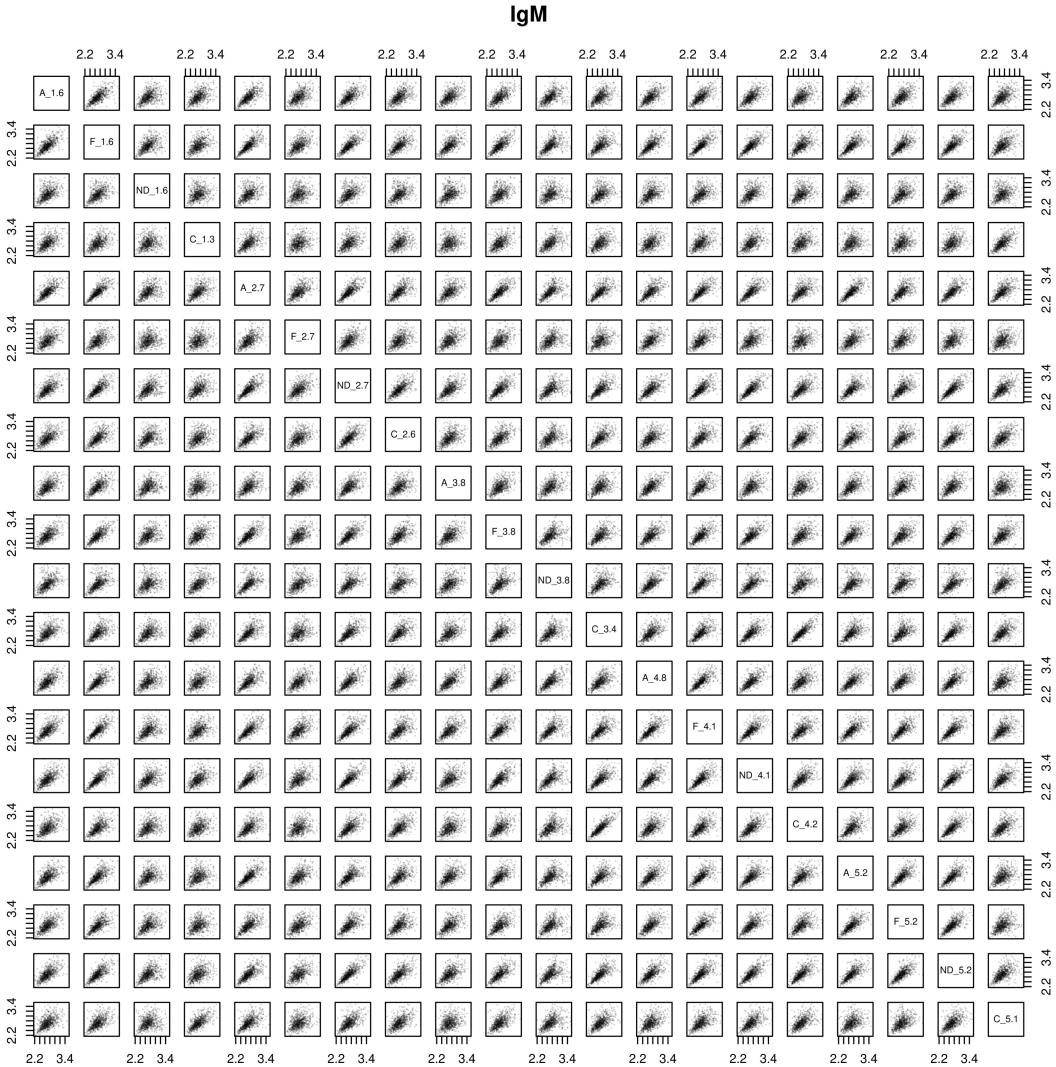
IgM
A_1.6
F_1.6
ND_1.6
C_1.3
A_2.7
F_2.7
ND_2.7
C_2.6
A_3.8
F_3.8
ND_3.8
C_3.4
A_4.8
F_4.1
ND_4.1
C_4.2
A_5.2
F_5.2
ND_5.2
C_5.1
2.2 3.4

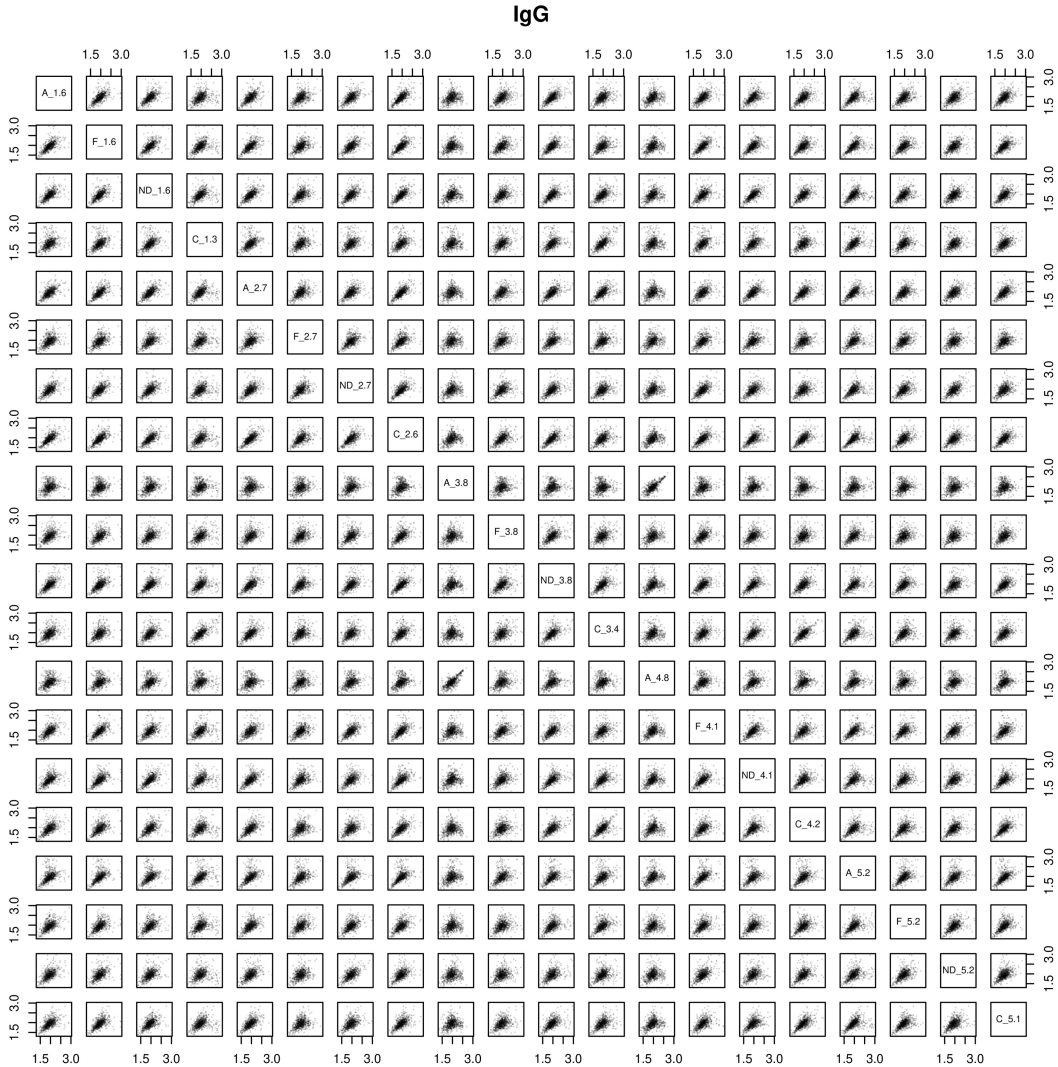
IgG
A_1.6
F_1.6
ND_1.6
C_1.3
A_2.7
F_2.7
ND_2.7
C_2.6
A_3.8
F_3.8
ND_3.8
C_3.4
A_4.8
F_4.1
ND_4.1
C_4.2
A_5.2
F_5.2
ND_5.2
C_5.1
1.5 3.0

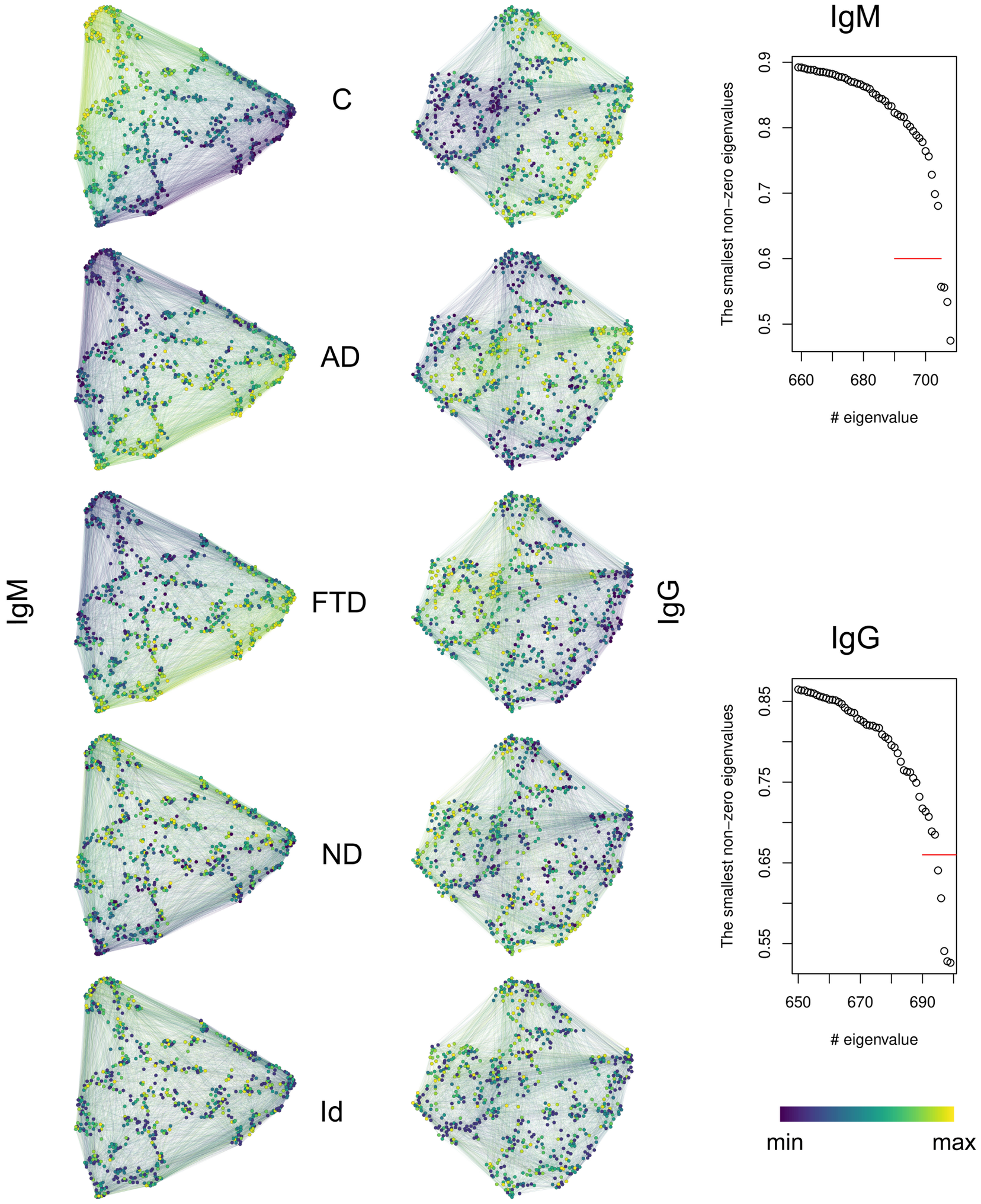
IgM
C
AD
FTD
ND
Id
IgG
IgM
The smallest non−zero eigenvalues
0.9
0.8
0.7
0.6
0.5
660
680
700
eigenvalue
IgG
The smallest non−zero eigenvalues
0.85
0.75
0.65
0.55
650
670
690
eigenvalue
min
max

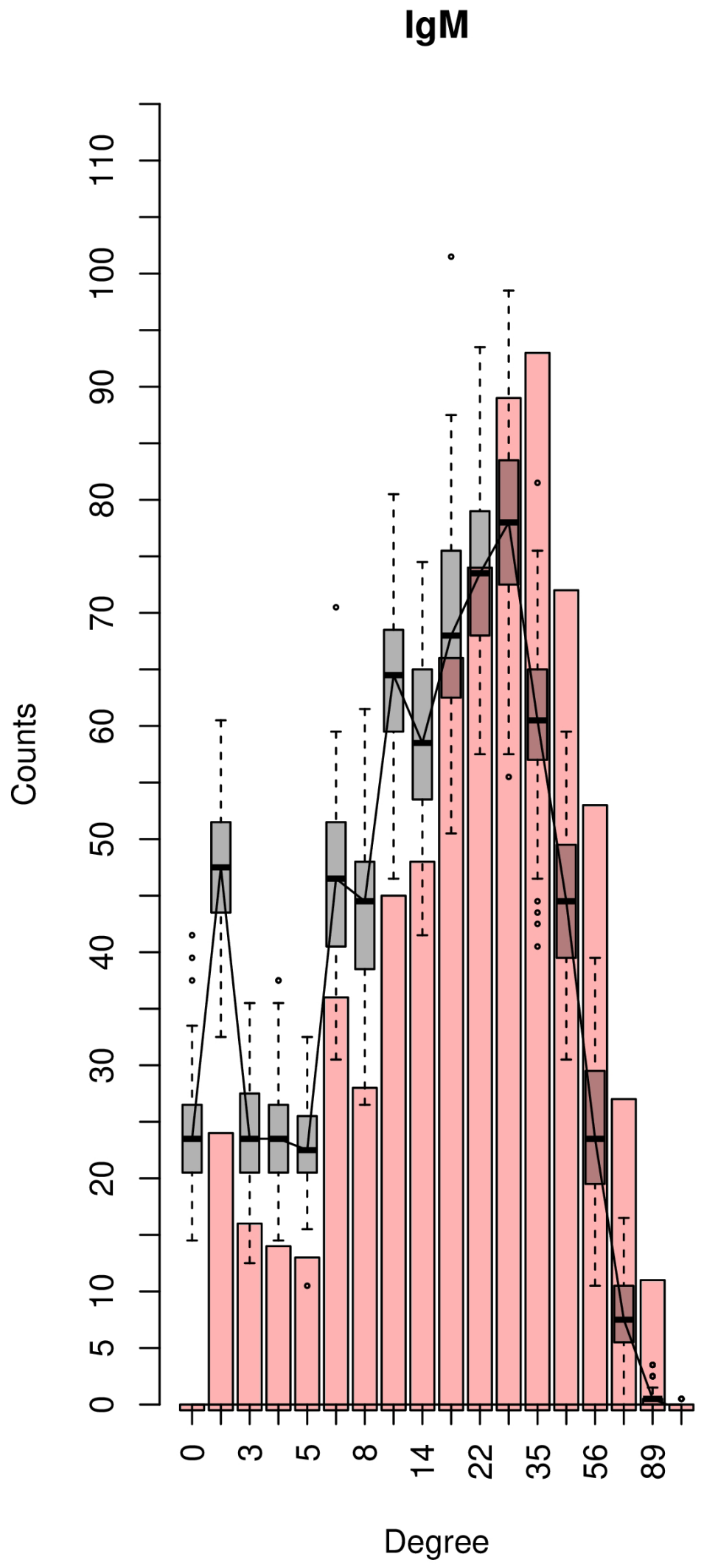
IgM
Counts
0
5
10
20
30
40
50
60
70
80
90
100
110
0
3
5
8
14
22
35
56
89
Degree

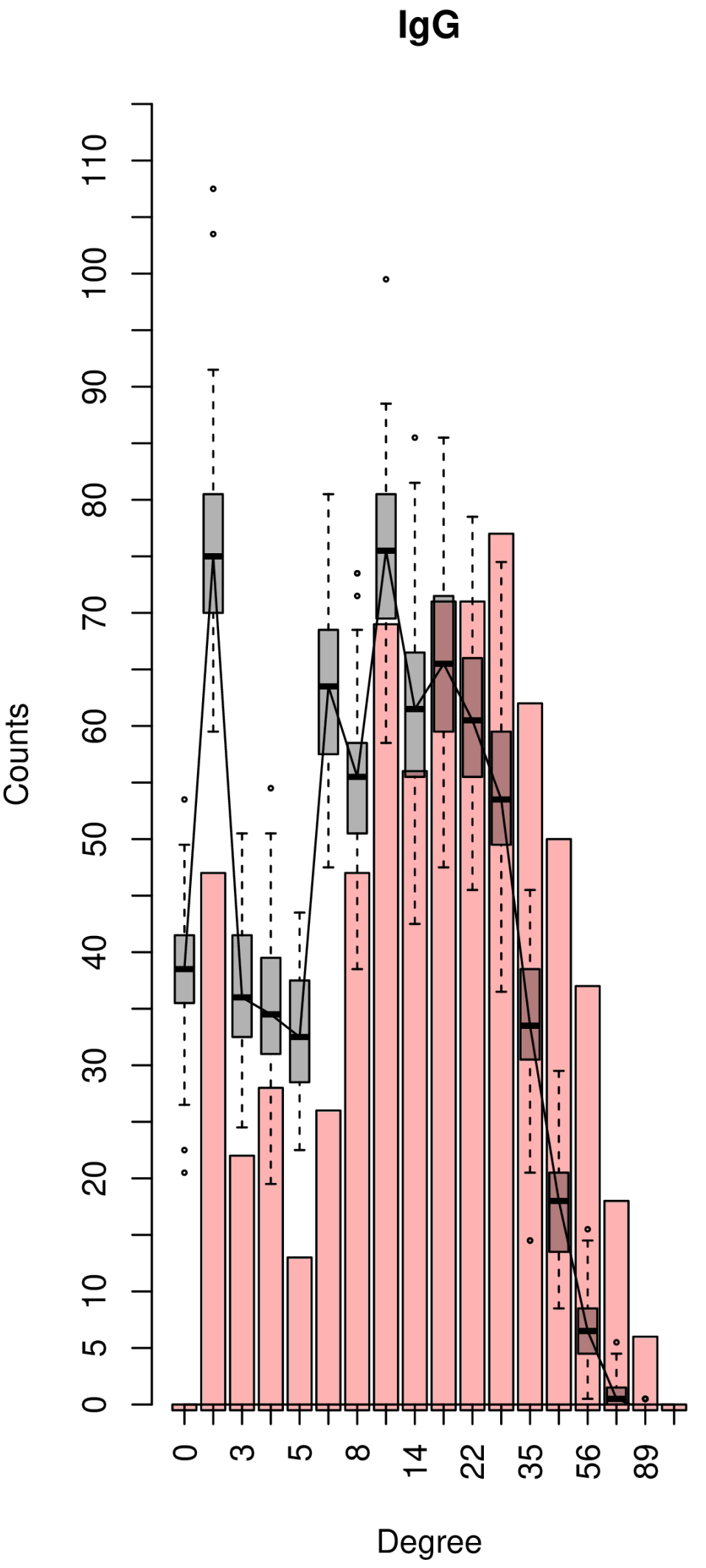
IgG
Counts
0
5
10
20
30
40
50
60
70
80
90
100
110
0
3
5
8
14
22
35
56
89
Degree

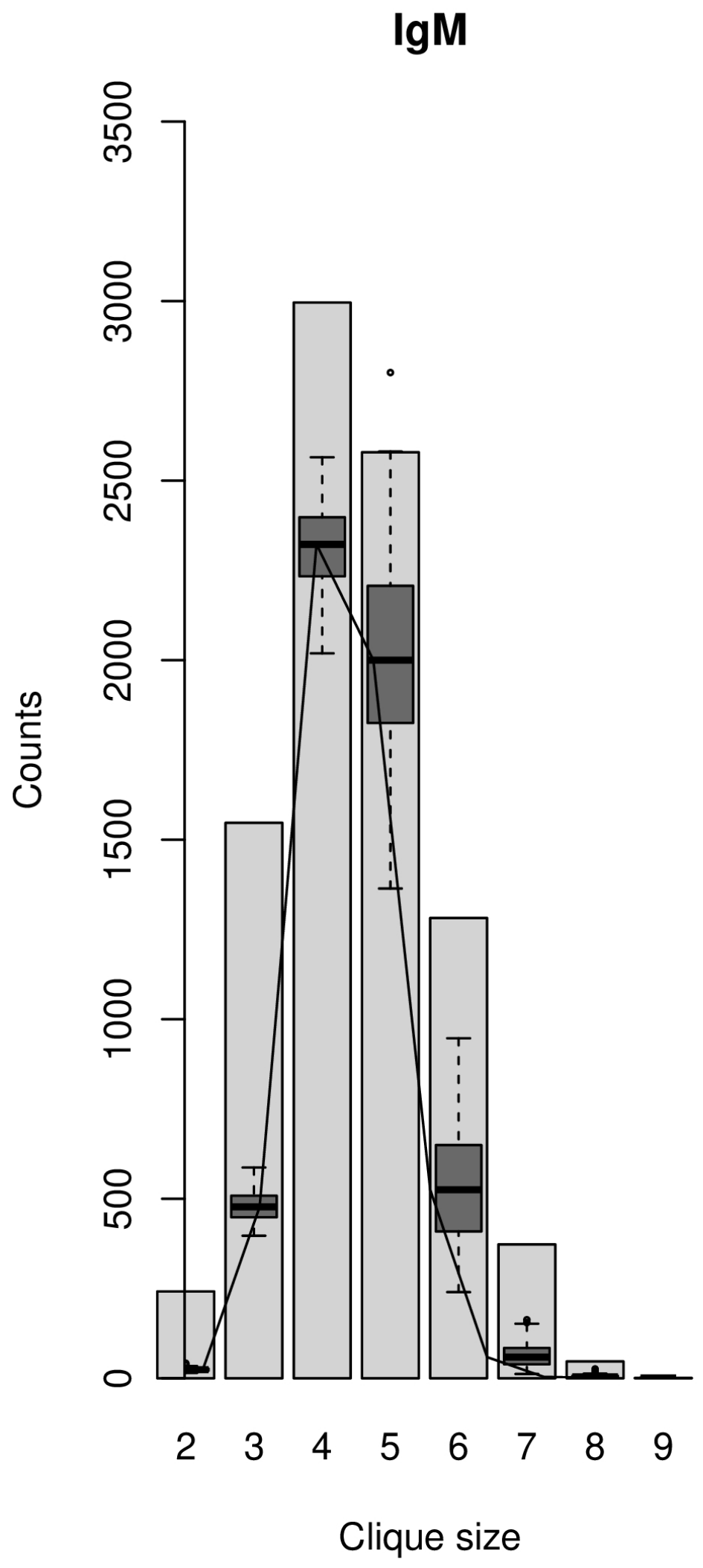
IgM
Counts
0
500
1000
1500
2000
2500
3000
3500
2
3
4
5
6
7
8
9
Clique size

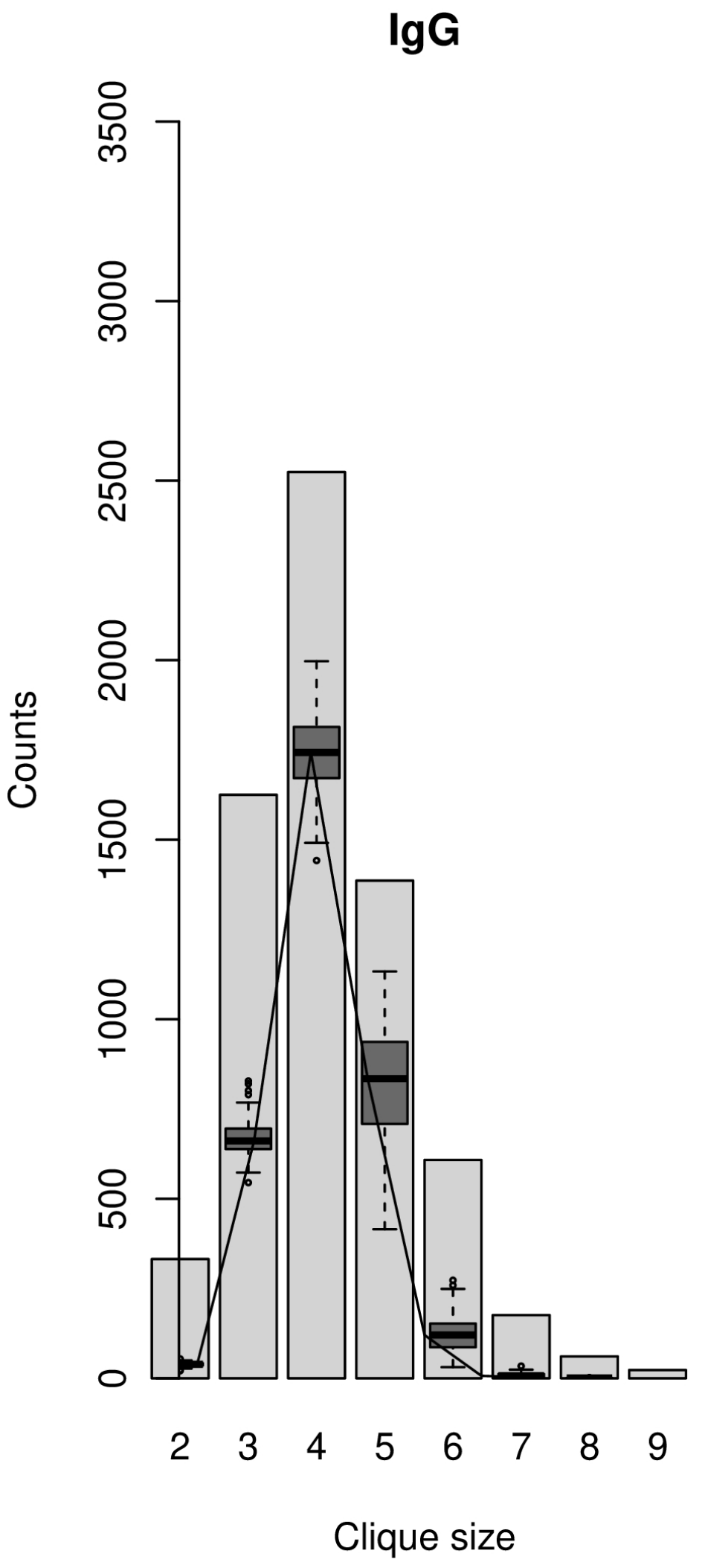
IgG
Counts
0
500
1000
1500
2000
2500
3000
3500
2
3
4
5
6
7
8
9
Clique size

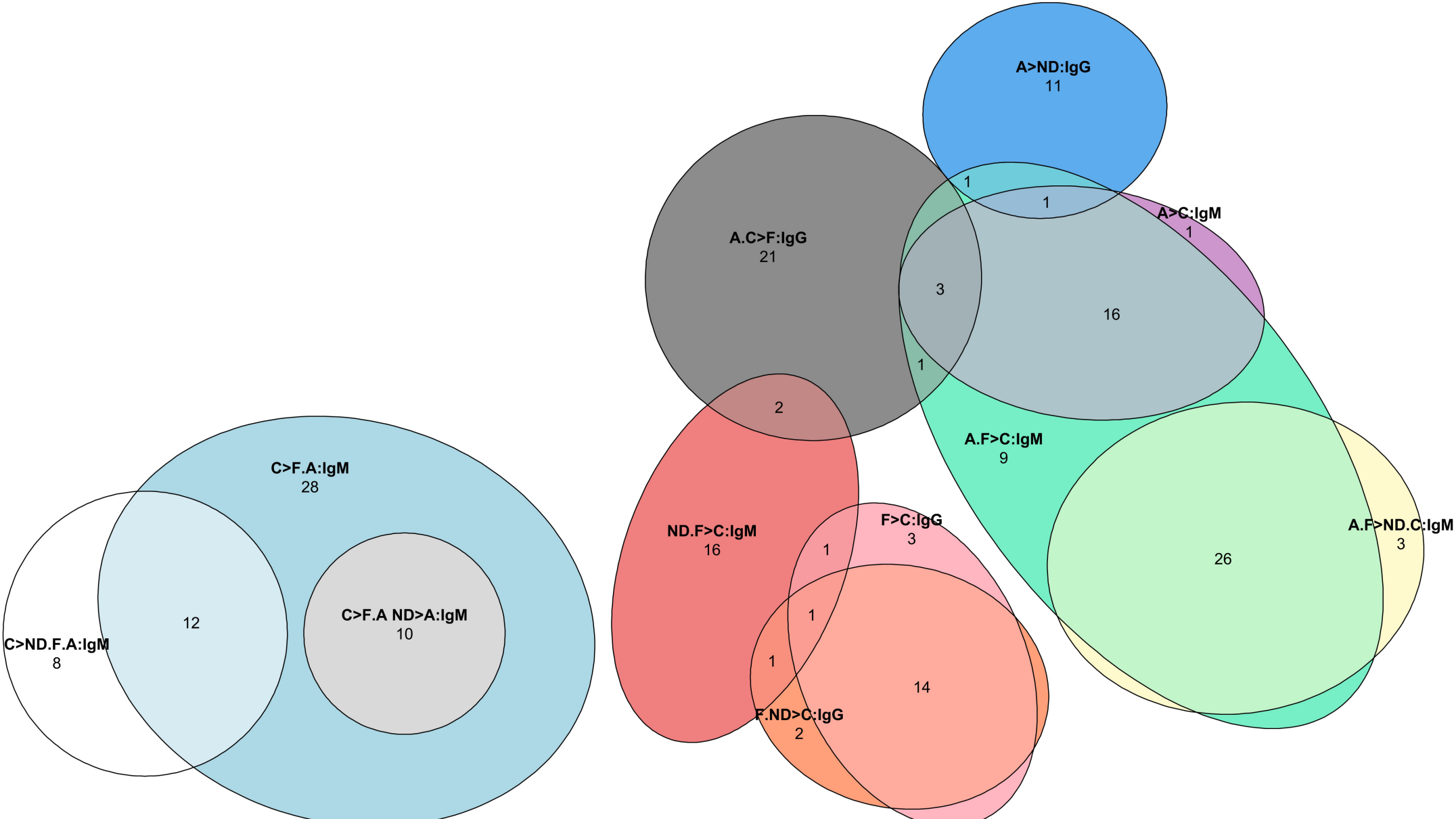
C>F.A:IgM
28
C>ND.F.A:IgM
8
12
C>F.A ND>A:IgM
10
A>ND:IgG
11
A.C>F:IgG
21
1
1
A>C:IgM
1
3
16
1
2
A.F>C:IgM
9
ND.F>C:IgM
16
F>C:IgG
3
1
1
1
14
F.ND>C:IgG
2
26
A.F>ND.C:IgM
3